RAPID PREDICTION OF FLOOD INUNDATION

by

Sophia Alevyzaki

Submitted for the degree of Master of Philosophy

Heriot-Watt University

School of Energy, Geoscience, Infrastructure and Society

June 2015

ABSTRACT

Historically, buildings have been built on floodplains ignoring the danger from the risk of flooding.

The need for large scale (national) and probabilistic flood risk assessment has resulted in the development of a number of rapid flood modelling methodologies.

These methods are approximate and generally ignore inertia in the estimation of flood extent. Therefore, the advantage of short run times of those rapid flood modelling methodologies is restricted by the limitation in the accuracy of the predicted results. On the other hand, full hydrodynamic models (such as TUFLOW) provide detailed predictions of the flood flow parameters, although they are time consuming to run. Consequently, the need for a new Rapid Flood Model which provides more detailed predictions is obvious.

In this thesis, several inflow volume scenarios were tested and results from both the RFIM and TUFLOW were compared in an attempt to provide a critical appraisal for the RFIM technique. This comparison showed that in a lot of relatively simple cases both models predicted similar flood parameters. Exceptions occur being where inertia has a significant influence on flood propagation and it is clear that care must be taken when applying the RFIM to such circumstances. The new Rapid Flood Model improved on this limitation for water level predictions. For most of the inflow volume cases investigated the new model displayed similar water level values to TUFLOW and the difference between these values reduced as the inflow volume increased.

Dedicated to my late father, my mother and sister for their support

and encouragement.

ACKNOWLEGMENT

I would like to thank my supervisors Professor Gareth Pender and Dr Steve Wallis for their support and supervision.

I would like to thank Dr Martin Krupka for providing the Rapid Flood Inundation Model (RFIM) and useful advice on its application, Dr Sylvain Neelz for his help on learning to use TUFLOW. I would also like to thank Dr Yang Liu for his comments and advice particularly on the development of his revised Rapid Flood Model.

Finally, I would like to thank Prof. Nigel Wright (University of Leeds) and Dr Grant Wright (Heriot-Watt University) for their useful comments.

ACADEMIC REGISTRY
Research Thesis Submission

Name*:*	**SOPHIA ALEVYZAKI**		
School/PGI:	**School of Energy, Geoscience, Infrastructure and Society - Institute for Infrastructure and Environment**		
Version: *(i.e. First, Resubmission, Final)*	**Final**	Degree Sought (Award **and** Subject area)	**MPhil** **Flood Risk Management**

Declaration

In accordance with the appropriate regulations I hereby submit my thesis and I declare that:

1) the thesis embodies the results of my own work and has been composed by myself
2) where appropriate, I have made acknowledgement of the work of others and have made reference to work carried out in collaboration with other persons
3) the thesis is the correct version of the thesis for submission and is the same version as any electronic versions submitted*.
4) my thesis for the award referred to, deposited in the Heriot-Watt University Library, should be made available for loan or photocopying and be available via the Institutional Repository, subject to such conditions as the Librarian may require
5) I understand that as a student of the University I am required to abide by the Regulations of the University and to conform to its discipline.

* *Please note that it is the responsibility of the candidate to ensure that the correct version of the thesis is submitted.*

Signature of Candidate*:*		Date:	19/6/2015

Submission

Submitted By *(name in capitals):*	**SOPHIA ALEVYZAKI**
Signature of Individual Submitting:	
Date Submitted:	19/6/2015

For Completion in the Student Service Centre (SSC)

Received in the SSC by *(name in capitals):*			
1.1 Method of Submission *(Handed in to SSC; posted through internal/external mail):*			
1.2 E-thesis Submitted (**mandatory for final theses)**			
Signature:		Date:	

TABLE OF CONTENTS

CHAPTER 1 –INTRODUCTION AND LITERATURE REVIEW

1.1 INTRODUCTION

Floods are natural hydrological phenomena **(PAGASA, 2009)**. There are very few countries worldwide that do not suffer a risk from flooding. Nowadays, this phenomenon is becoming more frequent and severe (to people and property) due to climate change. According to the UN reports the number of people living in areas of potential flood risk is approximately 1B (**Penning – Rowsell & Werrity, 2008**). Consequences from flooding are becoming more severe over the years. These consequences include environmental losses, economic damage and loss of life. Loss of life is considered to be the most important disaster (**Jonkman et al., 2008**). In 2011, 5202 deaths from flood were reported (**CRED, 2012, & Ballica et al., 2013**).

One of the countries that has suffered from floods over the years is the UK. The UK has a long history of flooding especially due to heavy rainfall and storm surge. It is estimated that 1.85 million homes, 185,000 commercial properties and approximately 5 million people were at risk from flooding in England and Wales (**Tunstall et al. 2004**). Since 2000, floods have caused over £4.5B worth of damage and especially the 2007 floods account for the £3B (**ABI, 2013**). The UK government has estimated that in the future £1.1B worth of damages will arise from flooding each year (**UK Parliament, 2013**). Flood Risk Management is an important factor for the UK government in terms of reducing environmental losses, property damages and loss of life.

The combination of the probability of occurrence of a flood event and the impact of that particular event define the flood risk (**Environment Agency, 2005**). These two factors mentioned above (probability, consequence) are affected by the *sources of risk* (rainfall, tides, waves etc), the *pathways* (rivers, flood defence infrastructure, topography (which can be modified by flood management measures)) and the *receptors of risk* (people, property, etc) (**Hall et al. 2003**).

The policies towards Flood Hazard Management that the UK governments have adopted over the past 50 years (since the end of the 2nd World war) have evolved as a result of changes in economic and social conditions, technology, information, knowledge etc, and also due to severe flood events (e.g. 1947, 1953, 1998 and 2000) which occurred and became *'a window of opportunity'* for catalytic policy change (**Tunstall et al. 2004**).

It is useful at this point to divide the phases of policy changes through the years into:

- land drainage: end of 2nd World War-late 1970s.
- flood defence: 1980s to 1990s.
- flood risk management: mid-1990s onwards.

The flood protection method that has been used since the 1990s is far from the traditional methods used in the past (i.e. land drainage and flood defence). It is more strategic and aims to *'manage the flood risks in terms of both probabilities and consequences'* (**Tunstall et al. 2004**).

'Flood Risk Management is the decision-making process which seeks to manage the reaction of the system to external perturbations recognising in particular that not all floods can be prevented' (**Tunstall et al. 2004**).

It is important here to notice that the protection method mentioned above is based on the combination of (**Tunstall et al. 2004**):

- *Flood abatement: prevention of flood waves.*
- *Flood control: prevention of floods.*
- *Flood alleviation: the reduction of flood impact*.

The category of artificial floods will be examined in this project where the term artificial floods describe floods that are caused due to human activities such as **(PAGASA, 2009)**:

- Failure of defence structures
- Mismanagement of defence structures

In the case of this particular thesis the consequences of failure of defence structures are examined, and the inundation arising from breaching or overtopping of a defence structure is simulated. This type of inundation can arise from either:

- Failure of the defence structure
- Mismanagement of the defence failure

Flood Risk Management measures are commonly assessed by the application of computer models. The flood hazard of an event is assessed by these models simulating the physical processes of the flood, by setting boundary conditions and predicting the

potential flood extent, depth and velocity (**Ballica et al., 2012, Hartanto et al., 2011, Beevers et al., 2012**).These models can be classified as 1D, 2D, 1D/2D, quasi-2D and 3D models. All hydrodynamic models are based on the mathematical conservation laws for mass and momentum. It is useful here to note that uncertainty, mainly, due to climate change is usually not included in flood risk numerical modelling. This could have implications on the usefulness of the results obtained from flood risk models (**van Vuren, 2005, & Warmink et al., 2010**). Efforts have been made to incorporate uncertainty in models in hydraulic modelling, flood mapping and inundation analysis, and flood risk management and assessment (**Smemoe et al., 2007, Baldassarre et al., 2009; 2010, & Hall et al., 2008**).

In recent years the popularity of 2D hydrodynamic models has increased. The most applied hydrodynamic model is TUFLOW. Although, they give reliable predictions of the flood parameters, they are time consuming. In order to reduce the computational cost the RFIM (Rapid Flood Inundation Model) was developed.

The aim of this thesis is to investigate whether the RFIM and TUFLOW predict similar flood parameters (such as water level, flood extent, flooding order, flood volume stored in each flooded cell, etc.) in various scenarios. In the cases where TUFLOW predicted more accurate results than RFIM due to the effect of inertia, the need for a new RFIM providing with as accurate as TUFLOW results but at the same time as fast as RFIM is obvious. Thus, another aim of the thesis is to develop a new Rapid Flood Model which will overcome the limitations of both the rapid flood modelling techniques (RFIM) and the shallow water equation model TUFLOW. Interpolation/extrapolation of the obtained TUFLOW results of two inflow volume scenarios will be used to develop this new model, similar to **Neelz et al (2007)**.

The thesis in the first part compares the predictions made by both flood models (i.e. RFIM and TUFLOW), for a series of benchmark DTMs and inflow volume scenarios. In the second part, a new RFIM is developed through linear interpolation/extrapolation of the obtained TUFLOW results of two extreme inflow volume scenarios. Those results (from the new RFIM) are compared to ones obtained from the RFIM, TUFLOW and simple interpolation/extrapolation and an overall conclusion is reached.

The rest of the thesis proceeds as follows: **Sections 1.2-1.4** provides a review of the literature; **Chapter 2** provides a description of work to be done; in **Chapter 3** the application of the new Rapid Flood Model is discussed. **Chapter 4** provides a detailed discussion of the findings and **Chapter 5** concludes. Supporting figures, tables and graphs are contained in **Appendices A** and **B** respectively.

1.2 MODELLING APPROACHES FOR FLOOD RISK MANAGEMENT:

1.2.1 INTRODUCTION TO MODELLING:

Computer modelling is now widely used in flood risk analysis, as it enables the simulation of real life phenomena in a matter that aids understanding and supports decision making. Using this simplified reality different scenarios can be tested and predictions of the future can be made.

Within flood risk management, there are different model types available (**WUP-FIN, 2004**)

- Hydrological models
- Hydrodynamic models
- Water quality models
- Meteorological models

In this thesis, only hydrodynamic models will be analysed (1D, 2D, 3D etc) and used as these focus on the water movement when a flood event occurs.

There are various types of hydrodynamic models which are classified based on their dimensionality, such as 1D, 2D, coupled 1D-2D, quasi-2D and 3D. However, all these types use approximately the same methodology in their set up:

- Develop the hydrodynamic model grid, considering the resolution of the grid, the grid size and the variation of the bathymetry.
- Determine the boundary conditions (upstream and downstream boundaries).
- Determine the physical parameters such as the bed roughness coefficient, the eddy viscosity, the density of water, the acceleration of gravity, etc.
- Finally, determine the time step necessary to ensure the numerical stability of the model.

1.2.2 FLOOD MODELS:

It is customary in flood modelling for three different types of mathematical models to be used. These types vary from the traditional 1D and 2D to the more complex 3D category (Table 1).

Method	Description	Typical run time	Outputs	Example models
1D	Solution of 1D St. Venant equation	minutes	Inundation extent (if floodplains are part of 1D model) Water depth	MIKE 11 HEC-RAS ISIS Etc.
2D	Solution of 2D shallow water equations	Hours or days	Inundation extent Water depth Depth-averaged velocities	TUFLOW MIKE 21 ISIS 2D TELEMAC 2D Etc.
1D/2D	Dynamically link of 1D river model and the 2D overland flow model	days	Inundation extent Water depth	MIKE FLOOD(i.e. combination of MIKE 11 / MIKE 21) Etc.
Quasi-2D	1D St Venant equation plus a storage cell approach to the simulation of floodplain flow	minutes	Inundation extent Water depth Water level	MIKE 11 HEC-RAS ISIS Etc.
3D	Reynolds averaged Navier-Stokes	days	Inundation extent Water depth Velocity in 3 dimensions	TELEMAC-3D MIKE 3 FLOW 3D Etc.
Rapid Flood Models	2D shallow water equations without considering the momentum conservation for the flood plain flow	seconds	Inundation extent Water depth Water level	RFIM RFSM

Table 1: Overview of inundation models

- ***1D approach:***

In the 1D modelling approaches, the river flow and the floodplain inundation can be simultaneously calculated with the solution of the modified St Venant equations. Precisely, the river channel is treated as a cross section set perpendicular to the flow direction while the floodplain is treated as an extended cross section of the river. In the 1D category, HEC-RAS, MIKE 11 and ISIS river modelling software are often used to construct models (**Syme et al. 2001, Lin et al. 2006 & Leandro 2008**).

The continuity or mass conservation equation (**Eq. 1**) and the momentum conservation equation (**Eq. 2**) influence the flood waves' movement. These two equations can be expressed as follows:

$$\frac{\partial Q}{\partial x}+\frac{\partial A}{\partial t}=0 \qquad \textbf{(Eq. 1)}$$

$$\frac{1}{A}\frac{\partial Q}{\partial t}+\frac{1}{A}\frac{\partial}{\partial x}\left[\frac{Q^2}{A}\right]+g\frac{\partial h}{\partial x}-g\left(S_o-S_f\right)=0 \qquad \textbf{(Eq. 2)}$$

(i) **(ii)** **(iii)** **(iv)** **(v)**

where Q (m^3/s) is the flow discharge in the channel, A (m^2) is the cross section surface area, x (m) is the distance along the channel, t (s) is the time, h (m) is the cross sectional averaged water depth, S_o is the bed slope in the longitudinal direction and S_f is the friction slope and g (m/s^2) is the acceleration due to gravity.

The momentum equation (**Eq. 2**) consists of the local acceleration or inertia term (**i**), the advective acceleration (**ii**), the pressure gradient (**iii**), the bed slope (**iv**), and the friction slope (**v**).

The friction slope can be expressed by Manning's, Darcy-Weisbach's or the Chezy's equation (**Ole et al. 2004, Environment Agency, 2009 & Syme et al. 2011**). However, Manning's equation is the most preferable in the UK.

The application of the **St Venant** equations is based on a number of theoretical assumptions being met:

- A small bed slope;
- The existence of hydrostatic pressure i.e. small streamline curvature and negligible vertical acceleration;
- Representations of channel conveyance obtained for the flow in steady state can account for the boundary friction and turbulence effects.

1D river models are capable of simulating flows over and through a variety of hydraulic structures, for example weirs, gates, sluices etc, and this is considered to be one of their main strengths. Another advantage of the 1D models is their short computational time.

Also, an important strength is the ability to combine the 1D modelling approaches with the 2D approaches. There are a number of ways for implementing such applications (**TUFLOW 2006, Environment Agency, 2009, Syme et al. 2001, Syme et al. 2004**):

- *Within a channel that one wishes to model partly in 1D and partly in 2D*
- *Between a 1D drainage network model and a 2D surface flood model*
- *Between a 1D river model and a 2D floodplain model*
- *Within a mainly 2D model where for example culverts are modelled in 1D, linking 2D cells between themselves*

- ***2D approach:***

The prediction of flood inundation in fully 2D flood models is based on the solution of the shallow water equations (**Wicks et al 2004, Pender et al. 2007 & Horritt et al. 2008**). The shallow water equations contain the mass conservation equation (**Eq. 3**) and the momentum conservation equation (**Eq. 4, Eq. 5**) on both the x and y directions and can be defined as a 2D dimension expansion of the 1D St Venant equations. These equations can be expressed as follows:

$$\frac{\partial h}{\partial t}+\frac{\partial hu}{\partial x}+\frac{\partial hv}{\partial y}=0 \qquad \textbf{(Eq. 3)}$$

$$\frac{\partial hu}{\partial t}+\frac{\partial (hu^2)}{\partial x}+\frac{\partial (huv)}{\partial y}+gh\frac{\partial h}{\partial x}-ghS_{0x}+ghS_{fx}=0 \qquad \textbf{(Eq. 4)}$$

(i) **(ii)** **(iii)** **(iv)** **(v)**

$$\frac{\partial hv}{\partial t}+\frac{\partial (hv^2)}{\partial x}+\frac{\partial (huv)}{\partial y}+gh\frac{\partial h}{\partial x}-ghS_{0y}+ghS_{fy}=0 \qquad \textbf{(Eq. 5)}$$

(i) **(ii)** **(iii)** **(iv)** **(v)**

where x (m) is the distance along the channel, t (s) is the time, h (m) is the cross sectional averaged water depth, u (m/s) is the velocity at the x direction, v (m/s) is the velocity at the y direction, S_o is the bed slope in the longitudinal direction and S_f is the friction slope and g (m/s^2) is the acceleration due to gravity.

The terms in the momentum equation are:
The local acceleration or inertia term (**i**), the advective acceleration (**ii**), the pressure gradient (**iii**), the bed slope (**iv**), and the friction slope (**v**).

It is essential here to define the term inertia, since it will be used frequently in Chapters 2 and 3.

'Inertia is the resistance of any physical object to a change in its state of motion or rest, or the tendency of an object to resist any change in its motion' (**Motte, 1846 & Burns, 2009**).

The most important assumptions for the application of the shallow water equations are:

- A small bed slope
- Steady state flow laws can be utilised for the representation of the bottom friction
- Hydrostatic pressure distribution over the depth

It is important to note that the shallow water equations can also include terms for the surface wind shear stress, the Coriolis force and head loss due to turbulent momentum exchange.

2D models do not require the predefinition of the flowpaths, thus, they can be used in areas where the flow follows the topography (e.g. through properties or along streets). However, they have a large computational cost, and also, accurate DTMs are essential (**Wang et al. 1997, Bates et al. 2005, Bradbrook, 2006, Pender et al. 2007, Pender et al. 2008 &, Environment Agency, 2009**).

Some of the most frequently used 2D modelling software packages are TELEMAC2D, TUFLOW, ISIS 2D, MIKE21 and the LISFLOOD-FP.

- ***1D-2D approach***

Recently, the linkage of the 1D modelling approach with the 2D approach has been proved to give more flexible models in terms of range of application than those produced from 1D and 2D models individually. When a 1D model is utilised, the river channel representation is efficient in computational terms and the model can handle the existence of structures. On the other hand, the 2D nature of the floodplain flow can be captured when a 2D approach is used. Consequently, 1D discretisation is used for the modelling of natural 1D elements (i.e. pipes and channels) while 2D methods are utilised for the calculation of the overland flow on floodplains (**Syme, 2001, Syme et al. 2004, Krupka, 2008 & Leandro, 2008**).

There are two techniques to couple these two modelling approaches: horizontal and vertical coupling. Watercourses and their floodplains can be modelled partly in 1D and partly in 2D through the utilisation of horizontal coupling. The horizontal coupling technique can also be used to connect the downstream extremity of a 1D model to 2D grid. In this technique the flow from the 1D enters the 2D model as a 'source', and the downstream boundary condition in the 1D model is given by the 2D model water level at the junction (**TUFLOW, 2006, Environment Agency, 2009**).

A continuous 2D grid overlying the 1D river model is used in the vertical coupling for the representation of a floodplain. The 1D model functions independently until the river level reaches bankfull level, at which point the water above this level is transferred to the 2D model (**Lin et al. 2006 & Environment Agency, 2009**).

These models, like 2D models, do not need to predefine the flow paths on the floodplain. So, they are more appropriate to be used for the modelling of floodplain inundation.

Commonly combined 1D-2D models are TUFLOW-ISIS and MIKE11-MIKE21 (i.e. MIKE FLOOD).

- ***Quasi-2D approach***

River flood modelling can be performed by 1D modelling approach. To model the floodplain flow a Quasi-2D approach is used (**Huang et al. 2007**). This can be accomplished in the following ways:

- Extension of 1D cross section onto the river floodplain. With this approach both the floodplain and the channel flow are calculated through the solution of the St Venant equations. And it is used mainly when there are no embankments or banks to separate the floodplain from the main channel, and also where floodplains are of limited transverse dimension. The disadvantage of this approach is the assumption that floodplain flow is parallel to the main channel.

- 2D storage cell method. This method solves the kinematic or diffusion wave equations in order to simulate the channel flow. A 2D floodplain simulation is linked to the channel flow simulation with a grid of square cells. Flow between cells

is estimated through the application of the Manning's equation (**Bates et al. 2005 & Horritt et al. 2008**).

- Storage cells with a spill relationship between the main channel and the floodplain. As mentioned before, the Quasi-2D models are used to account for the 2D nature of floodplain flow, although they do not discretize the terrain as a 2D computational grid; instead floodplains are treated as a system of storage cells. The communication of each cell with the neighbouring cells is established through a local 1D relationship (**Krupka, 2008**). Precisely, discharge relationships (usually based on weir flow equations) are utilised for the modelling of the flow between the 1D channel and the floodplain storage cells. Volume conservation is used for the computation of the water level in each storage cell. No momentum conservation on the floodplains is included in the Quasi-2D models, implying the instantaneous transfer of water from one end of the storage cell to the other (**Willems ert al. 2002 & Environment Agency, 2009**).

The benefit of quasi-2D models is that they only require short run time, although the calculation undertaken does not permit estimates of velocity and hence flood hazard.

- ***3D approach***

The *TELEMAC-3D*, the *MIKE 3* and *FLOW 3D* models are the three major ways to model flood inundation in 3 Dimensions (**DEFRA, 2006 & Li et al. 2006**). These particular models are based on the solution of the **Reynolds** averaged **Navier-Stokes** equations and can predict the water levels and the velocity (in 3 dimensions) in rivers and floodplains. Additional to the mass and momentum conservation, used in 2D approach, salinity and temperature conservation, as well as an equation of state relating local density to salinity, temperature and pressure are required (**DHI, Water and Environment, 2001**).

The RANS (Reynolds Averaged Navier-Stokes) equations are (**DHI, Water and Environment, 2001**):

$$\frac{\partial u_i}{\partial t} + \frac{\partial u_i u_j}{\partial x_j} + 2\Omega_{ij} u_j = -\frac{1}{\rho}\frac{\partial P}{\partial x_i} + g_i + \frac{\partial}{\partial x_j}(\nu_T \left\{ \frac{\partial u_i}{\partial x_j} + \frac{\partial u_j}{\partial x_i} \right\} - \frac{2}{3}\delta_{ij} k) \quad \textbf{(Eq. 6)}$$

$$\frac{\partial \rho}{\partial t} + \frac{\partial}{\partial x_j}(\rho u_j) = 0 \qquad \textbf{(Eq.7)}$$

Where ρ is the local density of the fluid, u_i the velocity in the x_i-direction, Ω_{ij} the Coriolis tensor, P the fluid pressure, g_i the gravitational vector, v_T the turbulent eddy viscosity, δ_{ij} Kronecker's delta, k the turbulent kinetic energy, and t denotes the time.

Coast contours and depth are described as accurately as possible with the selected grid size. The transport equations for salt and temperature are used together with an equation of state for the density of the water (**DHI, Water and Environment, 2001**):

$$\frac{\partial S}{\partial t} + \frac{\partial}{\partial x_j}(u_j S) = \frac{\partial}{\partial x_j}(D_S \frac{\partial S}{\partial x_j}) \qquad \textbf{(Eq.8)}$$

$$\frac{\partial T}{\partial t} + \frac{\partial}{\partial x_j}(u_j T) = \frac{\partial}{\partial x_j}(D_T \frac{\partial T}{\partial x_j}) + Q_H \qquad \textbf{(Eq.9)}$$

Where S is the salinity, T the temperature and Q_H the heat exchange with the atmosphere. D_S and D_T are the dispersion coefficients for salt and temperature, respectively.

The 3D modelling approaches are more appropriate to solve flow problems when turbulence and density variations are important factors. In more detail, they simulate unsteady flow considering bathymetry, density variations and external forces (i.e. meteorology, tidal elevations, etc.) (**DHI, Water and Environment, 2001**).

The main weaknesses of the 3D flood models are the large computational time and that they are data intensive.

- ***Rapid Flood Inundation model approaches (RFIM):***

This particular type of flood modelling has been developed recently and aims to predict the flood parameters in a timescale of seconds. Two models have been produced so far, one from Heriot-Watt University and the other from HR Wallingford. The analysis of both rapid models consists of two parts, the precalculation part and the inundation routine for the Heriot-Watt model, and preprocessing activities and hydraulic simulation

for the HR Wallingford model respectively. These models are based on continuity and the nearest neighbour principle to distribute water between cells and will be described later in detail (Section 1.3) (**Tarrant et al. 2006, Krupka et al. 2007a, b, Krupka, 2008, Lhome et al. 2008, Liu, 2008, Pender, 2011 & Pender et al. 2012**).

The development of those numerical models aims to investigate the consequences of flooding (such as flood extent, flood depth, flood hazard, etc.) in the cases of defence failure.

RFIM approaches are more appropriate to be used to investigate many flood volume scenarios in a short time frame when accuracy is not essential.

- ***Rapid inundation approaches based on Genetic Algorithms:***

It is important for risk assessment to know the flow velocities, since their combination with the depth is considered to have serious impacts (such as injuries, even death) onto people during flood events (**Krupka, 2008).** However, a limitation of the RFIM for flow velocity predictions is that they can predict the velocities only on the boundaries between two storage cells and not for each pixel (**Krupka, 2008**).

According to Krupka (**Krupka, 2008**) velocity predictions stemming from the RFIM are not as accurate as those obtained from hydrodynamic models.

The term Genetic Algorithms (GA) describes a method used in computing to determine solutions to search and optimization problems (**Mitchell, 1996, Whitley, 1994 & McCall, 2005**). These algorithms use techniques that replicate the principles of evolutionary biology namely reproduction, crossover and mutation. The methodology essentially involves initially the generation of many random individual solutions to provide an initial population. Each of these solutions is assigned a fitness evaluated through the objective function of the problem and, based on this; solutions are modified to form a new generation of solutions through the application of reproduction, crossover and mutation. 'A GA works iteratively by successively applying these three operators in each generation until a termination criterion is satisfied' **(Deb, 2001 & Deb, 2004**).

In particular, once the set of random solutions has been identified and their fitness determined, the reproduction operator is applied, selecting the fitter solutions and

forming a new generation (**Whitley, 1994, Mitchell, 1996, Deb, 2001, Deb, 2004 & McCall, 2005**). Next the crossover operator is applied, randomly matching pairs of 'parent' solutions to create a new solution, which shares some of the 'parent' characteristics. Mutation also assists in the creation of a new population of solutions, as it ensures that the characteristics found in the crossover are inherited by the 'child' solution. This generational process is repeated until the set termination condition has been reached (**Whitley, 1994, Mitchell, 1996 & McCall, 2005**).

Genetic Algorithms are currently being applied with RFIM based modelling using a non linear relationship between the residuals of predicted variables (arrival time, depth, velocity) and the predictive variables from a coarse grid model (**Liu, 2008**).

1.3 RAPID FLOOD MODELLING:

1.3.1 INTRODUCTION:

It is believed that the frequency and the scale of flooding will increase in the future due to climate change. In the UK, the planning authorities and the water companies have realized that it is not possible to eliminate the risk of flooding completely, however it is possible to reduce its consequences. For this reason, a range of numerical models have been developed in order to investigate the consequences of flooding in the cases of defence failure such as the overtopping of, and the breach in, a flood defence structure. Particularly, these models calculate the flood parameters such as flood extent, flow velocity, flood depth etc. and also the flood hazard (**Krupka et al. 2007**).

The current generation of inundation models can be divided in two categories (**Tarrant, 2006**):

- Simple inundation models which run very fast and do not require much information.
- Complex inundation models which in contrast to the simple ones require a long computation time and utilise much more detailed information.

The disadvantage of the simple inundation models is that they are not very accurate since they do not use detailed information. On the other hand, the disadvantage of the complex inundation models is that they cannot be used to investigate many different scenarios since they require a long time to run.

1.3.2 EXISTING RAPID FLOOD INUNDATION MODELS:

The Rapid Flood Inundation Model (RFIM) was developed at Heriot-Watt University in order to *'investigate the usage of a simple storage cell algorithm for the purpose of flood risk management'* (**Krupka et al., 2007a, b**). Precisely, it aims to predict the maximum flood inundation extent caused by the overtopping or breaching of flood defences (e.g. dykes). It was designed to run very quickly so that very many scenarios can be assessed in a short time frame, e.g. flood water ingress at different locations and of different water volumes. This particular model is used in combination with the MapInfo Professional software in order to produce maps, which depict the results in a clear way (**Krupka, 2008**).

Another rapid flood models was developed by the HR Wallingford, the Rapid Flood Spreading Methodology (RFSM). This model was created in order to support the Risk Assessment for Flood and Coastal Defence for Strategic Planning the so-called RASP approach. In particular, the model aimed to support the development of new flood spreading methods, which investigate different flood event scenarios (caused by defence failure and loading conditions) demanded by the RASP methods. This methodology provides with acceptable results both in terms of accuracy and time (**Tarrant, 2006**). It can be used to investigate different flood inundation scenarios and to predict the flood extent in each of these cases.

The RFSM aims to spread the water discharged from the defence failure (i.e. breached or overtopped flood defences) over the floodplain following the topography of the area (**Gouldby et al, 2008**).

Both the RFIM and the RFSM, in order to run very fast divide the analysis into two parts: precalculation part and inundation routine for the RFIM, and pre-processing activities and hydraulic simulation for the RFSM.

The corresponding parts of both models follow the same reasoning, but may differ slightly at points.

- ***PRECALCULATION PART / PRE-PROCESSING ACTIVITIES:***

In this part of the analysis the calculation mesh is generated. It entails identifying a series of accumulation areas with different shapes defined by the topography of the floodplain.

The input data of this process are the floodplain topography which is represented as a DTM (Digital Terrain Model), the location of the defences relative to the DTM (i.e. the location of the mid point of the defence) and the flood areas to be modelled (these areas are defined by the division of the whole floodplain area as described in **Tarrant, 2006 & Gouldby et al, 2008**).

The most important assumptions of this stage, in order to obtain all the relevant topographic information from the input data, are:

- *'The flow pathway follows the steepest slope of the topography, from the source of flooding to the accumulation areas.'*
- *'The pathway will remain the same independent of the event severity.'*

At the pre-processing stage, the floodplain is automatically divided into smaller accumulation areas and this division depends only on the ground elevations and the DTM grid density. This means that the water flow follows the underlying topography of the flood area. Apart from the construction of the accumulation areas, the identification of communication points (the lowest level that the water must reach in a given accumulation area to spill into another accumulation area) also takes place (**Tarrant, 2006 & Gouldby et al, 2008, Krupka et al., 2007b**).

The pre-processing calculation follows the following steps (**Tarrant, 2006**):

- Searching for the accumulation points (the lowest point of a given accumulation area).
- Building the accumulation areas: *'all the DEM cells associated to one accumulation point will form an accumulation area'.*
- Searching neighbours/communication points between accumulation areas: the lowest ground level of the DEM cells between two accumulated areas is selected as the communication level.
- Building the databases (level-volume database for each accumulation area and communication point database)

- Including the flood defences in the model.

In particular, this part provides most of the input used by the inundation routine. It is only run once for the whole floodplain and provides a definition of floodplain geometry for the inundation routine. Once the geometry is defined the inundation routine may be run for tens, hundreds or thousands of different flooding scenarios (**Krupka et al, 2007b**).

- ***INUNDATION ROUTINE / HYDRAULIC SIMULATION:***

In the case of flood event inundation routine / hydraulic simulations, firstly, the flood volumes obtained from each defence length become activated after being released into their neighbouring accumulation area (also referred to as adjacent impact zones) (Fig. 1). Following this, the water volume contained in an active accumulation area is compared with the appropriate communication volume level. Should the water reach the level of a communication point, then an excess volume is computed and released into the neighbouring accumulation area. This procedure is replicated across all communication points and areas, with reduced excess volumes for each repetition, down to the point when the excess becomes zero. In this way volume is preserved; following this the final flood depth grid can be obtained. A depth grid resolved to impact cell scale is obtained as a result (**Gouldby et al, 2008**).

The important steps that are followed are (**Tarrant et al, 2006**):

- *Activate accumulation areas*
- *Calculate the capacity of the active accumulation areas*
- *Check the relation between the capacity and inflow volume*
- *The active accumulation areas with excess are filled up*
- *The active accumulation areas without excess are filled up*
- *The compatibility of levels with the river is checked.*
- *Searching new accumulation areas to fill*
- *End of the inundation routine / hydraulic simulation*

An illustrated explanation of the inundation routine / hydraulic simulation is depicted in Fig. 1**.** In the inundation routine the flooding procedure is similar to that occurring following an actual breach in, or an overtopping of, a defence (Fig. 1). The volume of the flood water to be spread and the entry point of the water are specified by the

modeller. Originally, all the flood cells are dry. Once the breach has occurred the cell closest to the breach becomes active (flooded) and the rest are dry. Once this cell has flooded, adjacent cells become activated because of overtopping from the flooded one, which remains flooded but is inactive. The other cells remain dry. This procedure ends when all the floodwater has spread across the floodplain, at which point the total volume of all the flooded cells equals the floodwater volume (**Krupka et al, 2007b**).

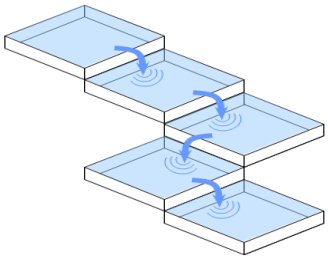

Fig. 1: Inundation process

1.3.3 APPLICATION OF THE RFIM AND THE RFSM TO THE RIVER THAMES:

Both models have been applied to the complex flood system of the River Thames (**Gouldby et al, 2008**). It is complex due to the different flood sources (high astronomical tides and meteorological surges) and also due to the variable floodplain topography.

The water volumes that enter the floodplain in extreme flood events, either as a result of a breached or overtopped structure, are used in the spreading of the floodwater across the floodplain. This is achieved through the use of an efficient flood-spreading method taking into account floodplain topography (described in Section 1.3.4). As a number of model runs were required for a full probabilistic analysis, the requisite fast spreading was ensured through the use of this particular method.

The RFIM was applied by **Krupka et al, (2007a)** on the Thamesmead and the Greenwich Embayments. On the other hand, the RFSM was applied westward along the Thames Estuary from Southend in the east to Teddington (**Reeder et al., 2007**).

1.4 INTRODUCTION OF A NEW RAPID FLOOD MODEL FOR THE ESTIMATION OF THE WATER LEVEL:

The advantage of the short run times of the RFIM is restricted by the limitation in the accuracy of the predicted results. In particular, the prediction of the flood parameters is

very general for each flooded cell (i.e. water level only); however, the computational time for a more detailed analysis, using hydrodynamic models such as TUFLOW, for each flooded cell separately is too large to be tractable in such a large scale analysis.

Therefore, the need of a new Rapid Flood Model which provides more detailed predictions including rate of flooding, while retaining the speed of simulation is obvious. A reduction in the computational cost can be achieved through linear interpolation/extrapolation of the obtained TUFLOW results of two extreme inflow volume scenarios.

1.4.1 OVERVIEW OF METHODOLOGY:

The improvement of the performance of fast inundation models was proposed by **Neelz et al.** (**2007a**), using statistical techniques. Fine Grid Models (FGM) give more accurate predictions due to their resolution of topography (e.g. 1m, 2m, etc.) and spatial resolution of output predictions. On the other hand, Coarse Grid Models (CGM) with resolution of topography of e.g. 10m, 50m, etc. predict less accurate (but in some respects informative) flood parameters with smaller computational cost than FGM. So, the improvement of CGM (Coarse Grid Model) predictions is achieved in **Neelz et al.** (**2007a, b**) through the use of linear interpolation. FGM and CGM predictions were obtained from two inflow volume scenarios, using TUFLOW, in order to estimate the residuals for each pair of FGM and CGM. An interpolation of those residuals gives an estimated residual which when added to the predicted CGM result achieves the improvement of the CGM prediction, as this would be more similar to a FGM prediction.

Similar to a FGM prediction, the water level and flow velocity were predicted using this method at a ~5 km^2 area of lowlands along the banks of the Thames Estuary in England (**Neelz et al. 2007a, b**). The main result of this investigation was that the CGM predictions of both flood parameters were greatly improved and were close to a FGM prediction. Similar to this technique, the new RFIM, described in this thesis, was developed.

The main differences between the method used in **Neelz et al.** (**2007a, b**) and the new RFIM developed in this thesis are:

- **Neelz et al.** (**2007a, b**) use statistical techniques to improve the results of CGM (10m and 50m resolution) predictions of water level and flow velocity in order for those to be comparable to the results of FGM (2m resolution) predictions. On the other hand, the new RFIM also uses statistics (i.e. linear interpolation/extrapolation) in order to improve the TUFLOW predictions of water level, making these comparable to the RFIM (for the new RFIM the DTM has the same resolution of 1m in all case studies). Therefore, the predictions of the new RFIM are as accurate as TUFLOW, and also, as fast as RFIM.

- **Neelz et al.** (**2007a, b**) applied this method to real topography (along the banks of the Thames Estuary in England), whereas, the new RFIM was applied to a series of artificial DTMs.

- Both **Neelz et al.** (**2007a, b**) and the new RFIM used the same hydrograph shape but with different values of peak discharge. Precisely, trapezoidal shape of hydrograph was used, as one would expect for tidally driven inundation.

1.4.2 NEW RAPID FLOOD MODEL:

Similar to this method, the new Rapid Flood Model introduced in this thesis, is based on the idea of linear interpolation for water level prediction; however, it refers to different inflow volumes of the same DTM. The absolute water level values of TUFLOW are contrasted to predicted water levels to estimate their residuals. The interpolated/extrapolated values of those residuals are added to the predicted values to provide with a more accurate representation of the water levels.

Trapezoidal shape hydrographs are used to represent the tidal character of the inflow volume (Fig. 2). As the breach occurs, high discharge levels are observed until a maximum value is reached, which lasts for a few hours until it starts to reduce. A number of different magnitudes of peak discharge were used varying from $Q_{\max} = 4.86\, m^3/s$ to $Q_{\max} = 34.72\, m^3/s$.

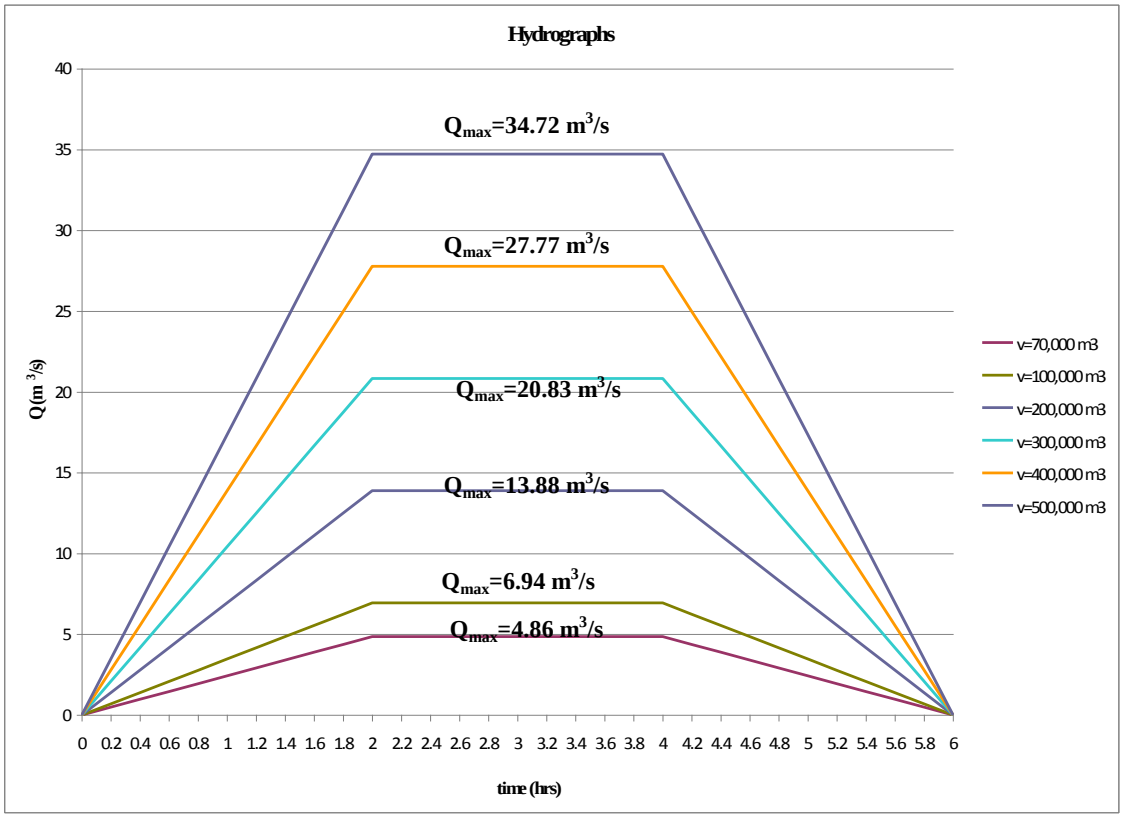

Fig. 2: Inflow hydrographs for the new RFIM

To assist the explanation of the used method, Fig. 3 and 4 have been created on a theoretical basis.

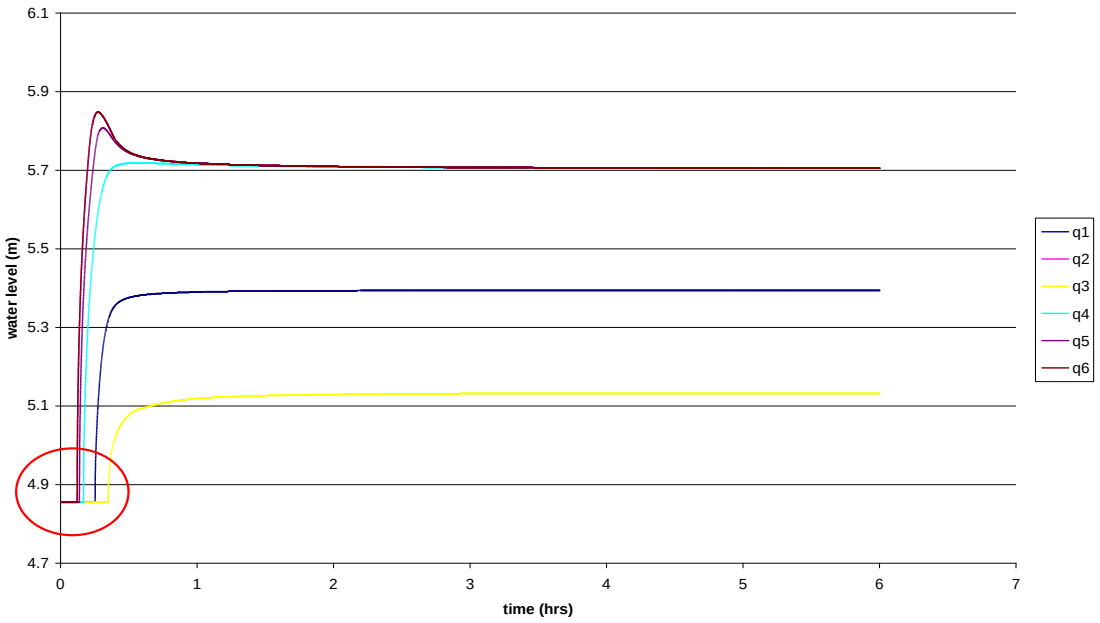

Fig. 3: Time series output for water level displaying time discontinuity for the same DTM

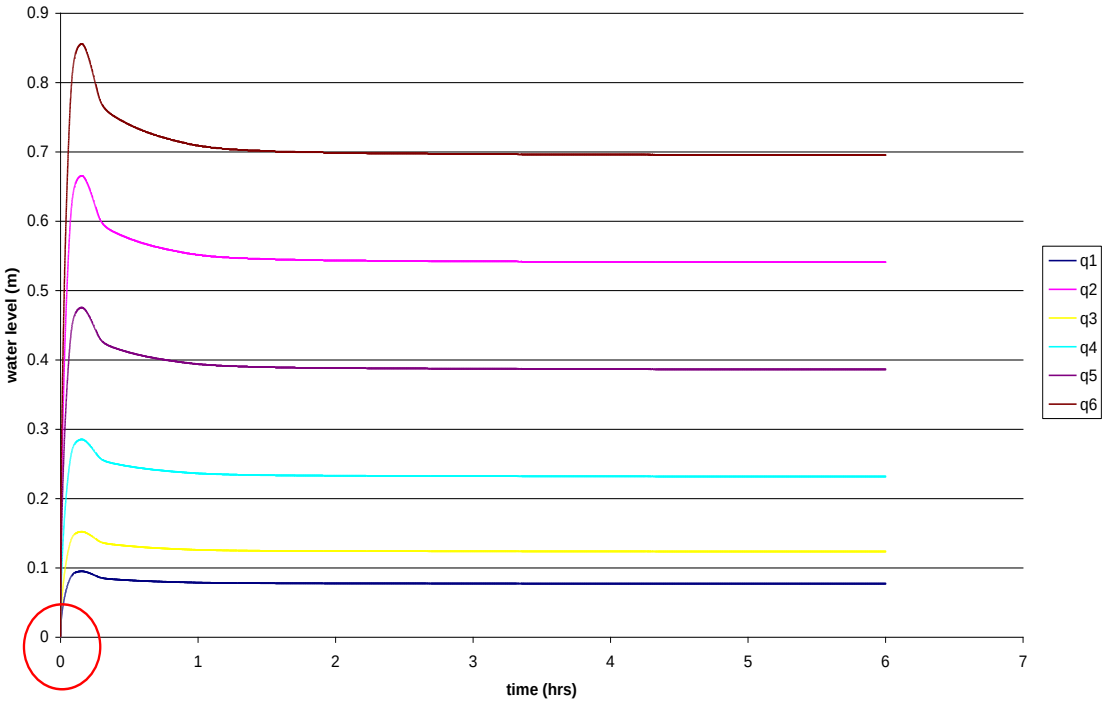

Fig. 4: Time series output for water level after normalisation of the same DTM

As observed in Fig. 3 the arrival time of the flood wave varies for different flood volume values of the same DTM. In order to have a more accurate analysis, the need of normalisation of the data on both the x and y axes arises. Direct interpolation/extrapolation with non-normalised data would provide inaccurate results. This normalisation procedure is exactly the same for flood parameters such as water level, water depth and flow velocity. In this thesis only the estimation of the water level takes place, therefore only the water level and arrival time normalisation is required.

Fig. 4 shows the normalised values of the water level starting from the origin of the axes (i.e. 0, 0).

Once the normalisation of the TUFLOW data has taken place, linear interpolation/extrapolation is undertaken using the following equation:

$$n_{pre}(q_i) = n(\tilde{q}_1) + [(n(\tilde{q}_2) - n(\tilde{q}_1)) \times \frac{q_i - \tilde{q}_1}{\tilde{q}_2 - \tilde{q}_1}] \ , \ \tilde{q}_2 > \tilde{q}_1 \qquad \textbf{(Eq. 10)}$$

where $n_{pre}(q_i)$ is the parameter (i.e. water level, arrival time) to be predicted at a given inflow discharge q_i , $n(\tilde{q}_1)$ and $n(\tilde{q}_2)$ are the normalised TUFLOW data of $\tilde{q}_1$ and

$\tilde{q}_2$ inflow discharge. It is important here to note that $\tilde{q}_1$ and $\tilde{q}_2$ refer to training data from where the predictions for the main training data (i.e. q_1 and q_2) are derived (Fig. 5). Also, i refers to q_1 and q_2.

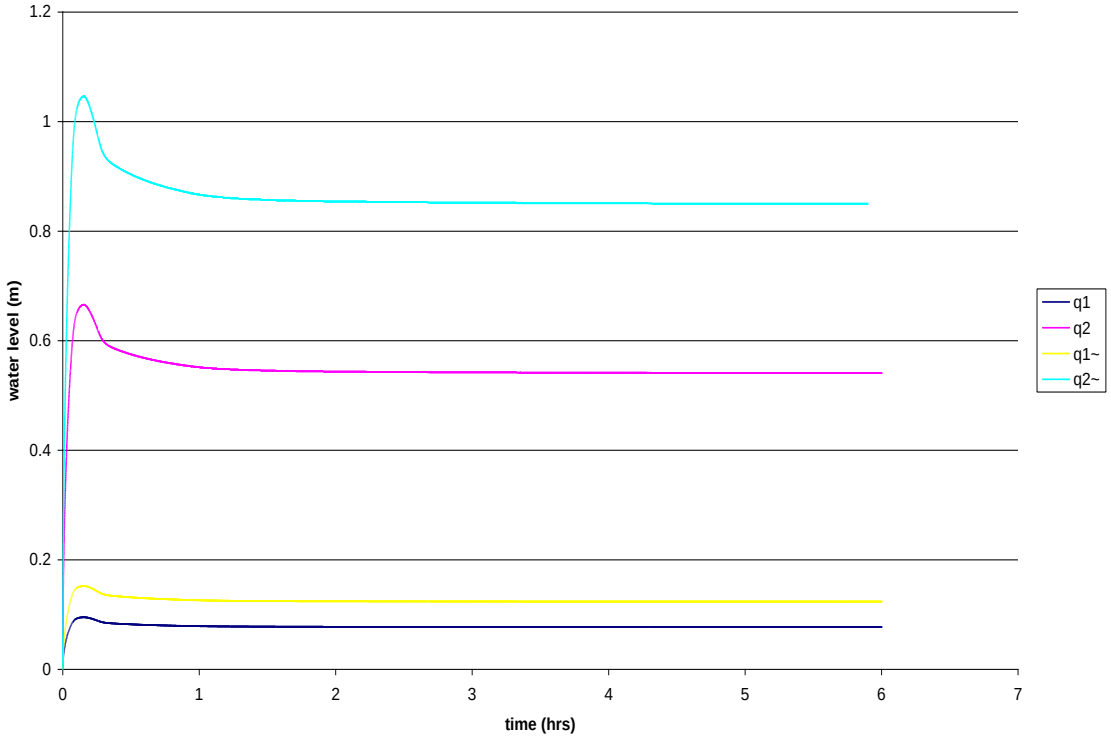

Fig. 5: $\tilde{q}_1$, $\tilde{q}_2$ (training data) used for the prediction of the main training data q_1, q_2)

Upon completion of the linear interpolation/extrapolation procedure, the data is returned to its original state prior to normalisation.

The predicted values ($n_{pre}(q_i)$) are used with the original TUFLOW data ($n_{TUFLOW}(q_i)$) to estimate their residual error ($\varepsilon(q_i)$) given by the following equation:

$$\varepsilon(q_i) = n_{TUFLOW}(q_i) - n_{pre}(q_i) \quad \textbf{(Eq. 11)}$$

Then using the following equation (**Eq. 12**) the predicted interpolated/extrapolated values for the residual error of q_i is obtained:

$$\varepsilon(q_j) = \varepsilon(q_1) + [(\varepsilon(q_2) - \varepsilon(q_1)) \times \frac{q_j - q_1}{q_2 - q_1}],\ q_2 > q_1 \qquad \textbf{(Eq. 12)}$$

where q_j is the inflow discharge to be investigated.

Finally, the above (**Eq. 12**) predicted error ($\varepsilon(q_j)$) is added to the predicted water level value for q_j inflow discharge ($n_{pre}(q_j)$) to obtain the improved water level data ($n'(q_j)$).

$$n'(q_j) = n_{pre}(q_j) + \varepsilon(q_j) \qquad \textbf{(Eq. 13)}$$

where $n_{pre}(q_j)$ is obtained by:

$$n_{pre}(q_j) = n_{pre}(q_1) + [(n_{pre}(q_2) - n_{pre}(q_1)) \times \frac{q_j - q_1}{q_2 - q_1}],\ q_2 > q_1 \qquad \textbf{(Eq. 14)}$$

The above methodology refers to a theoretical description of the water level prediction. In following section (Chapter 3) of this thesis, results of the application of this method will be described.

It has been established from the review of the available flood modelling techniques, from 1D to more complex 3D and rapid flood models (Section 1.2.2), that although, 2D and 3D are more accurate than 1D, they are more time consuming. On the other hand, rapid inundation models (RFIM and RFSM) have small computation time but lack accuracy. This thesis intents to introduce a model which is as accurate as 2D models, and as fast as rapid flood models using statistical techniques that have been successfully used in the past by **Neelz et al.** (**2007a, b**).

CHAPTER 2 – ANALYSIS OF WORK:

2.1 RFIM and TUFLOW comparison:

While the RFIM technique described in Section 1.3.2 provides very fast estimates of flood extent and depth, the simplifications necessary to obtain the computational speed result in the inertial effects of the flood wave being omitted from the simulation. It is therefore necessary to develop an understanding of when this simplification may result in the predictions from the technique diverging so far from real flood wave behaviour to limit their usefulness. To investigate this, the thesis compares the predictions made by the RFIM with those of a shallow water equation model TUFLOW, for a series of benchmark DTMs. The shallow water equation model includes a representation of inertial effects and therefore, provides what one would expect to be good quality predictions of flood inundation extent and depth.

An artificial DTM was chosen for the benchmark tests to provide clarity in the comparisons between RFIM and TUFLOW predictions were a real-life DTM to be used flow in complex areas of topography around structures such as bridges and buildings may mask the main area of interest in this study, namely, when is it necessary to include inertia in flood inundation simulations. To avoid this, a series of artificial benchmark DTMs have been developed in this thesis.

The artificial DTMs developed in this thesis are a network of inverted pyramids (depressions) on a rectangular pattern, they are modified in each case by inserting walls of varying sizes at the crest or at the boundaries between storage cells, and changing the slopes of the underlying topography on the i and j axes (e.g. Fig. 7a). The general characteristics of the DTMS include an area of 3,750,000 m^2 contained 15 storage cells 3 in the north-south direction and 5 in the east-west direction. The plan area of each storage cell was square, 501 m on the northing and 501 m on the easting. One important characteristic of all DTMs is the raised flat areas that have been introduced at the points where the storage cells meet (Fig. 7b). Without those the lowest link between four storage cells is the point with the lowest ground elevation. The reason for inserting these small flat areas ($50m \times 50m$) around the lowest link was therefore to avoid purely diagonal flow paths across the DTM**.** Also, the defence failure was located at the same position in all models (Fig. 7a,). To be more precise the failure occurred at the northwest corner of the DTM, having the following coordinates (x_coord = 544857,

y_coord = 180107-the x_coord and y_coord denote the coordinates on the east and north respectively).

The performance of the RFIM technique was assessed by comparing the order in which depressions flooded and the volume of the water retained with the predictions produced by TUFLOW.

Inflow conditions used in the simulations were bell shaped hydrographs with the total volume (V_{total}) and peak inflow (Q_{max}) chosen to be representative of the inflow expected through a breach in a coastal defence during one tidal cycle (**Wicks et al. (2004) and Alevyzaki, S. (2007)**) (Fig. 6).

In Alevyzaki, S. (2007) analysis was carried out for the determination of the boundary conditions for the application of the RFIM technique at coastal sites. The outcome of this was the overtopping of the coastal defence for V_{Total} between 50,000 m^3 and 400,000 m3, and breaching for values above V_{Total}=400,000 m^3. Here, the focus is on overtopping and so, V_{Total} between 70,000 m^3 and 400,000 m^3 were selected (Fig. 6). These hydrographs provide Q_{max} for each inflow volume scenario. The effects of the potential failure such as breaching could be the topic for future research.

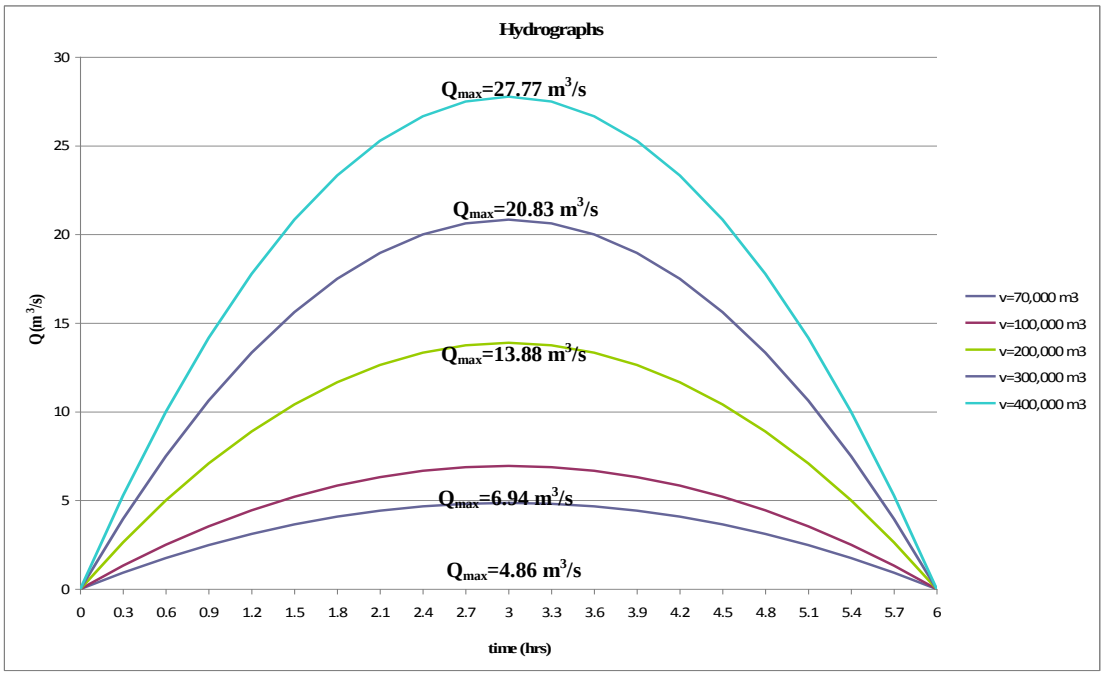

Fig. 6: Inflow hydrographs to the model domain

Table 2 provides a brief summary of all cases and flood volume scenarios investigated including the motivation behind each case study.

Case	Description	Volumes tested				Motivation
		V= 70,000 m^3	V= 100,000 m^3	V= 200,000 m^3	V= 400,000 m^3	
1	Introduction of flat areas around the lowest link	✓	✓	✓	✓	To avoid purely diagonal flow paths across the DTM
2	Two walls at the crest of storage cells C, H and M	✓	✓	✓	✓	To investigate the behaviour of the water as it reaches impermeable barriers
3	Two walls at the boundaries of the storage cells B, G and L	✓	✓	✓	✓	To investigate the behaviour of the water as it reaches impermeable barriers
4	Two walls at the boundaries of storage cells B, G and L, decreasing the slopes on both directions i and j	✓	✓	✓	✓	To assess the behaviour of the water in flat slopes
5	Two walls at the boundaries of the storage cells B, G and L, reducing the slopes on both directions i and j	✓	✓	✓	✓	To examine the behaviour of flood parameters in flatter topographies
6	Two walls at the boundaries of storage cells B, G and L, decreasing the elevation of the area between the walls by 0.5 m	✓	✓	✓	✓	To investigate the effect of smaller elevation between two walls
7	Two walls at the boundaries of storage cells B, G and L, reducing the elevation of the area between the walls by 0.5 m and reducing the area between the walls from 100m to 2m	✓	✓	✓	✓	To observe the effect of both a smaller elevation and area between two walls on the water spread
8	Four walls at the boundaries of some storage cells	✓	✓	✓	✓	To investigate the water behaviour as it reaches 4 walls

Table 2: DTM/volume configuration summary table

2.1.1 1st CASE STUDY: Introduction of flat areas around the lowest link:

- **Description of the DTM**

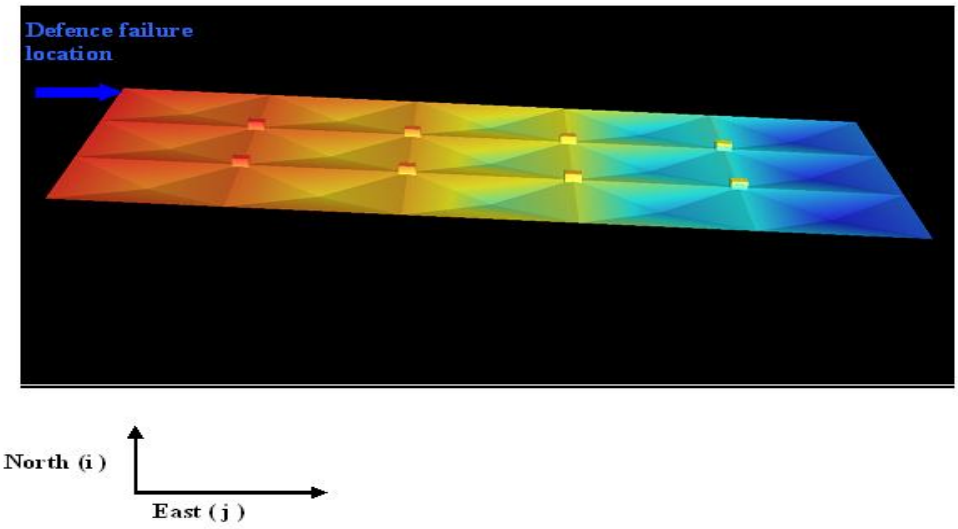

Fig. 7a: 3D view of the DTM flat areas around the lowest links

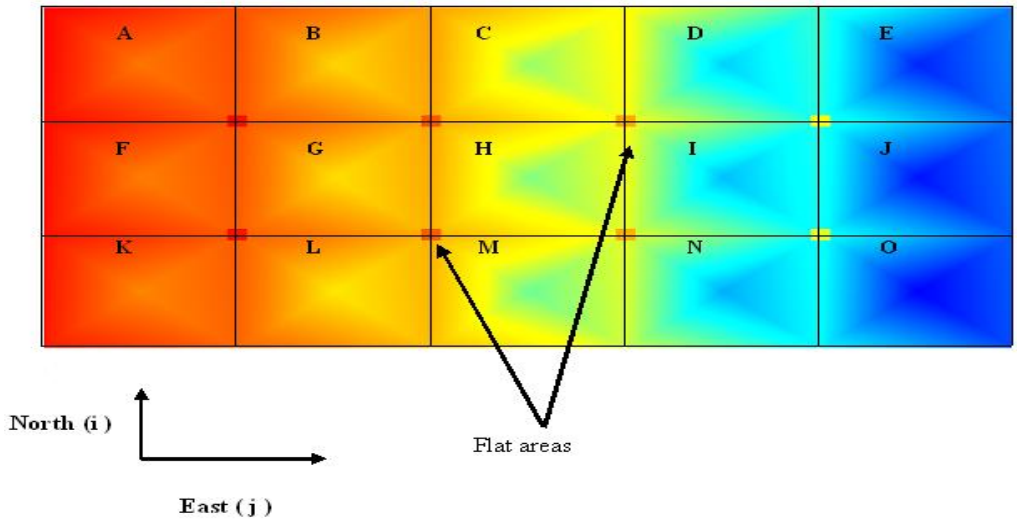

Fig. 7b: 2D view of DTM with flat areas around the lowest links

The characteristics of the terrain in this case study are mentioned in detail in Section 2.1. In this particular case study the terrain was inclined in both directions (Fig. 7a), in particular the slope in the north-south direction was i = 0.0002 and in east-west direction was j = 0.002. The investigation of the behaviour of the water in steep slopes was the reason for selecting these slopes. It is expected that steep slopes would affect the flood parameters and flood hazard more and so, it is selected as a benchmark case.

a. V_{total}=70,000 m^3 ($Q_{max} = 4.86 m^3/s$)

For the TUFLOW model the inflow volume is defined by a hydrograph (Fig. 6). The duration of time for the flooding for the hydrodynamic model was set to 6 hrs, with a

peak of flow $Q_{\max,TUFLOW} = 4.86 m^3/s$. The RFIM model uses an inflow volume (V_{total}) that is equal to that used by the TUFLOW model, giving a total inflow volume of 70,000 m^3 ($V_{total} = 70{,}000 m^3$).

RESULTS:

The flood extent obtained from the RFIM is contained within the first 5 storage cells (A to E) where the water spreads from the westerly direction (defence failure location) to the east. This can be observed from Fig. 8a where the numbers above the flooded cells denote the order in which they flood. The scale above the last flooded cell in all figures of flood extent predictions from both models (in all case studies) denotes the water depth in m. In this scenario the depth varies from 0.000 (white colour) to 0.4400 (dark blue) for both flood models.

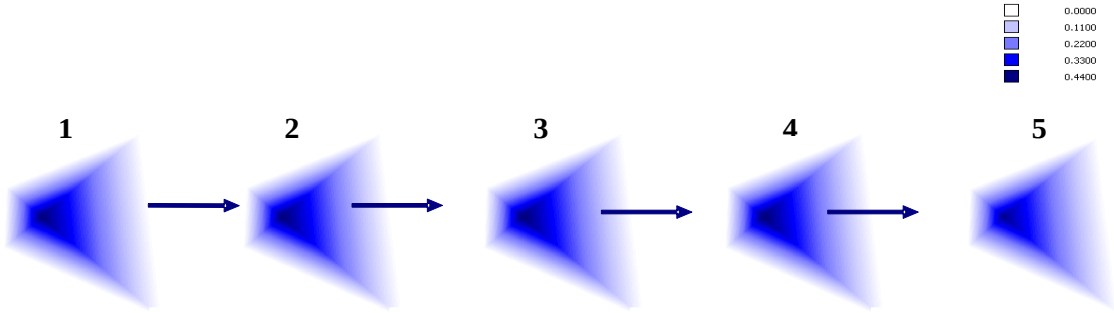

8a: RFIM

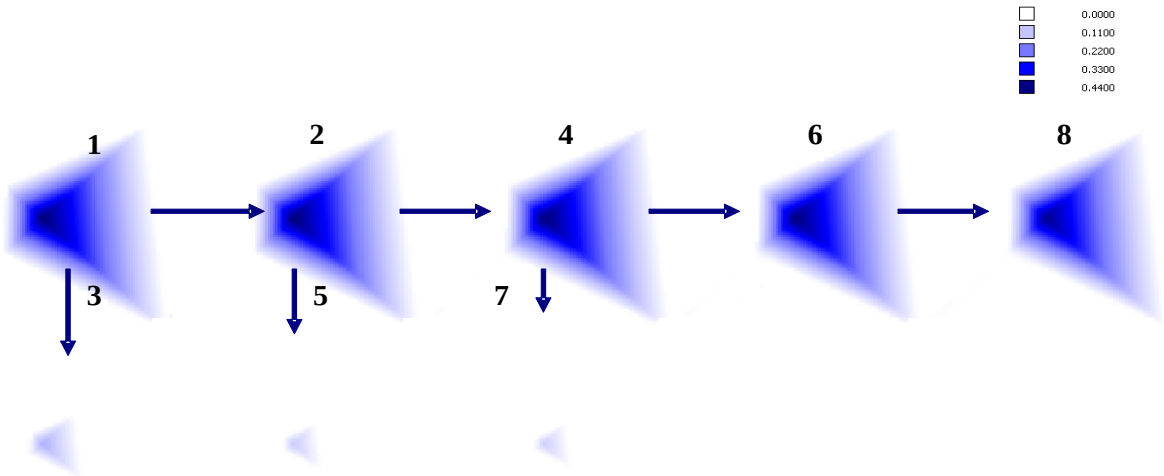

8b: TUFLOW

Fig. 8 a, b: Prediction of flood extent by RFIM & TUFLOW (scale shows the water depth in m) for: Introduction of flat areas around the lowest link
i=0.0002 j=0.002
V=70,000 m^3

Storage cell	RFIM Flood Volume (m^3)	RFIM Final water level in cell (m)	RFIM link level (m)	TUFLOW Flood Volume (m^3)	TUFLOW Final water level in cell (m)	Flood volume difference (m^3)	% Flood volume difference
A	14238	4.9	4.9	14248	4.9	10	+ 0.1
B	14421	3.9	3.9	14313	3.9	108	- 0.7
C	14606	2.9	2.9	14195	2.9	411	- 2.8
D	14789	1.9	1.9	14055	1.9	734	- 5
E	12278	0.87	0.87	12463	0.88	185	+ 1.4
F	-	-	-	507	4.5	507	-
G	-	-	-	176	3.45	176	-
H	-	-	-	151	2.44	151	-
I	-	-	-	-	-	-	-
J	-	-	-	-	-	-	-
K	-	-	-	-	-	-	-
L	-	-	-	-	-	-	-
M	-	-	-	-	-	-	-
N	-	-	-	-	-	-	-
O	-	-	-	-	-	-	-

Table 3a: Predicted flood volumes from RFIM and TUFLOW and % flood volume difference between the two models for:
Introduction of flat areas around the lowest link
i=0.0002 j=0.002
V=70,000 m^3

The flood volume in each cell, predicted from RFIM, varies from 12,200 m^3 to 14,790 m^3 (Table 3a). The flood volume is greater by about 200 m^3 comparing cells based on their flooding order, once the water spread is completed. The last flooded cell contains the lowest amount of flood water. This is a result of the fact that all the previous storage cells have absorbed their maximum flood potential (contain most of the flood water) leaving a smaller amount available to flood the final storage cell. So, the greatest share of the 70,000 m^3 is absorbed by the cells closest to the defence failure location leaving a smaller amount for the storage cell furthest away from the failure.

It is important to note that the arrows on the flood extent map predicted from RFIM (Fig. 8a) show the flooding direction. The beginning of the arrow shows the storage cell from where the water spreads, whilst the tip of the arrow demonstrates the storage cell which receives the water. The length of the arrow indicates the volume of the flood water remaining to be transferred. In this particular case, as can be observed from the flood extent map (Fig. 8a), the length of the arrows reduces by a small fixed amount denoting the decrease in the volume to be transferred, which implies that the volume reduces by a greater amount every time that the water moves from one flooded cell to the other.

The transmission of the predicted flood extent obtained from TUFLOW is not solely in the easterly direction as predicted by RFIM (Fig. 8b). After the failure occurs the water spreads on the east for the first two storage cells (the storage cell where the failure occurs and its eastern neighbour), then it moves from the failure occurrence flooded cell to its southern neighbour. Following this, the water is transferred from the flooded cell in the easterly direction from the failure location firstly to its eastern and then to its southern neighbour. These easterly and northerly direction spreadings are continued until the entire amount of the inundation volume (V_{total}) is spread.

The total number of predicted flooded cells from TUFLOW is 8 (Fig. 8b) with a range of flood volume from 151 m^3 to 14,320 m^3 contained in each of them (Table 3a). It can be noticed (Table 3a) that the flood volume increases gradually for the first two cells and then reduces significantly. This type of fluctuation continues for the remaining predicted flooded cells.

One important thing to notice is that, as mentioned in the description of the RFIM results, the arrows denote the water flow. The length of the arrows denotes the amount of flood volume to be spread. In contrast to the RFIM results, the length of the arrows varies from very small to large, since there is a wide variation of the spreading flood volume.

It can be observed that the flood extent is very similar between the two flood models but not exactly the same. TUFLOW demonstrated 3 additional flooded cells than RFIM. Although these 3 flooded cells contain a smaller amount of flood volume than the rest (Table 3a) (the flood volume in these cells varies from 151 m^3 to 507 m^3), and thus, they should not be ignored because they may affect the flood risk.

The corresponding flooded cells in the flood inundation models appear to have a small difference in terms of flood volume (Table 3a). The RFIM flood volume predictions are subtracted from the more accurate TUFLOW results. The percentage of the difference varies from +0.1% to -5.0%. The positive sign of the flood volume difference denotes that TUFLOW predicted a larger amount of flood volume than RFIM. On the other hand, the negative sign refers to a greater prediction from the RFIM. Thus, it can be concluded that for this particular case study both flood inundation models provide comparable predictions of inundation extent.

Another important observation is that the corresponding flooded cells in the two flood models display the same final water levels (Table 3a,).

The differences between the two models is attributable to the fact that TUFLOW contains the momentum equation which allows this model to simulate the effect of inertia causing the water to spread in two directions simultaneously; this behaviour is not captured by the RFIM.

b. V_{total}=100,000 m^3 ($Q_{\max} = 6.94 m^3/s$)

The effect can be seen further in Fig. 9 (Appendix A) which denotes the case of flood volume of 100,000 m^3 ($V_{total} = 100{,}000 m^3$) derived from a hydrograph of the same duration as before but with a peak of 6.94 m^3/s. With this greater value of inflow one would expect inertia to be more significant and the difference between the two modelling methods to be greater. All other conditions were the same as before; such as, the georeferencing data for the defence failure location and the time duration for the flooding used.

RESULTS:

When the total volume to be spread is 100,000m^3 ($V_{total} = 100{,}000 m^3$) for the RFIM the number of flooded cells increases to 7. The water spreads from the east (defence failure location) to the west for the first 5 flooded cells and then moves to the south for the remaining cells. This can be observed from Fig. 9a (Appendix A).

The flood volume in each cell varies from 14,100 m^3 to 14,800 m^3 (Table 3b, Appendix A). The final water volume contained in each of the first 4 cells (i.e. A-D) to flood displays a constant increase due to a flat slope of i = 0.0002. Then reduces significantly for the movement to cell E as the slope is steeper i.e. j = 0.002. Finally, for the remaining flooded cells (i.e. from E to O) the flood volume increases. Note that flood cell E contains the lowest flood water amount.

The predicted flood extent obtained from TUFLOW (Fig. 9, Appendix A) does not follow the same easterly and then southerly path as predicted by RFIM. After the failure occurs the water spreads on the east for the first two storage cells (the storage cell where the failure occurs and its eastern neighbour), and then, moves from the failure

occurrence point to its southern neighbour. Afterwards, the water spreads from the eastern neighbour of the failure location cell firstly to its eastern and then to its southern neighbour. These easterly and southerly direction spreadings are continued until flooded cell J is reached and then the water moves southerly to flood cell O where the spread of the entire amount of the inundation volume (V_{total}) is completed.

The predicted flooded cells from TUFLOW are 11 in number (Fig. 9b, Appendix A) with a range of flood volume from 420 m^3 to 18,130 m^3 contained in each of them (Table 3b, Appendix A). It can be noticed (Table 3b, Appendix A) that the flood volume displays a significant fluctuation. This type of increase and reduction continues until the flood cell I is reached. The movement to cell J increases the flood volume to its highest amount, which is followed by a significant reduction when moving from flood cell J to flood cell O.

TUFLOW displayed 4 additional flooded cells than RFIM. These 4 flooded cells must not be ignored as they contain a significant amount of flood volume (the flood volume in these cells varies from 420 m^3 to 1300 m^3) (Table 3b, Appendix A), large enough to affect the flood risk.

The corresponding flooded cells in the flood inundation models appear to have a great difference in terms of flood volume (Table 3b, Appendix A). The percentage of the difference varies from +0.1% to -70.6% (the greatest variations can be observed in storage cells E, J and O), thus, it can be concluded that for this particular case study, correct representation of momentum effects are important and TUFLOW is likely to provide better representation of flood inundation extent.

Another noticeable point is that both flood models display the same final water level for the storage cells A to E (for the RFIM) and storage cells A, B, C and E for TUFLOW. For the remaining two flooded cells (flooded cells J and O) the final water level is different (Table 3b, Appendix A).

Once more the two models differ as a result to the fact that TUFLOW contains the momentum equation which allows this model to simulate the effect of inertia. However, the differences are greater due to a larger momentum, which becomes more significant in terms of estimating the inertia effect.

c. V_{total}=200,000 m^3 ($Q_{max} = 13.88 m^3/s$)

The effect of inertia was once again investigated for this particular DTM (holding the boundary conditions unchanged) for a greater amount of inflow volume (V_{total}=200,000 m^3, $Q_{max} = 13.88 m^3/s$).

RESULTS:

As observed from Fig. 10a (Appendix A), the flood extent obtained from the RFIM is contained within 7 flooded cells. The inflow water volume flows from the failure occurrence cell to the east, flooding the first 4 storage cells (i.e. B-E) and to the south, flooding the remaining cells J and O.

The flood volume contained within each cell varies considerably as depicted in Table 3c (Appendix A). In particular, the flooded cell close to the defence failure, holds the smallest amount of water; however, the last cell to be flooded (i.e. storage cell O) contains the highest amount of flood water. It can be noticed that the final flood volume contained in the first 4 flooded cells (i.e. A-D) increases by about 200 m^3, when the cells are compared based on their flooding order, then displays significant increases for the remaining cells. This can be explained by the interaction of the two difference slopes (Fig. 10a, Appendix A). Precisely, the steeper slope of j = 0.002 affects the cells D, E, J and O more than the cells A-E.

The hydrodynamic model, on the other hand, predicted a greater flood extent for this case study (Fig. 10b, Appendix A). It predicted 4 additional flooded cells than RFIM. The flood water follows an interchangeable easterly and northerly direction spreading, similar to the flooding order observed for the inflow volume scenario of V_{total}=100,000 m^3.

The predicted flood volume varies from 4,200 m^3 to 55,900 m^3 approximately (Table 3c, Appendix A). For the first 2 flooded cells the flood volume increases gradually and then reduces significantly for the next 2 flooded cells. After that it increases greatly. This fluctuation continues until the last cell to flood is reached. The inundation volume reaches its highest amount at flooded cell O.

Both flood models predicted similar flood extents; however, the hydrodynamic model predicted 4 additional flooded cells with each containing a significant amount of flood water that can affect the risk of flooding (Table 3c, Appendix A).

The corresponding flooded cells appear to have similar water levels (Table 3c, Appendix A). Also, there is a great resemblance in terms of the amount of flood water contained within each of the corresponding flooded cells, evident from the small variation on the percentage of the flood volume difference. The flooded cell where the failure occurs (storage cell A), appears to have the smallest flood volume difference i.e. +0.1%. On the other hand, storage cell E displays the greatest flood volume difference i.e. -16%. It is also important to note that both flood models predicted that the last storage cell to be flooded (i.e. storage cell O) contained the highest amount of the flood volume.

The fact that TUFLOW contains the momentum equation, which allows the model to simulate the effects of inertia, may be the reason behind the differences between the two models.

d. V_{total}=300,000 m^3 ($Q_{max} = 20.83 m^3/s$)

A larger momentum was used for further investigation of the effect of inertia. The inflow hydrograph with a peak of flow $Q_{max} = 20.83 m^3/s$ (V_{total}=300,000 m^3), that was used had the same boundary conditions as the previous cases.

RESULTS:

Although the total volume to be spread was increased from V_{total}=200,000 m^3 to V_{total}=300,000 m^3, the flood extent predicted from RFIM did not change (Fig. 11a, Appendix A). It predicted 7 flooded cells with the same flooding order as in the previous case (i.e. for V_{total}=200,000 m^3).

The total flood volume contained within the first 4 storage cells (storage cells A- D) increases by 200 m^3 when compared according to their flooding order (Table 3d, Appendix A). There is a great increase of water from storage cell D to storage cell E. From there the volume increases by almost 20,000 m^3 for the remaining storage cells. Analogous to the case V_{total}=200,000 m^3 ($Q_{max} = 13.88 m^3/s$) the increase of 200 m^3

derives from the flat slope of i = 0.0002; however, the rise of 20,000 m^3 is due to the steeper slope of j = 0.002. It is also important to note that the last 3 flooded cells which contain most of the flood water, have the same water level.

Similar to the RFIM prediction, TUFLOW also predicted the same flood extent and flooding order as in the previous case, although the inserted flood volume had an increase of V=100,000 m^3 (Fig. 11b, Appendix A). Thus, 11 flooded cells were predicted containing a total volume of V_{total}=300,000 m^3. TUFLOW once again predicted 4 additional flooded cells than RFIM.

The flood volume contained within the first 4 flooded cells (i.e. storage cells A-D) was the same as in the previous case, which implies that the storage cells reached maximum water intake capacity (Table 3d, Appendix A). The remaining of the flood water is divided with a large variation between the remaining storage cells. Especially, storage cells E, J and O contain larger amounts of water than the others. It can be noticed that the volume increases by almost 15,000 m^3 between storage cells E to J and O. Also, the water level is the same for storage cells J and O.

The flood extent predicted from both models is very similar. The 4 additional flooded cells from TUFLOW contain a significant amount of water (approximately 9,000 m^3) which can affect the risk of flooding (Table 3d, Appendix A).

The corresponding flooded cells appear to have a small percentage of flood volume difference. The smallest difference appears in the first storage cell to be flooded (i.e. storage cell A) and it is +0.1%; however, the greatest (i.e. -18.3%) appears at storage cell E (Table 3d, Appendix A).

Another important observation is that for the first 4 corresponding flooded cells the predicted water level is the same; however, for the remaining cells, RFIM appears to display a greater value than TUFLOW (Table 3d, Appendix A).

These dissimilarities between the two models may stem from the fact that TUFLOW contains the momentum equation which allows this model to simulate the effect of inertia.

e. V_{total}=400,000 m^3 ($Q_{max} = 27.77 m^3/s$)

The differences between the two models were also examined for a flood volume of V_{total}=400,000 m^3 with a peak of flow $Q_{max} = 27.77 m^3/s$. The boundary conditions were the same as in the previous cases.

RESULTS:

One would expect that there would be a difference in the flood extent predicted from RFIM, since the inflow volume increased; however, both the flood extent and flooding order were the same as predicted in the previous case (i.e. for V_{total}=300,000 m^3) (Fig. 12a, Appendix A). RFIM once again predicted 7 flooded cells.

The predicted flood volume displays significant variation (Table 3e, Appendix A). The first 4 flooded cells (i.e. storage cells A-D) contain the same amount of water as in the previous case (i.e. for V_{total}=300,000 m^3) implying that maximum capacity has been reached. The remaining flooded cells contain more water than the others. An important observation is that the flood volume value increases by approximately 20,000 m^3 when comparing storage cells E, J and O in pairs. The justification of this occurrence, once again, is the same as in cases of V_{total}=200,000 m^3 ($Q_{max} = 13.88 m^3/s$) and V_{total}=300,000 m^3 ($Q_{max} = 20.83 m^3/s$). The last storage cell to be flooded is O and contains the maximum amount of flood water.

TUFLOW was expected to have predicted a different flood extent, i.e. having a greater number of flooded cells, since the total flood volume increased (Fig. 12b, Appendix A); however, TUFLOW predicted the same flood extent and flooding order as before (i.e. for V_{total}=300,000 m^3)..

The predicted volume for each flooded cell varied from small to large (Table 3e, Appendix A). It is important to notice that the first 4 flooded cells (i.e. storage cells A-D) contain the same flood volume as in the previous case (i.e. for V_{total}=300,000 m^3). The 4 additional flooded cells contain a flood volume of approximately V=14,000 m^3 each. The remaining flooded cells E, J and O contain the largest amount of flood water. It is important to note that the flood water value increases by almost 20,000 m^3, when comparing storage cells E, J and O according to their flooding order. The last storage cell to be flooded is storage cell O, which contains the maximum amount of flood water.

The corresponding flooded cells appear to have a small difference in terms of flood volume (Table 3e, Appendix A). A significant observation to be made is that both models have predicted the same flooded cells with the highest intake of flood water (i.e. storage cell E, J and O).

Also, one notices that the predicted water level is the same for the first 4 corresponding flooded cells (Table 3e, Appendix A). For the remaining cells, RFIM has predicted a higher value than TUFLOW.

Once more, the differences between the two models may be attributed to the fact that TUFLOW contains the momentum equation which allows this model to simulate the effect of inertia.

2.1.2 2nd CASE STUDY: Two walls at the crest of storage cells C, H and M:

- **Description of the DTM**

The representation of the terrain in this scenario has the same characteristics as described in Section 2.1 (Fig. 13a, Appendix A). Also, the gradient of the terrain in the east and in the north was the same as defined before (i = 0.0002 and j = 0.002 the slopes in the northerly and in the easterly directions, respectively). The main difference between this case study and the previous one was the walls that have been included as impermeable barriers at the crest of some storage cells (Fig. 13a, b, Appendix A). Both walls have the same size ($30m \times 700m$). The gap between them was 100m. The investigation of the water behaviour as it reaches impermeable barriers was the reason for inserting these walls at the crest of the storage cells.

a. V_{total}=70,000 m^3 ($Q_{\max} = 4.86 m^3/s$)

The inflow volume value for both flood models is $V_{total} = 70{,}000 m^3$. The hydrograph (Fig. 6, Section 2.1.1) from where this flood volume has been derived for the hydrodynamic model has the same time duration as previously and a flow peak of $Q_{\max,TUFLOW} = 4.86 m^3/s$.

RESULTS:

As can be observed from Fig. 14a (Appendix A) the water spreads from the left (defence failure location) to the right direction for the first 3 storage cells (until it

reaches the walls), then moves southerly flooding only one storage cell. Finally, the water is transferred from that flooded cell through the gap between the walls to its neighbouring storage cell on the right direction.

In this scenario the RFIM predicts 5 flooded cells (Fig. 14a, Appendix A) with a variable flood volume from 8,890 m^3 to 18,650 m^3 (Table 4a, Appendix A). For the first three flooded cells the flood volume increases gradually, and then it reduces significantly for the remaining cells. The last flooded cell contains the lowest amount of flood water.

The predicted flood extent obtained from the hydrodynamic model is similar to that obtained from the RFIM (Fig. 14b, Appendix A). The water spreads from the failure occurrence cell to its eastern neighbour, and then it moves from the defence failure location to its southern neighbour. These easterly and southerly direction spreadings are continued until the total amount of the inundation volume (V_{total}) is spread.

TUFLOW predicted 7 flooded cells, each of them containing a variable amount of flood volume from 176 m^3 to 18,400 m^3 (Table 4a, Appendix A). It can be observed (Table 4a, Appendix A) that the flood volume increases gradually for the first three flooded cells, and then it fluctuates greatly for the remaining flooded cells.

The arrow length once more fluctuates between very small to large values as a result of the variation of the spreading flood volume (Fig. 14b, Appendix A).

The predicted flood extents obtained from both flood models were very similar. TUFLOW predicted two additional flooded cells. Although the amount of the flood volume contained in these cells is small, they are large enough to have an effect on the flood risk and therefore ought not to be ignored.

There appears to be a small difference in terms of flood volume for the corresponding flooded cells in the flood inundation models (Table 4a, Appendix A). The difference in percentages varies from +0.1 % to -12.9%, thus, the conclusion can be that for this particular case study, both flood models can be used to predict the flood inundation extent, since the dynamic effects of flood wave propagation are insignificant.

The presence of the same final water level (Table 4a, Appendix A) in each of the corresponding flooded cells, for both flood models is another important observation.

b. V_{total}=100,000 m^3 ($Q_{max} = 6.94 m^3/s$)

The dynamic effects of flood wave propagation were further investigated in the following case scenarios by increasing the inflow volume and retaining the previous boundary conditions.

RESULTS:

For an inflow volume of V_{total}=100,000 m^3 ($Q_{max} = 6.94 m^3/s$) RFIM predicted, as expected, a greater number of flooded cells than in the previous case study (Fig. 15a, Appendix A). After the failure occurs, the water spreads from storage cell A to its first 2 southern neighbouring cells. From there the water moves through the gap between the two walls to the east, flooding the two remaining storage cells. Finally, it moves to the south to flood the last storage cell.

The 7 predicted flooded cells appear to have a small variation in terms of flood volume (Table 4b, Appendix A). The contained flood volume, once again, displays a gradual increase for the first two flooded cells, followed be a considerable increase. From there it reduces significantly and then increases gradually. These interchangeable increases and reductions continue until the total amount of flood volume has been spread. It is important to notice that the maximum amount of water is contained within storage cell C (where the wall is raised on its crest) and the minimum amount of water is contained within storage cell O (the last storage cell to flood).

TUFLOW predicted 3 additional flooded cells than in the previous inflow volume scenario, increasing the total number of flooded cells to 10 (Fig. 15b, Appendix A) and also, 3 additional flooded cells compared to RFIM. The flood water spreads the same way as in the previous scenario for the first 7 flooded cells, then it moves from storage cell H to the south, and finally, from storage cell J to the south.

There is a great variation in terms of flood volume (Table 4b, Appendix A). It increases gradually for the first 3 flooded cells and then reduces significantly for the next 2 flooded cells. These increases and reductions continue for the remaining flooded cells.

Both flood models predicted a similar flood extent, but TUFLOW displayed 3 additional flooded cells than RFIM (Table 4b, Appendix A). Each of these cells contained a significant amount of water which can affect the risk of flooding.

There appears to be a great difference in terms of flood volume for the corresponding flooded cells (Table 4b, Appendix A).The percentage of the flood volume difference varies from +0.1% to -61.0%, so the main conclusion from this is that the dynamic effects of flood wave propagation are significant and TUFLOW is likely to provide a better representation of the flood extent.

Another important point is that for the first 2 corresponding flooded cells (i.e. storage cells A and B) the water level is the same for both models (Table 4b, Appendix A). For the remaining corresponding flooded cells there is a small difference between the two models, with TUFLOW displaying larger values than RFIM.

c. V_{total}=200,000 m^3 ($Q_{max} = 13.88 m^3/s$)

For the greater inflow volume of V_{total}=200,000 m^3 ($Q_{max} = 13.88 m^3/s$) the RFIM predicted one additional flooded cell than in the previous scenario (V_{total}=100,000 m^3 ($Q_{max} = 6.94 m^3/s$)). In particular, 8 flooded cells were predicted following the same flooding order as before (Fig. 16a, Appendix A).

RESULTS:

The predicted flood volume shows a significant variation. Small values can be observed in storage cells A, B, C, H and I which are very close to the walls or the walls are on their crest, and these values are the same as in the previous inflow volume scenarios (i.e. V_{total}=70,000 m^3 ($Q_{max} = 4.86 m^3/s$) and V_{total}=100,000 m^3 ($Q_{max} = 6.94 m^3/s$)) (Table 4c, Appendix A), denoting that they have reached their maximum flood water capacity. It can be also noticed that the 3 remaining flooded cells with the maximum flood volume are located on the east of the terrain, which implies that the spreading of the water depends on the gradient of the terrain. This last observation can also be detected from Fig. 16a (Appendix A) where storage cell O is the cell with the maximum flood volume and is located on the southeast direction, where the slope of the terrain on the j direction is greater.

As RFIM predicted more flooded cells for an increase of inflow volume, TUFLOW displayed more flooded cells as well (Fig. 16b, Appendix A). It predicted 2 additional cells than it did on the inflow volume scenario of V_{total}=100,000 m^3 ($Q_{max} = 6.94 m^3/s$). The flood water followed the same east and south direction spreading as before.

One noticeable point is that the flood volume contained in specific storage cells (i.e. storage cells A, B, C, H and I) located very close to the walls or with walls located on their crest, have reached their maximum capacity, since, their flood volume values are the same as in the previous inflow volume scenario of V_{total}=100,000 m^3 ($Q_{max} = 6.94 m^3/s$) (Table 4c, Appendix A). The 3 storage cells on the east direction of the terrain (i.e. storage cells E, J and O) contain the 3 maximum flood volume values with storage cell O containing the maximum value of all flooded cells. This implies that in this case scenario the water spreading follows the topography of the terrain.

Both numerical models predicted a very similar flood extent in this case scenario. Especially, TUFLOW displayed 4 additional flooded cells than RFIM (Fig. 16, Appendix A). These cells, although they contain a small value of flood volume, they cannot be ignored because they may affect the risk of flooding. One important observation is that both models predicted the same flood volume values in storage cells very close to the walls as in the previous inflow volume scenario of V_{total}=100,000 m^3 ($Q_{max} = 6.94 m^3/s$) (Table 4c, Appendix A).

For the corresponding flooded cells there is a small variation in terms of flood volume difference (Table 4c, Appendix A). Although, the difference in percentage varies from +0.1% to -17.4%, it can be concluded that for this scenario TUFLOW can be used to predict the flood inundation extent since the dynamic effects of inertia are significant, as demonstrated in the volume contained in the additional flooded cells.

The final water levels at the corresponding flooded cells are observed to show close similarity (Table 4c, Appendix A).

d. V_{total}=300,000 m^3 ($Q_{max} = 20.83 m^3/s$)

Increasing the inflow volume by V=100,000 m^3 (i.e. V_{total}=300,000 m^3 ($Q_{max} = 20.83 m^3/s$)), both the flood extent and flooding order predicted from RFIM

remain exactly the same as described in the previous inflow volume scenario (Fig. 17a, Appendix A).

RESULTS:

It is important to note that most of the flooded cells contain the same flood volume as before, implying that maximum capacity has been reached (Table 4d, Appendix A); however, storage cells E, J and O i.e. the last storage cells to flood, located on the east direction, contain a greater water volume than before. It could be remarked that the extra volume of V=100,000 m^3, that was added to the V_{total}=200,000 m^3 of the previous inflow volume scenario, splits almost equally between the flooded cells on the east direction (i.e. storage cells E, J and O). Thus, these flooded cells show an increase of their flood volume of approximately 30,000 m^3 leaving once again the storage cell O to contain the maximum flood volume value. Therefore, from this it could be concluded that the slope of the terrain affects not only the direction of the water spreading but also the flood volume distribution.

The predicted flood extent from TUFLOW displayed 13 flooded cells i.e. one additional flooded cell than the previous inflow volume scenario of V_{total}=200,000 m^3 ($Q_{\max} = 13.88 m^3/s$) (Fig. 17b, Appendix A). The water spreads in the same way as before following the easterly and southerly direction.

It could be noticed that most of the predicted flooded cells contain the same volume as before (Table 4d, Appendix A). In particular, the storage cells F, G, M and N show an increase of approximately 4,000 m^3 and the storage cells E, J and O, which contained the maximum water volume, had an increase of approximately 30,000 m^3. So, it could be concluded that the water volume depends on the topography of the terrain.

The predicted flood extent obtained from both flood models was very similar but not the same (Fig. 17, Appendix A). To be precise, TUFLOW displayed 5 additonal flooded cells which cannot be ignored because they can affect the risk of flooding.

The corresponding flooded cells in the flood inundation models appear to have a small difference in terms of flood volume (Table 4d, Appendix A). The percentage of the difference varies between +0.1% and -19.6%, concluding therefore that for this particular scenario TUFLOW can be used to provide a good representation of the flood

inundation extent, since the dynamic effects of flood wave propagation are significant, since the additional cells contain an important amount of flood water and cannot be ignored.

For the corresponding flooded cells the existence of the same (or almost the same) final water levels is observed (Table 4d, Appendix A).

e. V_{total}=400,000 m^3 ($Q_{max} = 27.77 m^3/s$)

For a greater inflow volume of V_{total}=400,000 m^3 ($Q_{max} = 27.77 m^3/h$), RFIM predicted 8 flooded cells as predicted in the inflow volume scenarios of V_{total}=200,000 m^3 and V_{total}=300,000 m^3 (Fig. 18a, Appendix A).

RESULTS:

Although the flood extent and flooding order were the same as in the previous scenarios, there was a difference in the flood volume value of the easterly flooded cells i.e. storage cells E, J and O (Table 4e, Appendix A). There was an increase of approximately 30,000 m^3 for each, meaning that the increase of 100,000 m^3 of the total inflow volume that was used on the previous scenario (i.e. V_{total}=300,000 m^3 ($Q_{max} = 20.83 m^3/s$)) split almost equally between those 3 flooded cells. It can also be noted that for those flooded cells the flood volume increased by 60,000 m^3 compared to the V_{total}=200,000 m^3 scenario (Tables 4c, 4d, 4e, Appendix A). Once again, the conclusion drawn is that the flood volume spreading depends on the slope of the terrain. The remaining predicted flooded cells have the same flood volume values as before, implying that they have reached their maximum capacity.

TUFLOW was expected to have predicted a greater flood extent since there was an increase of the inflow volume; however, it predicted the same 13 flooded cells as in the previous scenario (i.e. V_{total}=300,000 m^3) (Fig. 17b and Fig. 18b, Appendix A). It can also be noticed that the flooding order remained the same.

Although the flood extent is the same, the flood volume value is different in some of the flooded cells (Table 4e, Appendix A). To be more precise, storage cells E, J and O have an increase of approximately 30,000 m^3 in their contained flood volume compared to the previous scenario of V_{total}=300,000 m^3. It also can be noted that they display an

increase of 60,000 m^3 from the scenario of V_{total}=200,000 m^3 (Tables 4c, 4d, 4e, Appendix A). From these, it could be concluded that the volume spread depends on the terrain topography, since; these storage cells are on the east direction from the breach location. There was also a small increase for storage cells G, M and N; however, the remaining predicted flooded cells retain the same values as in the previous scenarios, meaning that they have reached their maximum capacity (Tables 4d, 4e, Appendix A).

Both inundation models predicted a similar flood extent (Fig. 18, Appendix A). Especially, TUFLOW displayed 5 additional flooded cells than RFIM, which contain smaller flood volume compared to the corresponding flooded cells, but cannot be ignored because they can affect the risk from flooding (Table 4e, Appendix A).

The flood volume for the corresponding flooded cells between the two models appears to display only slight differences (Table 4e, Appendix A). The difference in percentages varies from +0.1% to -19.4%, hence, TUFLOW can be used in the prediction of the flood inundation extent, since the dynamic effects of flood wave propagation are significant, as the 5 additional flooded cells have stored a substantial amount of flood volume.

The presence of the same or almost the same final water levels (Table 4e, Appendix A) in each of the corresponding flooded cells, for both models is another important observation.

2.1.3 3rd CASE STUDY: Two walls at the boundaries of the storage cells B, G and L:

- **Description of the DTM**

The terrain in this scenario (Fig. 19a and Fig. 19b, Appendix A) has the same characteristics as mentioned in Section 2.1. The main difference between this case study and the two previous cases is the introduction of 2 walls at the boundaries of the storage cells B, G and L, with a size of these walls being $30m \times 700m \times 7m$. These walls were raised at the boundaries in order to examine the behaviour of the water as it reaches impermeable barriers. It is important here to note that this particular DTM is very similar to the ones of cases 4-7 (thus, the same figure (Fig. 19 a, b, Appendix A) is going to be used for those cases); although the differences are not obvious neither in 2D

nor in 3D view. The results, on the other hand, display evident differences which will be analysed further in the following sections (Sections 2.1.4 – 2.1.7).

a. V_{total}=70,000 m^3 ($Q_{max} = 4.86 m^3/s$)

The inflow volume used was the same for both the RFIM and TUFLOW. Particularly, this inflow volume has been calculated from a hydrograph (Fig. 6, Section 2.1.1) for TUFLOW, which has time duration of 6 hrs and a flow peak of $Q_{max,TUFLOW} = 4.86 m^3/s$.

RESULTS:

The predicted flood extent from RFIM is contained within the first two storage cells and the next two storage cells on the south of the second cell. The water spreads from the left to the right direction and then to the south direction (Fig. 20a, Appendix A).

It can be observed from Fig. 20a (Appendix A) that this case study predicts 4 flooded cells each of them containing a flood volume between 14,200 m^3 and 22,400 m^3 (Table 5a, Appendix A). The flood volume increases gradually as the water spreads from one flooded cell to the other.

For TUFLOW the water spreads from the defence failure location firstly to its neighbouring storage cell on the east and then on the southerly direction (Fig. 20b). Then from the neighbour of the failure location on the east the water spreads firstly to its neighbouring storage cell on the east and then on the south. Finally, the water moves from the storage cell H to its eastern neighbour.

The 7 predicted flooded cells contain a flood volume which varies from 510 m^3 to 18,900 m^3 (Table 5a, Appendix A). It can be observed that the flood volume increases gradually for the first two flooded cells and then reduces greatly. Then it fluctuates for the remaining flooded cells.

There is a strong similarity in the flood extent predicted from both flood models, although TUFLOW displayed a greater number of flooded cells. In particular, it predicted three additional flooded cells. The flood volume contained in each of these

three flooded cells varies from 520 m^3 to 14,400 m^3, implying that they have a substantial effect on the flood risk.

There appears to be a small difference in terms of flood volume for the corresponding flood cells in the flood inundation models (Table 5a, Appendix A). The percentage of the difference varies from +0.1% to -92.5%, therefore, both flood inundation models can be used to predict the flood extent since the effects of the momentum are insignificant.

The existence of very similar final water level (Table 5a, Appendix A) in each of the corresponding flooded cells is another important observation. TUFLOW displayed a slightly greater water level than the RFIM.

In a similar manner as previously, the differentiation between the two models may be explained by the fact TUFLOW contains the momentum equation which allows this model to simulate the effect of inertia.

b. V_{total}=100,000 m^3 ($Q_{max} = 6.94 m^3/s$)

For a total volume of 100,000 m^3 the number of flooded cells predicted from RFIM increased to six (Fig. 21a, Appendix A). As in the previous case study with the inflow volume of 70,000 m^3, the water moves from the failure location to its eastern neighbouring cell, and then to the next storage cell on the south. From there the water spreads firstly to its eastern and then to its southern neighbouring cell. Finally, the water moves from the storage cell H to its eastern neighbouring cell.

RESULTS:

The flood volume contained within the flooded cells varies from 7,240 m^3 to 29,070 m^3 (Table 5b, Appendix A). The volume increases gradually for the first three cells and then greatly for the following cells. After that it reduces gradually for the remaining flooded cells.

For a greater amount of inflow volume ($V_{total} = 100{,}000 m^3$) TUFLOW predicted a greater number of flooded cells, as expected (Fig. 21b, Appendix A). Particularly, the number of predicted flooded cells rose to 8, each of them containing a variable flood volume between 1,270 m^3 and 18,600 m^3 (Table 5b, Appendix A). It demonstrated two

more cells than RFIM of which each contained a flood volume which varies from 1,270 m^3 to 12,400 m^3 (Table 5b, Appendix A). These flood volume values show that these flooded cells are large enough to affect the flood risk.

The flood volume follows the same flooding order for the first 7 flooded cells as in the previous inflow volume scenario of V_{total}=70,000 m^3 and finally, the water moves from the storage cell I to its easterly neighbouring storage cell (Fig. 21b, Appendix A).

The corresponding flooded cells appear to have a great difference in terms of flood volume (Table 5b, Appendix A). The percentage of the difference varies from +0.1% to +96.8%, thus, TUFLOW is more appropriate to be used for the prediction of flood inundation extent.

Another noticeable point is that both models display the same final water level for storage cell A (failure location). For the remaining corresponding flooded cells the final water level differs, with TUFLOW displaying slightly greater values (Table 5b, Appendix A).

Once more the differences between the two models may be credited to the fact that TUFLOW contains the momentum equation which allows this model to simulate the effects of inertia. However, the differences are greater due to a larger momentum, which becomes more significant in terms of estimating the inertia effect.

c. V_{total}=200,000 m^3 ($Q_{max} = 13.88 m^3/s$)

For a greater amount of inflow volume (i.e. V_{total}=200,000 m^3 ($Q_{max} = 13.88 m^3/s$)) the RFIM predicted a greater flood extent as expected (Fig. 22a, Appendix A). In particular, it displayed 3 additional flooded cells than in the previous scenario.

The water spreads in the same way as in the previous scenario (i.e. for V_{total}=100,000 m^3 ($Q_{max} = 6.94 m^3/s$)) following the easterly and southerly direction; however, on storage cell J it moves on the southerly (storage cell E) and then on the northerly direction (storage cell O) (Fig. 22a, Appendix A).

RESULTS:

It can be noticed from Table 5c (Appendix A) that RFIM has predicted a variation of flood volume in each flooded cell. However, some of the flooded cells such as storage cells A, B, G, H and L contain the same flood volume as in the previous inflow volume scenario (i.e. V_{total}=100,000 m^3 ($Q_{max} = 6.94 m^3/s$)), thus, implying that these storage cells have reached their maximum flood volume capacity. The remaining of the predicted flooded cells have increased their flood volume.

The flood extent derived by TUFLOW is different from the one obtained for an inflow volume of V_{total}=100,000 m^3. For this scenario TUFLOW predicted 12 flooded cells, 4 additional cells than previously (Fig. 22b, Appendix A).

The flood volume is spreading following the southerly and northerly direction as before; however, in this particular scenario, there is also a northerly spreading into storage cell J. The water at this particular storage cell firstly moves to the south and then to the north direction.

It was expected that for a greater inflow volume, TUFLOW would have predicted greater values of flood volume for all predicted flooded cells (Tables 5b, 5c, Appendix A). However, this was not the case, since there are some storage cells such as cells A and B which contained the same flood volume as before (i.e. for V_{total}=100,000 m^3), implying that these storage cells reached their maximum flood volume capacity. The remaining flooded cells had an increase in flood volume which was either very small (e.g. for storage cell G the increase was 90 m^3) or very large (e.g. for storage cell O the increase was almost 43,500 m^3) (Table 5c, Appendix A).

For this particular inflow volume scenario both flood models displayed a very similar flood extent (Fig. 22, Appendix A). However, TUFLOW, once again, predicted 3 additional flooded cells than RFIM. Each of these 3 flooded cells contains an important amount of flood volume which can affect the risk of flooding (Table 3c, Appendix A).

Although, the flood volume difference for the corresponding flooded cells appears to be smaller than in the previous inflow volume scenario, it has a great variation from +0.1% to -48.6% (Table 5c, Appendix A). Therefore, it should be concluded that for this

particular scenario TUFLOW is more appropriate to be used for flood extent prediction purposes due to significant effects of inertia.

Another important point is that for the corresponding flooded cells both models have predicted very similar final water levels (Table 5c, Appendix A). TUFLOW in some flooded cells displayed slightly greater values than RFIM.

d. V_{total}=300,000 m^3 ($Q_{max} = 20.83 m^3/s$)

Increasing the inflow volume to be spread to V_{total}=300,000 m^3 ($Q_{max} = 20.83 m^3/s$), one could expect that RFIM would have predicted a greater flood extent than in the previous inflow volume scenarios. However, this was not the case, since RFIM predicted the same 9 flooded cells as before (i.e. for V_{total}=200,000 m^3 ($Q_{max} = 13.88 m^3/s$)) with the same flooding order as well (Fig. 23a, Appendix A).

RESULTS:

A great variation in terms of the flood volume contained in each flooded cell was predicted (Table 5d, Appendix A). There were some flooded cells which contained the same flood volume as in the case of V_{total}=200,000 m^3, implying that for this particular case study maximum capacity has been reached in terms of flood volume. These storage cells either contain the walls (storage cells B, G and L) or they are close to storage cells which have the walls (storage cells A, H and I) (Fig. 19b, Appendix A). The remaining of the predicted flooded cells increased their flood volume by almost 30,000 m^3 from the previous case study scenario (Table 5d, Appendix A). Another noticeable point is that the last cells to ne flooded (i.e. storage cells E, J and O) contain the maximum values of flood volume with storage cell O containing the maximum value of all (Table 5d, Appendix A). Thus, it could be concluded that the flood volume spread depends on the slope of the terrain.

When the total volume to be spread is V_{total}=300,000 m^3 ($Q_{max} = 20.83 m^3/s$) for TUFLOW the total number of flooded cells is 12, the same as in the previous case study of Vtotal=200,000 m^3 (Fig. 23b, Appendix A). The water follows the same easterly and southerly direction spreading as before.

In terms of flood volume, TUFLOW predicted the same flood volume values as previously for storage cells A and B (Table 5d, Appendix A). The remaining of the predicted flooded cells had either a very small (i.e. storage cell G had 16m^3 increase) or very large (i.e. storage cell O had almost 30,000m^3 increase) increase.

Both inundation models displayed a similar flood extent (Fig. 23, Appendix A), with TUFLOW having predicted 3 additional flooded cells than RFIM. Each of these 3 flooded cells contains a significant amount of flood volume (Table 5d, Appendix A).

There appears to be a small difference in terms of flood volume for the corresponding flooded cells (Table 5d, Appendix A). The percentage of the difference varies from +0.1% to -12.5%, thus, for this particular scenario TUFLOW can be used for the flood inundation prediction purpose, since there are significant effects of the flood wave propagation.

Both models display the same or similar water levels for the corresponding flooded cells (Table 5d, Appendix A), although, TUFLOW displays slightly greater values than RFIM.

e. V_{total}=400,000 m^3 ($Q_{max} = 27.77 m^3/s$)

For a total volume of V_{total}=400,000 m^3 ($Q_{max} = 27.77 m^3/s$) RFIM predicted the exact same flood extent as in the cases of V_{total}=200,000 m^3 and V_{total}=300,000 m^3 (Fig. 22a, 23a and 24a, Appendix A), thus, the flooding order was the same as well.

RESULTS:

Although the inundation extent was the same, the predicted flood volume varied across cells (Table 5e, Appendix A). Only, storage cells A, B, G, H, I and L contained the same flood volume as before, having either the wall at their boundary or located close to cells with walls at their boundary. The remaining of the predicted flooded cells displayed increases of approximately 30,000 m^3, meaning that the increase from V_{total}=300,000 m^3 to V_{total}=400,000 m^3 was split almost equally among storage cells E, J and O. These cells are located on the east direction of the terrain and contain the maximum values of flood volume; with storage cell O containing the maximum value of all. Hence, the flood volume spreading depends on the slope of the terrain.

TUFLOW displayed a greater flood extent for V_{total}=400,000 m^3 than for V_{total}=300,000 m^3 (Fig. 23b and 24b, Appendix A), predicting 2 additional flooded cells. Although, the contained flood volume in these flooded cells is very small (178m^3 and 271 m^3), they should not be ignored because they may affect the flood risk (Table 5e, Appendix A).

Two of the flooded cells (i.e. storage cells A and B) appear to contain the same flood volume as in the previous scenarios of V_{total}=70,000 m^3, V_{total}=100,000 m^3, V_{total}=200,000 m^3 and V_{total}=300,000 m^3 (Table 5e, Appendix A). The remaining of the predicted flooded cells have either a small (i.e. storage cell G) or a large (i.e. storage cell O) rise. Storage cells E, J and O located on the east side of the terrain raise their volume by 30,000 m^3, implying that the increase from V_{total}=300,000 m^3 to V_{total}=400,000 m^3 divides almost equally between these cells. Storage cell O appears to have the maximum flood volume value of all predicted flooded cells. Hence, for this particular case study, the flood volume spreading depends on the slope of the terrain.

The flood extent obtained from both flood models is similar; however, TUFLOW displayed 5 additional flooded cells (Fig, 24, Appendix A). The contained flood volume in those 5 flooded cells varies from very small to small (Table 3e, Appendix A).

The corresponding flooded cells appear to exhibit a small difference in terms of flood volume, which varies from +0.1% to -14.2%, thus, it could be concluded that for this case study, TUFLOW is more appropriate for flood inundation extent purposes (Table 5e, Appendix A). That is the result of the significant effect of the momentum equation.

Another important observation is that for the corresponding flooded cells both flood models predicted similar final water levels, with TUFLOW displaying slightly greater values than RFIM (Table 5e, Appendix A).

2.1.4 4th CASE STUDY: Two walls at the boundaries of storage cells B, G and L, decreasing the slopes on both directions i and j :

- **Description of the DTM**

The DTM in this case scenario is similar to the case study 3 (Section 2.1.3) (Fig. 19a and Fig. 19b, Appendix A); however, the distinction between them is that the slopes on the north and east direction have been changed and have the same values i.e. i = 0.001 and j = 0.001, in order to assess the behaviour of the water in flat slopes.

a. V_{total}=70,000 m^3 ($Q_{max} = 4.86 m^3/s$)

The predicted from RFIM flood extent begins with the water moving from the failure location firstly to its neighbouring storage cell on the easterly and then on the southerly direction (Fig. 25a, Appendix A). From the easterly neighbour of the defence failure location the water progresses to the southerly direction.

RESULTS:

The flood volume contained in each of the predicted flooded cells varies from 7,600 m^3 to 16,300 m^3 (Table 6a, Appendix A). The total volume reduces gradually as it spreads from one storage cell to the other.

The flood extent obtained from TUFLOW starts with the water spreading from the failure location firstly to its easterly and then to its southerly neighbouring storage cell (Fig. 25b, Appendix A). From the easterly neighbour of the failure location the water moves to the south; finally, from the southing neighbouring cell of the failure location to the south direction.

Each of the predicted flooded cells contained a flood volume which varies from 5,050 m^3 to 16,970 m^3 (Table 6a, Appendix A). The flood volume reduces gradually for the first two flooded cells and then increases significantly. After that reduces gradually for the next flooded cell and greatly for the remaining flooded cells.

The flood extent predicted from both flood models is very similar (Fig. 25, Appendix A). The number of flooded cells is the same for both models; however the last flooded cell is different.

The corresponding flooded cells in the flood inundation models appear to have a small difference in terms of flood volume (Table 6a, Appendix A). The percentage of the difference varies from -0.2% to +10.0%, therefore, both flood models can be utilised in the flood extent prediction, since the effects of momentum are insignificant.

Once more, it is important to observe that there is a very similar final water level (Table 6a, Appendix A) for the corresponding flooded cells for both flood models, with TUFLOW displaying slightly larger final water level values.

b. V_{total}=100,000 m^3 ($Q_{max} = 6.94 m^3/s$)

For a further investigation of the dynamic effects of inertia, different inflow volume scenarios were used for this particular floodplain topography.

RESULTS:

Precisely, for an inflow volume of V_{total}=100,000 m^3 ($Q_{max} = 6.94 m^3/s$) RFIM predicted the exact same flood extent as in the previous inflow volume scenario of Vtotal=70,000 m^3 (Fig. 26a, Appendix A).

Those 5 flooded cells have similarities with the 5 flooded cells from the previous inflow volume scenario, not only in terms of flooding order but also, in terms of the contained flood volume (Table 6b, Appendix A). All flooded cells; apart from the last cell to be flooded (i.e. storage cell L) contained the same flood volumes as before, which imply that they reached their maximum flood volume capacity. On the other hand, storage cell L, which was the last cell to be flooded, had an increase of 30,000 m^3 in its volume. These 30,000 m^3 was the increase of V_{total} from V_{total}=70,000 m^3 to V_{total}=100,000 m^3 which means that all of this increase was transferred to storage cell L. Another important point to notice is that storage cells B and F contain almost the same amount of flood volume.

For a V_{total}=100,000 m^3 ($Q_{max} = 6.94 m^3/s$) the hydrodynamic model displayed a different flood extent than V_{total}=70,000 m^3 ($Q_{max} = 4.86 m^3/s$) (Fig. 26b, Appendix A). In particular, TUFLOW predicted one additional flooded cell. The water follows the same path in terms of spreading. Precisely, it moves following an interchangeable easterly and southerly direction.

Although most of the predicted flooded cells were the same as before, only two of them contained the same flood volume (Table 6b, Appendix A). Those cells were the storage cell where the failure occurs and its neighbour on the east direction. The remaining cells had either a very small (i.e. storage cell F had an increase of 5 m^3) or large increase (i.e. storage cell K had an increase of almost 7,000 m^3).

Both flood models appear to display a similar flood extent, with TUFLOW predicting more flooded cells than RFIM (Fig. 26, Appendix A). In both models the water follows an easterly-southerly direction of spreading.

For the corresponding flooded cells there is a large difference in terms of flood volume (Table 6b, Appendix A). The percentage of this difference varies from +2.3% to -42.0%, hence, TUFLOW is better for use in terms of inundation extent purposes, because the dynamic effects of inertia are significant.

For the corresponding flooded cells the predicted final water levels are very similar, with TUFLOW having predicted slightly greater values than RFIM.

c. V_{total}=200,000 m^3 ($Q_{max} = 13.88 m^3/s$)

As the total volume increases to V_{total}=200,000 m^3 ($Q_{max} = 13.88 m^3/s$), RFIM displayed slightly different flood extent than before (i.e. for V_{total}=100,000 m^3) (Fig. 27a, Appendix A). It predicted one additional flooded cell.

RESULTS:

The flooding order is the same as previously, meaning that it follows the same interchangeable easterly and southerly direction. It can also be noticed from Tables 6b and 6c (Appendix A) as the total volume increases from V_{total}=100,000 m^3 to V_{total}=200,000 m^3 the storage cell which contains the failure location and its neighbour cells on the east and south direction contain the same amount of flood water as before; however, the remaining cells have a variation of increase. Another important observation is that storage cells B and F, as well as K and G, contain almost the same volume in pairs. It could be noticed that both storage cells B and G, which have the walls, contain slightly smaller values than storage cells F and K. Also, in terms of flood volume, the cells where the walls are located (i.e. storage cells B, G and L) contain greater values of flood water, with storage cell L containing the maximum value of all cells.

The hydrodynamic flood model, once again, predicted a greater flood extent for a greater inflow volume (Fig. 27b, Appendix A). It predicted one additional flooded cell. After all cells that are located on the west of the walls (i.e. storage cells A, B, F, G, K

and L), have flooded, the water moved through the gap between the two walls to the neighbour cell.

The failure occurrence cell and its eastern and southern neighbouring cells, contain the same flood volume as before (i.e. for V_{total}=100,000 m^3) (Table 6c, Appendix A). All other cells display increases in their flood water values. It could be noted here that storage cells B and F, as well as cells K and G, have similar flood volume values in pairs, with F and K displaying slightly greater values. Storage cells B, G and L, which contain high values of flood volume with cell L containing the maximum value, enclose the two walls on their boundary.

Once again, although both models predicted a very similar inundation extent, TUFLOW displayed a greater number of flooded cells (Fig. 27, Appendix A). Although that cell contained a small amount of flood water, it could affect the risk of flooding, thus, it should not be ignored.

For the corresponding flooded cells, there is a small difference in terms of flood volume which varies from +2.3% to +10.0%, hence, both models are appropriate to provide a good representation of the flood extent, since the effects of inertia are insignificant (Table 6c, Appendix A)

Once again, for the corresponding flooded cells the predicted final water levels are very similar; however, TUFLOW displayed slightly larger values than RFIM (Table 6c, Appendix A).

d. V_{total}=300,000 m^3 ($Q_{max} = 20.83 m^3/s$)

For a greater inflow volume (i.e. V_{total}=300,000 m^3 ($Q_{max} = 20.83 m^3/s$)) RFIM predicted more flooded cells than in the case of V_{total}=200,000 m^3 as expected (Fig. 28a, Appendix A). This increase of 100,000 m^3 moved through the gap between the two walls to the easterly and then to the southerly direction.

RESULTS:

As in the previous inflow volume scenario (i.e. V_{total}=200,000 m^3) storage cells B and F, G and K as well as the additional cells I and M in pairs, contained similar volumes (Table 6d, Appendix A).

The hydrodynamic model predicted 2 additional flooded cells than in the previous inflow volume scenario (i.e. V_{total}=200,000 m^3) (Fig. 28b, Appendix A). The water follows the same path in terms of spreading.

It can be noticed from Table 6d (Appendix A) that TUFLOW predicted the same flood volume values as in the previous inflow volume case study (i.e. V_{total}=200,000 m^3) for storage cells A, B and F. This implies that those cells have reached their maximum flood volume capacity. All other cells had a large increase.

Although both models displayed a very similar flood extent, the RFIM displayed one additional flooded cell.

For the corresponding flooded cells, there is a large difference in terms of flood volume which varies from +2.3% to -41.3%, thus, the conclusion is that in this particular case study, both models can be used in the flood extent prediction.

Once again, the predicted final water levels are very similar for the corresponding flooded cells, with TUFLOW displaying slightly larger values than RFIM (Table 6d, Appendix A).

e. V_{total}=400,000 m^3 ($Q_{max} = 27.77 m^3/s$)

Increasing the total volume by 100,000 m^3 from the previous inflow volume scenario (i.e. V_{total}=400,000 m^3 ($Q_{max} = 27.77 m^3/s$)), the flood extent predicted a small change for RFIM (Fig. 29a, Appendix A). One additional cell was flooded. The water followed the same interchangeable easterly and southerly direction in terms of spreading as in the previous inflow volume scenarios.

RESULTS:

This increase of 100,000 m^3 of the inflow volume showed that the majority of the predicted flooded cells reached their maximum water capacity, since they contained the same amount of flood water as in the case of V_{total}=300,000 m^3 (Tables 6e and 6d, Appendix A). Only 2 of the predicted flooded cells have an increase in their flood volume (i.e. storage cells N and O).

Storage cells B and F, G and K, I and M in pairs contained very similar amounts of flood volume (Table 6e, Appendix A), with cell L, which includes one of the walls at its boundary, containing the maximum amount of flood volume. Therefore, the walls rather than the slope of the terrain displayed a greater role in terms of the flood volume spreading, since the floodplain terrain was very flat.

For a total volume of V_{total}=400,000 m^3 TUFLOW displayed a greater inundation extent than before (Fig. 29b, Appendix A). The number of the predicted flooded cells increased to 12. The flow path was the same as previously, where the water followed an easterly-southerly direction of spreading.

It can be observed from Tables 6d and 6e (Appendix A) that most of the predicted cells had an increase in their flood volume, the exception being the cell where the failure occurs and its neighbours which have already reached their maximum flood volume capacity. The maximum amount of flood water is stored in cell L, which contains a wall on its boundary. It can therefore be concluded that the location of the walls, and not the slope of the terrain, display a great role in terms of the flood water spreading.

As observed in Fig. 29 (Appendix A), both models displayed a very similar inundation extent, with TUFLOW displaying slightly greater number of flooded cells.

There appears to be a large difference in terms of the flood volume which varies from +2.3% to -33.0% for the corresponding flooded cells (Table 6e, Appendix A). Thus, the conclusion can be reached that for this inflow volume scenario, TUFLOW can be utilised in the flood extent prediction.

One more point to observe is that there are very similar final water level values for the corresponding cells (Table 6e, Appendix A). TUFLOW, however, displayed slightly greater values than RFIM.

2.1.5 5th CASE STUDY: Two walls at the boundaries of the storage cells B, G and L, reducing the slopes on both directions i and j:

- **Description of the DTM**

The DTM in this case scenario is similar to case study 3 (Section 2.1.3) (Fig. 19a and Fig. 19b, Appendix A); however, the distinction between them is that the slopes on the

north and east direction are reduced and have the same values (i.e. i = 0.0002 and j = 0.0002). This is assessed in order to examine the behaviour of flood parameters such as number of flooded cells, water depth, water level, etc. in flatter topographies.

a. V_{total}=70,000 m^3 ($Q_{max} = 4.86 m^3/s$)

The RFIM predicted 3 flooded cells (Fig. 30a, Appendix A). Precisely, the flood spreading was contained within the storage cells where the failure defence occurred and its neighbours on the easterly and southerly direction. The water spreads firstly from the defence failure location to its eastern and then to its southern neighbour.

The flood volume enclosed in each of the predicted flooded cells varies from 4,730 m^3 to 61,100 m^3 (Table 7a, Appendix A). The greatest share of the inflow volume of $V_{total} = 70{,}000 m^3$ is absorbed by the failure location leaving a smallest amount, which is shared equally, to the remaining of the flooded cells (Fig. 30a, Appendix A).

The hydrodynamic model predicted 3 flooded cells as well (the failure location and its neighbours on the easterly and southerly direction) (Fig. 30b, Appendix A). The spreading of the total volume starts from the failure location, and then moves firstly to its easterly and then to its southerly neighbour.

RESULTS:

Each of the flooded cells contains a predicted flood volume which varies from 3,000 m^3 to 62,600 m^3 (Table 7a, Appendix A). This volume reduces greatly for the first two flooded cells and then increases gradually for the last flooded cell.

It can be observed that both models predicted the same flood extent and the same flooding order of the flooded cells (Fig. 30, Appendix A).

Both flood models predicted the maximum flood volume to be contained within the failure location, however they did not predict the same value (TUFLOW displayed a greater value than RFIM) (Table 7a, Appendix A). The RFIM predicted the same flood volume amount for the remaining flooded cells in contrast to TUFLOW which predicted different values. In the last two flooded cells the RFIM displayed a greater value than TUFLOW.

Another observation is the existence of similar final water level (Table 7a, Appendix A) in each of the corresponding flooded cells, for both flood inundation models. TUFLOW displayed a greater value for the breach location and the last flooded cell than RFIM.

There is a small difference in terms of the flood volume for the corresponding flooded cells in the flood inundation models (Table 7a, Appendix A); the percentage of the difference varies from +2.5% to -36.6%, therefore, both models can be used for the prediction of flood extent, since the momentum effects are insignificant.

b. V_{total}=100,000 m^3 ($Q_{max} = 6.94 m^3/s$)

The flood extent and the flooding order derived by the RFIM was the same as in the previous case study despite the increase of the total volume (Fig. 31a, Appendix A). The failure location contains the maximum flood volume, dividing equally the residual volume between the remaining of the flooded cells.

RESULTS:

The flood volume in each cell varies from 20,230 m^3 to 61,100 m^3 (Table 7b, Appendix A). The volume decreases greatly and then remains stable.

TUFLOW displayed the same flood extent and flooding order as before, despite the increase of the total volume (Fig. 31b, Appendix A).

The flood volume predicted from TUFLOW varies from 17,590 m^3 to 62,610 m^3 (Table 7b, Appendix A). The volume reduces greatly for the first two flooded cells and then increases gradually. It can be observed from Table 7b (Appendix A) that the breach location contains the maximum flood volume, leaving a smaller amount to the rest of the flooded cells.

Although both models predicted the same flood extent, the flood volume contained in the cells was different (Fig. 31, Table 7b, Appendix A). Both models predicted that the maximum flood volume is contained in the failure location cell; however TUFLOW displayed a greater amount than the RFIM. Also, the RFIM predicted that the remaining amount of the flood volume splits equally between the remaining cells in contrast to TUFLOW which predicted different amount for both models.

There appears to be a small difference in terms of flood volume for the corresponding flooded cells in the flood inundation models (Table 7b, Appendix A). The percentage of the difference varies from -1.8% to -13.1%, thus, both models can be utilised for the flood inundation prediction purposes. That is the result of the insignificant effects of the momentum equation.

Another important observation is the existence of similar final water level (Table 7b, Appendix A) in each of the corresponding flooded cells, for both flood models.

c. V_{total}=200,000 m^3 ($Q_{max} = 13.88 m^3/s$)

The flood extent obtained from RFIM was greater than that of the previous scenario (Fig. 32a, Appendix A). Increasing the total volume to be spread, RFIM predicted two additional flooded cells. The flooding order is the same as previously for the first 3 flooded cells. Then the water spreads to the south from the easterly neighbour of the failure location cell, and also, from the south neighbour of the failure location.

RESULTS:

The cell which contains the failure and both its neighbours contain very similar flood water values (Table 7c, Appendix A). Especially, for the cell where the failure occurs (i.e. storage cell A), it has reached its maximum flood volume capacity, since it contains the same amount as in the previous scenarios (**V_{total}**=70,000 m^3 and V_{total}=100,000 m^3). On the other hand, both cells B and F have increased their flood volume by approximately 41,000 m^3. The remaining predicted flooded cells contain the exact same amount of flood water.

For a greater inflow volume (i.e. V_{total}=200,000 m^3) TUFLOW displayed a greater number of flooded cells (Fig. 32b, Appendix A). The flow path was exactly the same for the first 3 flooded cells as before. Then the water spread to the south firstly from the easterly neighbour cell of the failure location and then from the southerly neighbour cell.

The cell where the failure occurs and its neighbour cells contained similar amounts of flood water (Table 7c, Appendix A). Especially cells B and F have increased their volumes by almost 45,000 m^3 as the total volume to be spread increases.

Both flood models displayed the exact same flood extent and the same flow path (Fig. 32, Appendix A). Although, both models predicted the same flooded cells, there is a large difference in terms of flood volume. This difference varies from +2.0% to -54.3%, so, it could be concluded that for this particular case, both models can be used to predict the flood extent since the dynamic effects of inertia are insignificant. It is important to note that the smallest percentage is located not on the cell where the failure occurs, as it is the case for previous scenarios, but on its eastern neighbouring cell. Both models predicted the same cell (i.e. storage cell F) which contained the maximum flood volume.

The final water levels predicted from both models were very similar, with TUFLOW displaying slightly larger values than RFIM (Table 7c, Appendix A).

d. V_{total}=300,000 m^3 ($Q_{max} = 20.83 m^3/s$)

Although the inflow volume has been increased by 100,000 m^3 compared to the previous scenario, and one would expect that RFIM would obtain greater inundation extent, this was not the case. RFIM predicted the exact same flood extent with the same flooded cells (Fig. 33a, Appendix A).

RESULTS:

As it is observed from Tables 7c and 7d (Appendix A), the first 3 flooded cells (i.e. storage cells A, B and F) contain the same flood volume as before, although there was an increase of the total volume. This means that these cells reached their maximum value capacity. The 2 remaining predicted cells display an increase of approximately 51,000 m^3 and although their values are very similar they are not the same as in the previous scenarios.

As the total volume to be spread increased, the total number of the cells to be flooded from TUFLOW increased (Fig. 33b, Appendix A). For an inflow volume of V_{total}=300,000 m^3 TUFLOW displayed 6 flooded cells; one additional cell than in the previous scenario.

The first 3 flooded cells (i.e. storage cells A, B and F) retained the same flood volume as in the previous scenarios (Table 7d, Appendix A). The rest of the flooded cells increased their contained flood volume gradually. One important thing to note is that the

flood volume of cell A and B, and F and G in pairs are very similar, with cells that are located on the east i.e. cells B and G having slightly greater values than the others.

The flood extent obtained by TUFLOW, although very similar with that obtained by RFIM, it displays a small difference (Fig. 33b, Appendix A). It predicted one additional flooded cell than RFIM. For the corresponding flooded cells on both models the flow path is exactly the same.

Although both models displayed a very similar inundation extent there is a large difference in terms of flood volume for the corresponding flooded cells. This difference varies from +2.0% to -51.2%. Thus, for this case TUFLOW is the most appropriate to predict the flood extent, since the dynamic effects of the flood wave propagation are significant.

For the corresponding flooded cells both models displayed similar final water level values (Table 7d, Appendix A), with TUFLOW displaying slightly greater values.

e. V_{total}=400,000 m^3 ($Q_{max} = 27.77 m^3/s$)

Increasing the total volume from V_{total}=300,000 m^3 to V_{total}=400,000 m^3 RFIM predicted one additional flooded cell than previously (Fig. 34a, Appendix A). For the first 5 flooded cells the flow path was exactly the same as before.

RESULTS:

As in the previous inflow volume scenarios, the first 3 flooded cells have reached their maximum flood volume capacity (Table 7e, Appendix A). The remaining of the predicted flooded cells display increased volume and especially for cells G and F the increase was about 6,000 m^3. It is important to note that storage cells A, B and F have very similar flood volume values. This is also the case for cells G and K.

For a greater inflow volume TUFLOW predicted a greater flood extent (Fig. 34b, Appendix A); it predicted one additional flooded cell. The flow path was the same as before, also the water was transferred through the gap between the walls to the first cell on the east of the gap.

The first 4 flooded cells (i.e. storage cells A, B, F and G) reached their maximum flood volume capacity since they contain the same amount as before (Table 7e, Appendix A). It is important to mention that cells A and B, and F and G have very similar amounts of flood water. The remaining predicted cells display increased flood volume.

The flood extent obtained from both models is very similar but not exactly the same, since TUFLOW displayed one additional flooded cell than RFIM (Fig. 34, Appendix A). The flow path for the corresponding flooded cells on both models is exactly the same.

There is a small difference in terms of flood volume between the two models. This difference varies from +2.0% to -17.1%, hence, TUFLOW can be used in terms of flood inundation extent purposes, since the effects of momentum equation are significant (Table 7e).

Both models predicted the same cell to contain the maximum flood volume. That cell (i.e. storage cell L) is located on the south – east direction from the failure location and there is a wall at its boundary (Table 7e, Appendix A). This implies that for this particular case the walls, rather than the slope of the terrain, display a great role in terms of the flood water spreading.

The predicted final water levels for the same cells on both models are very similar (Table 7e, Appendix A). TUFLOW, once again, displayed slightly larger values than RFIM.

2.1.6 6th CASE STUDY: Two walls at the boundaries of storage cells B, G and L, decreasing the elevation of the area between the walls by 0.5 m:

- **Description of the DTM**

The DTM in this case scenario is similar to the case study 3 (Section 2.1.3) (Fig. 19a and Fig. 19b, Appendix A); however, the distinction between them is that the elevation of the area between the walls is reduced by 0.5m. The reason for this case was to investigate the effect of smaller elevation between the walls.

a. V_{total}=70,000 m^3 ($Q_{max} = 4.86 m^3/s$)

The predicted inundation extent from RFIM is contained within the first 2 storage cells, and then the water is transferred to the cell on the south direction. From there, it passes through the gap between the two walls to the two cells on the easterly direction (Fig. 35a, Appendix A).

There appears to be a small variation in terms of the flood volume, contained in each of the 5 predicted flooded cells (Table 8a, Appendix A). The volume increases gradually for the first 2 flooded cells and then reduces gradually for the following cell. This fluctuation continues for the remaining cells until the entire amount of the total volume has been spread.

RESULTS:

The flood extent for TUFLOW is contained within 6 flooded cells (Fig, 35b, Appendix A). The water is transferred from the cell where the failure occurs firstly to its eastern and then to its southern neighbour. From the eastern neighbour of the failure location cell the water spreads to the cell on the south direction. Finally, it is transferred through the gap between the two walls to the two cells in the easterly direction.

The contained flood volume in each of the predicted flooded cells has a large variation from 506 m^3 to approximately 18,600 m^3 (Table 8a, Appendix A). It can also be observed that there is a large fluctuation of the flood volume as the water is transferring from one cell to the other.

Both flood models predicted a very similar flood extent with a very similar flow path (Fig. 35, Appendix A). However, TUFLOW displayed one additional flooded cell which although it contains a small amount of flood water, it could affect the flood risk.

The corresponding flooded cells appear to have a large difference in terms of flood volume difference (Table 8a, Appendix A). This varies from +0.1% to -57.9%, so, TUFLOW is more appropriate to provide a better representation of the flood extent, since the dynamic effects of the flood wave propagation are significant. Another important point is that both models predicted that the maximum flood volume is contained in storage cell B.

An additional important observation is the existence of similar final water levels for the corresponding cells (Table 8a, Appendix A). TUFLOW predicted greater values than RFIM.

b. V_{total}=100,000 m^3 ($Q_{max} = 6.94 m^3/s$)

The flood extent obtained from RFIM can be observed in Fig. 36a (Appendix A). The obtained inundation extent was greater for a greater inflow volume as expected. In particular, 2 additional flooded cells were predicted than in the previous inflow volume scenario, increasing the total number of flooded cells to 7. The flow path was the same as before. The water moves from the storage cell where the failure occurred, to its neighbour on the east, then to the south. From there it spreads to the east for the next three storage cells and finally to the south.

RESULTS:

It is noticeable that RFIM predicted 7 flooded cells each of them containing a variable flood volume from 9,600 m^3 to 16,970 m^3 (Table 8b, Appendix A). The volume increases gradually for the first two flooded cells, then reduces gradually. After that it fluctuates for the remaining cells. The last flooded cell contains the lowest amount of flood volume. This is a result of the fact that all the previous cells have absorbed their maximum flood potential (contain most of the flood water) leaving a smaller amount to the last cell to be flooded.

One important observation is that storage cells A, B, G and H (i.e. cells which either have a wall on their boundary or are located next to cells with a wall on their boundary) contain the exact same volume as in the previous total volume scenario (i.e. V_{total}=70,000 m^3 ($Q_{max} = 4.86 m^3/s$)) (Table 8b, Appendix A), implying that they have reached their maximum flood volume capacity.

As the total volume to be spread increases gradually, the total number of flooded cells also rises gradually for TUFLOW (Fig. 36b, Appendix A). Particularly, 2 additional cells were flooded as the inflow volume was increased to V_{total}=100,000 m^3. The flow path was the same as previously. The water after the failure occurred spreads firstly to the easterly and then to the southerly direction. Then from the eastern neighbour of the failure location cell it spreads to the south. From there the water moves firstly to the east

and then to the south. These easterly and southerly direction spreadings are continued until the entire amount of the inundation volume is spread.

The predicted flooded cells from TUFLOW are 8 (Fig. 36b, Appendix A) with a range of flood volume between 1270 m^3 and 18,600 m^3 (Table 8b, Appendix A). It can be noticed (Table 8b, Appendix A) that the volume increases gradually for the first two flooded cells, and then fluctuates for the remaining cells. It is important to note that the cells A and B contain the same flood volume as before and the rest of the predicted flooded cells have a variation of flood volume increase (Table 8b, Appendix A).

The flood extent is very similar between the two models (Fig. 36, Appendix A). TUFLOW displayed a greater number of flooded cells. In particular, it demonstrates two additional cells than RFIM. Although, these 2 flooded cells contain less amount of flood water than the other cells (Table 8b, Appendix A) (the flood volume in these cells varies from 1270 m^3 to 1,620 m^3), they should not be ignored because they may be large enough to affect the flood risk.

Both models predicted that storage cell B contains the maximum flood volume of all predicted cells (Table 8e, Appendix A).The corresponding flooded cells in the two models appear to have a small difference in terms of flood volume (Table 8b, Appendix A). The percentage of the difference varies from +0.1% to +22.1%, therefore, both models are appropriate for the prediction of the flood extent, due to the insignificant effect of the momentum.

Similar final water levels (Table 8b, Appendix A) exist in each of the corresponding flooded cells, for both flood models. TUFLOW displayed greater values than RFIM.

c. V_{total}=200,000 m^3 ($Q_{max} = 13.88 m^3/s$)

As the total volume to be spread is increased to V_{total}=200,000 m^3 ($Q_{max} = 13.88 m^3/s$), the number of flooded cells rises to 8 (Fig. 37a, Appendix A). Therefore, one additional cell is flooded than in the previous inflow volume scenario. The water followed the exact same path for the first 7 flooded cells and then from cell J it is transferred to the cell on the north direction.

RESULTS:

The volume contained in cells A, B, G, H and I is the same as before, meaning that they have reached their maximum capacity of flood volume (Table 8c, Appendix A). The remaining predicted cells (i.e. E, J and O) increased their volume approximately by 30,000 m^3. This implies that the 100,000 m^3 of the increase of the V_{total} from V_{total}=100,000 m^3 to V_{total}=200,000 m^3, splits almost equally between those cells. Also, the cells which are located on the easterly direction of the terrain and have steep slopes contain the 3 highest values of flood volumes. So, it could be concluded that for this particular case, the slope plays a great role in terms of the flood volume spreading.

For great value of inflow volume, TUFLOW predicted more flooded cells (Fig, 37b, Appendix A). Precisely, 4 additional cells were flooded compared to the previous scenario of V_{total}=100,000 m^3. In general, the water follows the same path as before.

It is important to notice that the amount of flood volume remains the same for each predicted cell, such as cells A, B, G, H and I (Table 8c, Appendix A), implying that they have reached their maximum flood volume capacity. All other predicted cells display an increase in their contained volume.

The predicted flood extent from both models is very similar, with the water following a very similar flow path (Fig. 37, Appendix A). However, TUFLOW displayed a greater number of flooded cells than RFIM.

The corresponding flooded cells appear to have a large variation in terms of flood volume (Table 8c, Appendix A). The percentage of the difference varies from +0.1% to -34.7%, hence, TUFLOW is more appropriate for the prediction of the flood extent, due to significant effects of inertia.

Similar water levels exist in each of the corresponding flooded cells, for both flood models (Table 8c, Appendix A). TUFLOW displayed greater values than RFIM.

d. V_{total}=300,000 m^3 ($Q_{max} = 20.83 m^3/s$)

Although the inflow volume increased by 100,000 m^3 compared to the previous total volume scenario (i.e. from V_{total}=200,000 m^3 to V_{total}=300,000 m^3), the flood extent was

exactly the same as before (Fig. 38a, Appendix A). RFIM predicted the exact same 8 flooded cells and the water followed the same flow path.

RESULTS:

In terms of the predicted flood volume contained in each of the cells, there is a small difference in contrast to the previous inflow volume (i.e. V_{total}=200,000 m^3) (Table 8d, Appendix A). Only storage cells E, J and O, which are located on the easterly direction of the DTM, had an increase of their flood volume. The steep slopes of the terrain imply that the last cells to be flooded will attract more water. The remaining cells contained the same amount of flood water, since they reached their maximum flood volume capacity. To be more precise, the flood volume increase was approximately 30,000 m^3 for each cell. This implies that the increase of 100,000 m^3 of the inflow volume split almost equally between those cells. It could be concluded from the above that for this particular scenario, the slope of the terrain displays a great role in terms of the flood volume spreading.

For a greater inflow volume TUFLOW displayed a greater number of flooded cells (Fig. 38b, Appendix A). In particular, for an inflow volume of Vtotal=300,000 m^3, 14 flooded cells had been predicted; however, the water follows the same flow path as before.

As was expected, as more water is spread to the terrain, more water is stored in each of the predicted flooded cells (Table 8d, Appendix A). In general, it could be concluded that for the majority of the predicted cells, the contained flood water increased gradually. Once again, for cells A, B, H and I maximum flood volume capacity has been reached. One important thing to notice is that for cells E, J and O their contained flood volume increased by about 30,000 m^3.

The predicted inundation extent obtained from both flood models was very similar with very similar flow path (Fig. 38, Appendix A). However, once again, TUFLOW displayed more cells than RFIM. It predicted 4 additional flooded cells, each of them containing a significant amount of flood water, which should not be ignored, since they may affect the flood risk.

For the same predicted cells for both models, there appears to be a small difference in terms of the flood volume (Table 8d, Appendix A). The percentage of this difference varies from +0.1% to -28.0%, so, TUFLOW could be used to predict the flood extent, since the dynamic effects of inertia are significant. One important observation is that both models predicted that the storage cell O (which is affected by the steep slopes more than the other cells because it is the last cell on the easterly direction to be flooded) contained the maximum flood volume.

Another point to observe is the existence of very similar final water levels for the corresponding flooded cells (Table 8d, Appendix A), with TUFLOW displaying slightly greater values than RFIM.

e. V_{total}=400,000 m^3 ($Q_{max} = 27.77 m^3/s$)

The flood extent predicted from RFIM for a total spreadable volume of V_{total}=400,000 m^3 ($Q_{max} = 27.77 m^3/s$) was exactly the same, with an identical flow path, as in the previous inflow volume scenario of V_{total}=300,000 m^3 (Fig. 39a, Appendix A).

RESULTS:

Since the cells A, B, G, H and I reached their maximum flood volume capacity from the previous inflow volume scenario; the increase of 100,000 m^3 of the V_{total} was split almost equally between the cells E, J and O (Table 8e, Appendix A). Those cells are located on the easterly direction of the DTM and the steep slopes of the terrain imply that these last cells to be flooded will attract more water. It could, therefore, be concluded that for this particular scenario the slopes of the DTM display a great role in terms of flood water spreading.

Although the inflow volume increased by 100,000 m^3 compared to the previous scenario, and one would expect that TUFLOW would predict a greater flood extent that was not the case (Fig. 39b, Appendix A). For a total volume of V_{total}=400,000 m^3 ($Q_{max} = 27.77 m^3/s$) TUFLOW predicted an identical inundation extent to the one obtained for V_{total}=300,000 m^3, and in which also the water followed the exact same flow path.

As was observed from the previous inflow volume scenario (i.e. V_{total}=300,000 m^3 ($Q_{max} = 20.83 m^3/s$)), storage cells A, B, H and I reached their maximum inflow volume capacity (Table 8e, Appendix A). The rest of the predicted flooded cells had a gradual increase of their flood volume, with cells E, J and O having an increase of about 30,000 m^3; their volumes were the highest of all predicted cells. So, for this particular case, the slopes of the terrain display a great role in terms of the flood water spreading.

The predicted flood extent from both models was very similar with a similar flow path (Fig. 39, Appendix A). However, TUFLOW predicted 4 additional flooded cells than RFIM. Each of those cells contained a significant amount of flood volume which could affect the flood risk.

There appears to be a small difference in terms of flood volume for the corresponding flooded cells (Table 8e, Appendix A). The percentage of the difference varies from +0.1% to -24.5%, thus, for this particular case, TUFLOW is more appropriate to predict the flood extent, since there are significant effects of inertia. Both models predicted that storage cell O contained the maximum amount of flood water.

Another important observation is the existence of very similar final water levels for the corresponding flooded cells (Table 8e, Appendix A), with TUFLOW displaying slightly greater values than RFIM.

2.1.7 7th CASE STUDY: Two walls at the boundaries of storage cells B, G and L, reducing the elevation of the area between the walls by 0.5 m and reducing the area between the walls from 100m to 2m.

- **Description of the DTM**

The DTM in this case scenario is similar to the case study 3 (Section 2.1.3) (Fig. 19a and Fig. 19b, Appendix A); however, the distinction between them is that the elevation of the area between the walls is reduced by 0.5m and also, the area between the walls is smaller. This case is assessed in order to observe how both smaller elevation and area between the two walls would affect the water spread.

a. V_{total}=70,000 m^3 ($Q_{max} = 4.86 m^3/s$)

The flood extent of a total spreadable volume of V_{total}=70,000 m^3 ($Q_{max} = 4.86 m^3/s$, (Fig. 6, Section 2.1.1) can be observed in Fig. 40a (Appendix A), where the water is transferred from the cells where the failure occurs to the east, then to the cells on the south and finally it spreads through the small gap between the two walls to the east.

RESULTS:

The contained volume in each of the predicted flooded cells has a small variation from approximately 9,500 m^3 to 16,970 m^3 (Table 9a, Appendix A). There is also a small fluctuation of the volume values. It is important here to note that the cells which either contain a wall on their boundary (i.e. storage cells B and G) or are located next to cells with a wall on their boundary (i.e. cells A and H) contain large values of flood volume.

The inundation extent obtained by TUFLOW can be seen in Fig. 40b (Appendix A), where the water spreads from the failure location firstly to the east and then to the south direction. From the eastern neighbour of the failure location it spreads to the south. It is important here to note that the water does not travel to the cells that are located east of the gap, meaning that it never travels through the gap, so, it floods only the cells west of the gap.

TUFLOW predicted a large variation of flood volume from 506 m^3 to 19,090 m^3 approximately (Table 9a, Appendix A). One important observation is that the cells which contain a wall on their boundary (i.e. cells B, G and L) contain high flood volume values. The maximum flood volume is contained in the cell where the gap is located (i.e. storage cell G).

The flood extent obtained by the two flood models is very different (Fig. 40, Appendix A). Also, the flow path is completely different for the two models. The flood from RFIM extends in the area outside the gap; however, this is not the case for TUFLOW (here no water travels through the gap and therefore no cells beyond the gap are flooded).

There appears to be a small difference in terms of the flood volume for the corresponding flooded cells (Table 9a, Appendix A). The percentage of the difference varies from +0.1% to +25.2%, thus, for this particular inflow volume scenario,

TUFLOW can be utilised to give a representation of the flood extent, since the effects of inertia are significant, although, RFIM predicted more cells than TUFLOW.

One more point to be raised is the existence of similar final water levels for the corresponding flooded cells (Table 9a, Appendix A), with TUFLOW displaying greater values than RFIM.

b. V_{total}=100,000 m^3 ($Q_{max} = 6.94 m^3/s$)

The number of the flooded cells increased as the total volume to be spread increased from V_{total}=70,000 m^3 to V_{total}=100,000 m^3. The flood extent obtained from the RFIM can be observed in Fig. 41a (Appendix A), where the water follows the same path as previously for the first 5 flooded cells and then it spreads firstly to the east and finally, to the south.

RESULTS:

The flood volume contained in each cell varies from 10,500 m^3 to 16,970 m^3 (Table 9b, Appendix A). The flood volume increases gradually for the first two flooded cells, and then reduces gradually for the next two cells. This type of increase and reduction continues until the entire amount of the inflow volume is spread. The flood volume stored in cells A, B and H was the same as in the previous scenario, implying that they reached their maximum flood volume capacity. The rest of the predicted flooded cells had a gradual volume increase.

Although the inflow volume increased to V_{total}=100,000 m^3 ($Q_{max} = 6.94 m^3/s$) the predicted flood extent was exactly the same as in V_{total}=70,000 m^3, meaning that no water passed through the gap. The flood extent predicted from TUFLOW (Fig. 41b, Appendix A) is different from the one obtained from the RFIM. The water spreads from the failure location to the east and then to the south. Finally, from the eastern flooded cell of the defence failure location (i.e. storage cell B) the water spreads to the south.

The flood volume contained in each of the 5 predicted cells of TUFLOW (Table 9b, Appendix A) varies from 1,270 m^3 to 38,500 m^3. It can be noticed (Table 9b, Appendix A) that the volume increases gradually for the first two flooded cells, and then reduces greatly; then increases significantly and gradually. The cells A and B contained the same amount of flood volume as before, so, they reached their maximum flood volume

capacity. One important thing to note is that cells B, G, and L, which contain a wall on their boundary, contain high flood volume values with cell O containing the maximum flood volume of all.

The flood extent obtained from both flood models is very different. The RFIM predicted 4 additional flooded cells than TUFLOW (Fig. 41, Table 9b, Appendix A).

The corresponding flooded cells in the flood inundation models appear to have a great difference in terms of flood volume (Table 9b, Appendix A). The percentage of the difference varies from +0.1% and +76.8%, therefore, for this case study TUFLOW is more appropriate to provide a better representation of flood inundation extent than RFIM.

One more point to be raised is the existence of similar final water level (Table 9b, Appendix A) in each of the corresponding flooded cells, for both flood models. TUFLOW displayed greater values than the RFIM.

c. V_{total}=200,000 m^3 ($Q_{max} = 13.88 m^3/s$)

The flood extent obtained by RFIM for an inflow volume of V_{total}=200,000 m^3 ($Q_{max} = 13.88 m^3/s$) is identical to that obtained for a total spreadable volume of V_{total}=100,000 m^3 (Fig. 42a, Appendix A). However, one additional cell was flooded. The flooding order of the predicted flooded cells was the same as before.

RESULTS:

One important observation is that the majority of the predicted cells contained the exact same amount of flood water as in previous inflow volume scenarios, implying that their maximum capacity of flood volume has been reached (Table 9c, Appendix A). Only the 3 cells, which are located on the east of the DTM and are affected more by the steep slopes (i.e. storage cells E, J and O), increased their volume by about 30,000 m^3. This means that the rise of 100,000 m^3 in the total volume splits almost equally between these particular cells. Therefore, it could be concluded that for this particular inflow volume scenario, the slopes of the DTM display a great role in terms of the flood volume spreading.

For this greater inflow volume TUFLOW predicted an identical flood extent to the previous scenario (V_{total}=100,000 m^3) (Fig. 42b, Appendix A). The flood extended only between the cells that are located on the west side of the walls, meaning that no water was transferred through the gap. Therefore, the following conclusion could be reached: for this particular scenario, the smaller area between the walls (i.e. gap) displayed a great role in terms of the flood water spreading.

It can be observed from Table 9c (Appendix A) that apart from the cell where the failure occurs (i.e. storage cell A), which has reached its maximum flood volume capacity, the remaining of the predicted cells display a gradual increase of their volume, compared to the previous inflow volume scenario. Especially for the cells B, G and L, which have a wall on their boundary, the volume increased by 30,000 m^3, meaning that the increase of 100,000 m^3 of the inflow volume split almost equally between those cells.

The flood extent obtained by both flood models is different (Fig. 42, Appendix A). RFIM predicted a flood that is extended not only on the west side of the walls, but also on the east side. On the other hand, TUFLOW predicted an extent that covers only the cells that are located on the west side of the wall, implying that the smaller gap between the walls does not allow the water to travel through the gap, to flood the cells on the east of the walls.

The large difference between the two flood models can be observed not only from the flood extent (Fig. 42, Appendix A), but also from the flood volume difference of the corresponding flooded cells (Table 9c, Appendix A). The percentage of that difference varies from +0.1% to +292.6%, so, for this particular inflow volume scenario, TUFLOW is the most appropriate to give a good representation of the flood extent, since the dynamic effects of inertia (due to the reduction of the area between the two walls) are significant.

The existence of very similar final water levels of the corresponding flooded cells can be observed in Table 9c (Appendix A). TUFLOW displayed greater values than RFIM. One important thing to notice is that the final water levels predicted from TUFLOW for the cells B, G and L are exactly the same.

d. V_{total}=300,000 m^3 ($Q_{max} = 20.83 m^3/s$)

Increasing the inflow volume by 100,000 m^3 compared to the previous scenario (i.e. V_{total}=200,000 m^3), one would expect that RFIM would predict a greater flood extent; however, this was not the case (Fig. 43a, Appendix A). RFIM predicted the exact 8 flooded cells as before with the same flow path. It could be concluded that both the smaller area between the walls and the reduction of the elevation of the area close to the gap allowed the water to travel through the gap and flood the cells on its easterly direction.

RESULTS:

Although the extent was the same as before, the same observation can not be made for the contained flood volume in each of the predicted cells (Table 9d Appendix A). Most of the cells contained the same volume as before; however, 3 of the predicted cells (i.e. storage cells E, J and O), affected by the steep slopes of the terrain, had an increase in volume of about 30,000 m^3 each. This implies that the 100,000 m^3 increase of the total volume is divided almost equally between those cells. Therefore, the slopes on the terrain display a great role in the flood volume spreading.

The small area between the walls prevented the water be transferred through it to the cells on the easterly direction of the walls (Fig. 43b, Appendix A). Also, the decrease of the elevation of the area close to the gap between the walls caused most of the water to travel to the cell on the south direction (i.e. storage cell L).

Apart from the cell where the failure occurs (i.e. storage cell A), which contained the same amount of flood volume as before, the remaining cells displayed gradual increase (Table 9d, Appendix A). Especially, the storage cells B, G and L which have a wall on their boundary had an increase of almost 30,000 m^3 of their flood volume, suggesting that the increase of the total volume is divided almost equally between those cells.

It can be observed from Fig. 43 (Appendix A) that the flood extent obtained by the two models is different. RFIM predicted a flood that is extended to cells on either the easterly and westerly side of the walls; however, TUFLOW predicted a flood that covers cells only on the westerly direction of the walls.

The large difference between the predictions of the two models can be observed not only in terms of flood extent (Fig. 43, Appendix A), but also in terms of flood volume (Table 9d, Appendix A). The percentage of the difference for the corresponding flooded cells varies from +0.1% to +501.5%, so, TUFLOW can be used to predict the flood extent, despite the greater number of flooded cells predicted from RFIM. The dynamic effects of the flood wave propagation are more significant, due to the reduction of the area between the two walls.

The corresponding flooded cells have very similar final water levels (Table 9d, Appendix A). TUFLOW displayed greater values than RFIM. It is important to note that TUFLOW predicted the same final water level for cells B, G and L.

e. V_{total}=400,000 m^3 ($Q_{max} = 27.77 m^3/s$)

The predicted from RFIM flood extent was the same as before, although the inflow volume was raised to V_{total}=400,000 m^3 ($Q_{max} = 27.77 m^3/s$) (Fig. 44a, Appendix A). The same 8 cells have been flooded following the exact same flow path as previously.

RESULTS:

One important thing to observe in Table 9e (Appendix A) is that storage cells E, J and O, have an increase of approximately 30,000 m^3 in their contained amount of flood volume. So, for this scenario the slopes of the terrain displayed a great role in terms of the flood volume spreading.

The hydrodynamic flood model predicted the same 5 flooded cells as previously (Fig. 44b, Appendix A). So, it could be deducted that the smaller gap area prevented the water from travelling to the easterly direction, and also, the reduction of the elevation of the area close to the gap caused most of the flood volume to be transferred to the cell on the south (i.e. storage cell L).

Only the cell where the failure occurs (i.e. storage cell A) has the same flood volume as before and the rest of the predicted cells displayed a gradual increase (Table 9e, Appendix A). Especially the cells B, G and L, which have a wall on their boundary and contained the highest values of the flood volume, have a volume increase of 30,000 m^3.

The predicted flood extent from both flood models is very different (Fig. 44, Appendix A). RFIM has predicted flooded cells not only on the westerly but also on the easterly direction of the walls. On the other hand, TUFLOW displayed flooded cells only on the westerly direction of the walls.

There appears to be a large difference in terms of flood volume for the corresponding flooded cells (Table 9e, Appendix A). This difference varies from +0.1% to +709.5%, hence, for this particular scenario, TUFLOW can be utilised to predict the flood extent.

The predicted final water levels are very similar for the corresponding flooded cells (Table 9e, Appendix A). TUFLOW displayed greater values than RFIM.

2.1.8 8th CASE STUDY: Four walls at the boundaries of some storage cells:

- **Description of the DTM**

The DTM of this particular case study (Fig. 45a,b, Appendix A) has the same characteristics regarding the number of storage cells in the northing and easterly direction, the plan area of each storage cell, the resolution and the slope in the northing and easterly directions as the previous case studies.

In order to investigate the behaviour of the water as it reaches barriers, 4 walls were raised at the boundaries of some storage cells (Fig. 45b, Appendix A).

a. V_{total}=70,000 m^3 ($Q_{max} = 4.86 m^3/s$)

The inundation obtained from RFIM is extended from the failure location cell to the east, then to the south and finally to east flooding the cell where the gap between the walls is located (i.e. storage cell M) (Fig. 46a, Appendix A). It can be noticed that the water does not pass through the gap between the walls, so, it remains contained within the wall boundaries.

The flood volume contained in each of the 5 predicted cells varies from 7,680 m^3 to 19,990 m^3 approximately (Table 10a, Approximately B). The flood volume increases gradually for the first 3 flooded cells as the water is spread to more cells, and then reduces significantly for the remaining ones. Storage cells B and G contain almost the same amount of flood water. The flooded cell which contains the minimum value of

flood volume is the storage cell M which is the last cell to be flooded and which also contains the gap between the walls.

RESULTS:

The hydrodynamic flood model predicted 6 flooded cells (Fig. 46b, Appendix A). From Fig. 45b, it could be concluded that the flood extent is contained within the boundaries set by the wall, and no water is transferred to other cells outside the wall set boundaries.

The predicted flood volumes from TUFLOW that are contained in each of the predicted cells have a large variation from 506 m^3 to 19,100 m^3 approximately (Table 10a, Appendix A).

The flood extent obtained by both models is very similar (Fig. 46, Appendix A). Their difference is that TUFLOW displayed one additional cell than RFIM. This cell should not be ignored although it contains a small flood volume value, because it may affect the flood risk. The flow path is similar for both models.

For the corresponding flooded cells there is a large difference in terms of flood volume (Table 10a, Appendix A). This difference has a variation from +0.1% to -54.4%, so, for this particular case study, both models are appropriate to predict the flood extent, since the dynamic effects of inertia are insignificant.

The final water levels for the corresponding cells were very similar; however, TUFLOW displayed slightly greater values than RFIM (Table 10a, Appendix A).

b. V_{total}=100,000 m^3 ($Q_{max} = 6.94 m^3/s$)

The flood extent for V_{total}=100,000 m^3 ($Q_{max} = 6.94 m^3/s$) is identical to that obtained by RFIM for V_{total}=70,000 m^3 ($Q_{max} = 4.86 m^3/s$) (Fig. 47a, Appendix A). The water remains within the cells that cover the area set by the walls. The water follows the exact same path as previously (Fig. 47a, Appendix A).

RESULTS:

The predicted flood volume for each of the flooded cells varies from 14,240 m^3 to 38,080 m^3 (Table 10b, Appendix A). The flood volume contained within the first 4

flooded cells remains the same as in the previous inflow volume scenario (V_{total}=70,000 m^3 ($Q_{max} = 4.86 m^3/s$)), so they reached their maximum flood volume capacity. However, for the last flooded cell which contains the gap between the walls and it is surrounded by the 3 walls, the volume is increased by approximately 31,000 m^3 (Table 8b, Appendix A). This particular cell is the cell which contains the maximum amount of flood water.

The predicted flood extent from TUFLOW is shown in Fig. 47b (Appendix A). The flood extent as well as the flooding order are identical to the one obtained in V_{total}=70,000 m^3 (Fig. 47b, Appendix A). This means that the amount of water was not enough to spread outside the area set by the walls.

TUFLOW predicted 6 flooded cells (Fig. 47b, Appendix A). This means that the hydrodynamic model predicted one additional cell than the RFIM. The amount of the flood volume contained in each of the flooded cells varies from 1,270 m^3 to 32,500 m^3 (Table 10e, Appendix A). The flood volume increases gradually for the first three flooded cells and then reduces greatly. After that it increases significantly. It is important to note that the cell where the failure occurs, the two cells with a wall on their boundary and the cell on the south of those (i.e. storage cells A, B, G and L) contain the same amount of water as before (i.e. for V_{total}=70,000 m^3), which means that they reached their maximum flood volume capacity (Table 10b, Appendix A).

Both flood models predicted a similar flood extent. Their difference is that TUFLOW predicted one additional flooded cell than the RFIM. Although, this cell contains less amount of flood volume than the other cells (Table 10b, Appendix A), it should not be disregarded as it may be large enough to affect the flood risk.

There appears to be a small difference in terms of flood volume for the corresponding flooded cells in the flood inundation models (Table 10b, Appendix A). The percentage of the difference varies from +0.1% to -14.6%, hence, for this particular case study both flood inundation models can be used for flood risk management purposes. One important observation is that both models predicted that the maximum amount of flood volume is contained in storage cell M and the minimum in the cell where the failure occurs (i.e. storage cell A) (Table 10b, Appendix A).

The differences between the two models may be attributed to the fact that TUFLOW contains the momentum equation which allows this model to simulate the effect of inertia.

c. V_{total}=200,000 m^3 ($Q_{max} = 13.88 m^3/s$)

Increasing the amount of water to be spread to V_{total}=200,000 m^3, the number of flooded cells rises into 9 (Fig, 48a, Appendix A). The flow follows the same path as in the previous inflow volume scenarios (i.e. V_{total}=70,000 m^3 and V_{total}=100,000 m^3) for the first 5 flooded cells and then the water passes through the gap between the two walls to the cell on the north. From there it is transferred to the cells on the easterly direction and finally to the cell on the southerly direction.

RESULTS:

Storage cells A, B, G and L reached their maximum flood volume capacity from the previous total volume scenario (i.e. for V_{total}=100,000 m^3), thus, they contain the same amount of water as before (Table 10c, Appendix A). The remaining of the predicted cells display an increase in their contained flood volume. In general, as the water is transferred from one cell to the other, the flood volume displays a fluctuation of increases and reductions (e.g. increase from A to B & G, but decrease from G to H etc.).

For a greater inflow volume, TUFLOW predicted 3 additional flooded cells than in the case of V_{total}=100,000 m^3 (Fig. 48b, Appendix A). The number of the flooded cells rose to 9. The amount of inflow volume was large enough, so, the water is transferred from the gap between the walls to the cell on the north direction, and then to its two eastern neighbouring cells.

The contained flood volume in each of the predicted cells increased apart from the cells A, B, G and L, which contained the same volume as before, since they reached in the previous inflow volume scenario (i.e. V_{total}=100,000 m^3) their maximum flod volume capacity (Table 10c, Appendix A).

The predicted inundation extent is very similar for both models (Fig. 48, Appendix A). Although both models predicted the same number of 9 flooded cells, these cells are not the same; however, both models follow a very similar flow path.

In terms of flood volume for the corresponding flooded cells in both models, there is a small difference (Table 10c, Appendix A), which varies from +0.1% to +19.2%, so, both models are appropriate to display the flood inundation prediction, since the effects of inertia are insignificant.

The final water levels are very similar for the corresponding flooded cells on both models (Table 10c, Appendix A); however, TUFLOW displayed slightly greater values than RFIM.

d. V_{total}=300,000 m^3 ($Q_{max} = 20.83 m^3/s$)

For an increase of 100,000 m^3 of the total volume (i.e. from V_{total}=200,000 m^3 to V_{total}=300,000 m^3) the flood extent was not greatly affected (Fig. 49a, Appendix A). In general, it was the same as for V_{total}=200,000 m^3, and only one additional cell flooded. The flow path was exactly the same as before.

RESULTS:

One important observation to be made in terms of flood volume is that the majority of the flooded cells have reached their maximum flood volume capacity, once they appear to contain the same amount of flood water as in the previous inflow volume scenario (Table 10d, Appendix A). Only the last 3 flooded cells (i.e. storage cells E, J and O) display an increase in their volume by approximately 30,000 m^3. So, it could be concluded that the 100,000 m^3 total volume increase is divided almost equally into these 3 cells which are located on the east direction of the terrain. Therefore, for this particular case, the slope of the terrain plays a great role in terms of the water spreading, since the 3 cells containing the highest flood volume values are located in areas of steep slopes.

The total number of flooding cells, for TUFLOW, increased to 12 since there was an increase of the inflow volume of 100,000 m^3 (Fig. 49b, Appendix A). Both the flood extent and the flow path were the same as before; however, 3 additional cells were flooded. The cells A, B, G, H, I, L and M, meaning the cells that have a wall on their boundary or are located next to a cell with a wall have reached their maximum flood volume capacity (Table 10d, Appendix A). The remaining cells displayed a variation of volume increase. It is important to note that the 3 cells that are located on the east of the terrain contain high values of flood volume. So, one would notice that the slope displays

a great role in terms of flood volume spreading, since the cells located in areas with steep slopes contain large values of flood volume. Especially for cell O which contains an increased volume of about 50,900 m^3.

Both models displayed a very similar inundation extent with a very similar flow path (Fig. 49, Appendix A). However, TUFLOW predicted 2 additional flooded cells than RFIM. These cells contain a significant amount of flood volume, so, they could affect the flood risk.

The corresponding flooded cells appear to have a small difference in terms of flood volume (Table 10d, Appendix A). The percentage of the difference varies from +0.1% to +18.4%, so, for this particular inflow volume scenario, both models can be used to predict the inundation extent, since there are insignificant effects of inertia. Another important thing to observe is that both models predicted the same storage cell containing the maximum flood volume (i.e. storage cell M).

The final water levels predicted from both models are very similar (Table 10d, Appendix A); however, TUFLOW displayed slightly greater values than RFIM.

e. V_{total}=400,000 m^3 ($Q_{\max} = 27.77 m^3/s$)

The effect of inertia can be seen further in Fig. 50 (Appendix A) which denotes the case of flood volume of 400,000 m^3 ($V_{total} = 400{,}000 m^3$), derived by a hydrograph of the same duration as before and a flow peak of $Q_{\max,TUFLOW} = 27.78 m^3/s$ (Fig. 6, Section 2.1.1).

RESULTS:

For an inflow volume of 400,000 m^3 for the RFIM the flood extent was the same as before, following the same path as previously (Fig. 50a, Appendix A).

It appears that the majority of the predicted flooded cells (i.e. storage cells A, B, G, H, I, L and M) contain the same amount of flood water as before, since they have reached their maximum flood volume capacity (Table 10e, Appendix A). The remaining flooded cells (i.e. storage cells E, J and O) appear to have an increase in volume of about 30,000 m^3. These cells, which are located on the east direction of the terrain, contain large

values of flood volume. Thus, it could be concluded that for this case the slope displays a great role in terms of the water spreading, since those cells are located in an area where the slope forces the water to transfer to the easterly direction. In particular, storage cell O contains the maximum flood volume of all flooded cells.

For a greater inflow volume TUFLOW predicted more flooded cells (Fig. 50b, Appendix A). In particular, 2 additional cells have been flooded compared to the previous inflow volume scenario (i.e. V_{total}=300,000 m^3). The flow path was very similar with that followed in the previous scenario.

The flood extent obtained from TUFLOW is very similar to that obtained from the RFIM (Fig. 50b, Appendix A).

The predicted flooded cells from TUFLOW are 12 (Fig. 50b, Appendix A) with a range of flood volume from 27 m^3 to 84,760 m^3 (Table 10e, Appendix A). It can be observed from Table 10e (Appendix A) that the flood volume increases gradually for the first 3 flooded cells, then reduces gradually for the next two flooded cells and once more increases greatly for the next cell. This type of fluctuation continues for the remaining flooded cells.

One important thing to notice is that most of the predicted cells (i.e. storage cells A, B, G, H, I, L and M) contain the same volume as previously and the rest of the predicted cells display an increase of their contained water volume (Table 10e, Appendix A). Especially for cells E, J and O, which are located on the east of the terrain, contain larger amounts of water, with cell O containing the maximum amount of flood volume. Thus, the conclusion can be reached for this particular scenario, the slope displays a great role in terms of water spreading, since the cells with the maximum amount of volumes are located on the easterly direction of the DTM.

TUFLOW displayed a greater number of flooded cells. Precisely, it predicted four additional cells than the RFIM. These 4 cells must not be ignored as they contain a significant amount of flood volume (the flood volume in these cells varies from 27 m^3 to 14,280 m^3) (Table 10e, Appendix A), large enough to affect the flood risk.

Storage cells A, B, G, H, I, L and M contain the same amount of flood volume as before and the cells E, J and O, which are located on the east direction of the terrain, contain maximum values of flood volume. This implies that the slope for this particular case, plays a great role in terms of the water spreading, since the slope of the terrain forces the water to travel to the east direction of the DTM.

The corresponding flooded cells in the flood inundation models appear to have a small difference in terms of flood volume (Table 10e, Appendix A). The percentage of the difference varies from +0.1% to -13.0%, thus, the conclusion to be drawn is that both models can be used for flood extent prediction purposes, due to insignificant effects of inertia.

Another thing to be noticed is that both models display similar final water levels for the same flooded cells (Table 10e, Appendix A). TUFLOW displayed greater values than the RFIM.

Finally, Table 11 provides a summary of the results of the flooded cells and the minimum and the maximum % of flood volume difference obtained from all cases that were investigated.

	1st Case study	*2nd Case study*	*3rd Case study*	*4th Case study*	*5th Case study*	*6th Case study*	*7th Case study*	*8th Case study*
V=70,000 m³								
RFIM	5 flooded cells	5 flooded cells	4 flooded cells	5 flooded cells	3 flooded cells	5 flooded cells	5 flooded cells	5 flooded cells
TUFLOW	8 flooded cells	7 flooded cells	7 flooded cells	5 flooded cells	3 flooded cells	6 flooded cells	5 flooded cells	6 flooded cells
MIN % FLOOD VOLUME DIFFERENCE	+0.1	+0.1	+0.1	+2.3	+2.5	+0.1	+0.1	+0.1
MAX % FLOOD VOLUME DIFFERENCE	-5.0	-12.9	-92.5	+10.0	-36.6	-57.9	+25.2	-54.4
V=100,000 m³								
RFIM	7 flooded cells	7flooded cells	6 flooded cells	5 flooded cells	3 flooded cells	7 flooded cells	7 flooded cells	5 flooded cells
TUFLOW	11 flooded cells	10 flooded cells	8 flooded cells	6 flooded cells	3 flooded cells	8 flooded cells	5 flooded cells	6 flooded cells
MIN % FLOOD VOLUME DIFFERENCE	+0.1	+0.1	+0.1	+2.3	+2.5	+0.1	+0.1	+0.1
MAX % FLOOD VOLUME DIFFERENCE	-70.6	-61.0	+96.8	-42.6	-13.1	+22.1	+76.8	-14.6
V=200,000 m³								
RFIM	7 flooded cells	8 flooded cells	9 flooded cells	5 flooded cells	5 flooded cells	8 flooded cells	8 flooded cells	9 flooded cells
TUFLOW	11 flooded cells	12 flooded cells	12 flooded cells	7 flooded cells	5 flooded cells	12 flooded cells	5 flooded cells	9 flooded cells
MIN % FLOOD VOLUME DIFFERENCE	+0.1	+0.1	+0.1	+2.3	+2.5	+0.1	+0.1	+0.1
MAX % FLOOD VOLUME DIFFERENCE	-16.0	-17.4	-48.6	+10.0	-54.3	-34.7	+292.6	+19.2
V=300,000 m³								
RFIM	7 flooded cells	8 flooded cells	9 flooded cells	10 flooded cells	5 flooded cells	8 flooded cells	8 flooded cells	10 flooded cells
TUFLOW	11 flooded cells	13 flooded cells	12 flooded cells	9 flooded cells	6 flooded cells	14 flooded cells	5 flooded cells	12 flooded cells
MIN % FLOOD VOLUME DIFFERENCE	+0.1	+0.1	+0.1	+2.3	+2.5	+0.1	+0.1	+0.1
MAX % FLOOD VOLUME DIFFERENCE	-18.3	-19.6	-12.5	-41.3	-51.2	-28.0	+501.5	-18.4
V=400,000 m³								
RFIM	7 flooded cells	8 flooded cells	9 flooded cells	11 flooded cells	6 flooded cells	8 flooded cells	8 flooded cells	10 flooded cells
TUFLOW	11 flooded cells	13 flooded cells	14 flooded cells	12 flooded cells	7 flooded cells	14 flooded cells	5 flooded cells	14 flooded cells
MIN % FLOOD VOLUME DIFFERENCE	+0.1	+0.1	+0.1	+2.3	+2.5	+0.1	+0.1	+0.1
MAX % FLOOD VOLUME DIFFERENCE	-19.2	-19.4	-14.2	-33.0	-17.1	-24.5	+709.5	-13.0

Table 11: DTM/ volume configuration summary table

CHAPTER 3 – COMPARISON OF NEW APPROACH WITH RFIM, TUFLOW AND STATISTICS

- **Application of the new Rapid Flood Model**

To examine whether the new Rapid Flood Model is indeed as fast as RFIM and as accurate as TUFLOW, the methodology was applied to the 8 DTM scenarios that were analysed in Section 2.1. The results of this application were then compared to the corresponding results obtained from RFIM, TUFLOW and simple linear interpolation/extrapolation. Therefore, the methodology of the new Rapid Flood Model, as described in Section 1.4.2 (following the methodology of Neelz et al (2007), described in Section 1.4), was applied to the 8 DTM scenarios that were analysed in Section 2.1. To be more precise, specific points located at the centre of the flooded cells (i.e. H1, H8, H15, etc.) (Fig. 51) were selected, based on their DTM position (i.e. defence failure location, close to a wall or the gap between two walls, etc.).

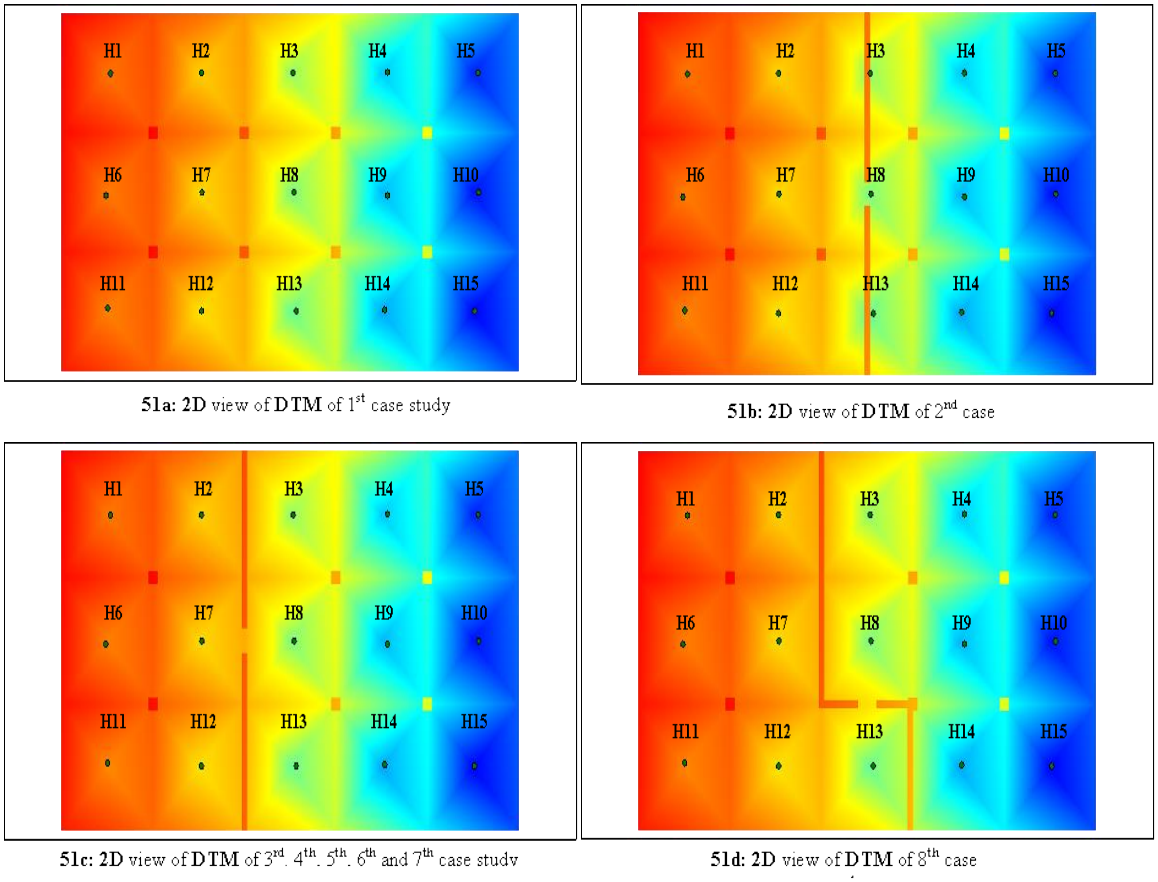

51a: 2D view of DTM of 1st case study

51b: 2D view of DTM of 2nd case

51c: 2D view of DTM of 3rd, 4th, 5th, 6th and 7th case study

51d: 2D view of DTM of 8th case

Fig. 51 a, b, c, d: 2D view of DTM of all case studies including H points

The particular points (located at the centre of the flooded cells) investigated, were chosen based on their DTM position (Fig. 51). Specifically, point H1 was selected in all case studies, since it is contained in the cell where the failure occurs, and is the begging

of the flow path. Also, point H15 is examined in most of the cases, as it is the last cell to be flooded and it is important as the water has finished spreading. The remaining training points were selected due to their location close to the gap between the two walls (e.g. before or after the gap). The importance of the behaviour of the water as it passes through the gap was the reason for the selection of those particular points.

The two main training data sets used were those obtained from two hydrographs of V_{total}=100,000 m^3/s ($Q_{max} = 6.94 m^3/s$) and V_{total}=400,000 m^3/s ($Q_{max} = 27.77 m^3/s$) respectively. The new model's linear interpolation of the training sets gives the water level prediction for V_{total}=200,000 m^3/s ($Q_{max} = 13.88 m^3/s$) and V_{total}=300,000 m^3/s ($Q_{max} = 20.81 m^3/s$). On the other hand, linear extrapolation of the same data sets, provides the water level prediction for V_{total}=70,000 m^3/s ($Q_{max} = 4.86 m^3/s$) and V_{total}=500,000 m^3/s ($Q_{max} = 34.72 m^3/s$) (Fig. 2, Section 1.4.2). This training data set was chosen as representative of an expected typical tidal or storm surge event as mentioned in Chapter 2.

These results are compared to those obtained from RFIM, TUFLOW and simple linear interpolation/extrapolation of TUFLOW results. To assist in the analysis graphs (i.e. Fig. 52-83, Appendix B) have been created.

It is important here to note that although RFIM, as referred in Section 1.4, does not predict the water level at each time step; calculations were made using the following method:

- Estimate the total volume at each time step (i.e. time = 0, 1, 2, …,6 hrs) of the hydrographs (Fig. 2, Section 1.4.2) through the simple formulas of the area under the curve.

- Using the above results of the total volume, RFIM is run providing the results of the water depth at each time step.

- Finally, the water level is predicted by the summation of the water depth and the terrain of the DTM:

$$z(i, j) = h(i, j) + terrain(i, j) \qquad \textbf{(Eq. 11)}$$

Table 12 provides a summary of the specific points located at the centre of certain flooded cells examined for each case study.

CASES / POINTS	1	2	3	4	5	6	7	8
H1	✓	✓	✓	✓	✓	✓	✓	✓
H2					✓		✓	
H3								
H4								
H5	✓							
H6				✓	✓			
H7			✓	✓	✓	✓	✓	✓
H8		✓	✓			✓		✓
H9								✓
H10								
H11					✓			
H12			✓	✓				✓
H13								
H14								
H15	✓	✓	✓			✓		

Table 12: Points/Cases investigated summary table

3.1 1st CASE STUDY: Introduction of flat areas around the lowest link:

- **H1**

The water level predictions obtained from the application of the new RFIM at point H1 (Fig. 51a, Chapter 3), which is located at the centre of the flooded cell where the defence failure occurs, are compared to the ones obtained from RFIM, TUFLOW and simple linear interpolation/extrapolation of TUFLOW data. This comparison is shown in Fig. 52. It is important here to note that the phrase new_model included in the legend of all graphs, refers to the new Rapid Flood Model.

The first observation to be made in Fig. 52 is that the starting point of the water level for all models (i.e. RFIM, TUFLOW, linear extrapolation and new model) is the same.

Although, it was expected that the water level would remain stable for a short time period and then start to increase, this was not the case. It seems that the level rises almost as soon as the cell starts to flood. This may occur because H1 is located at the cell where the failure occurs.

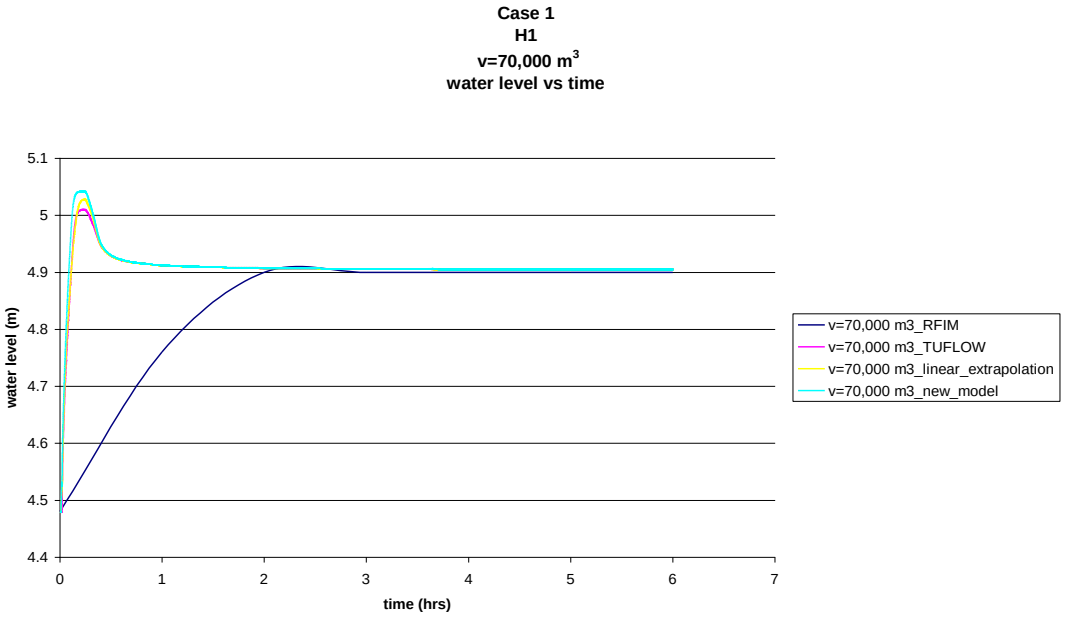

52a

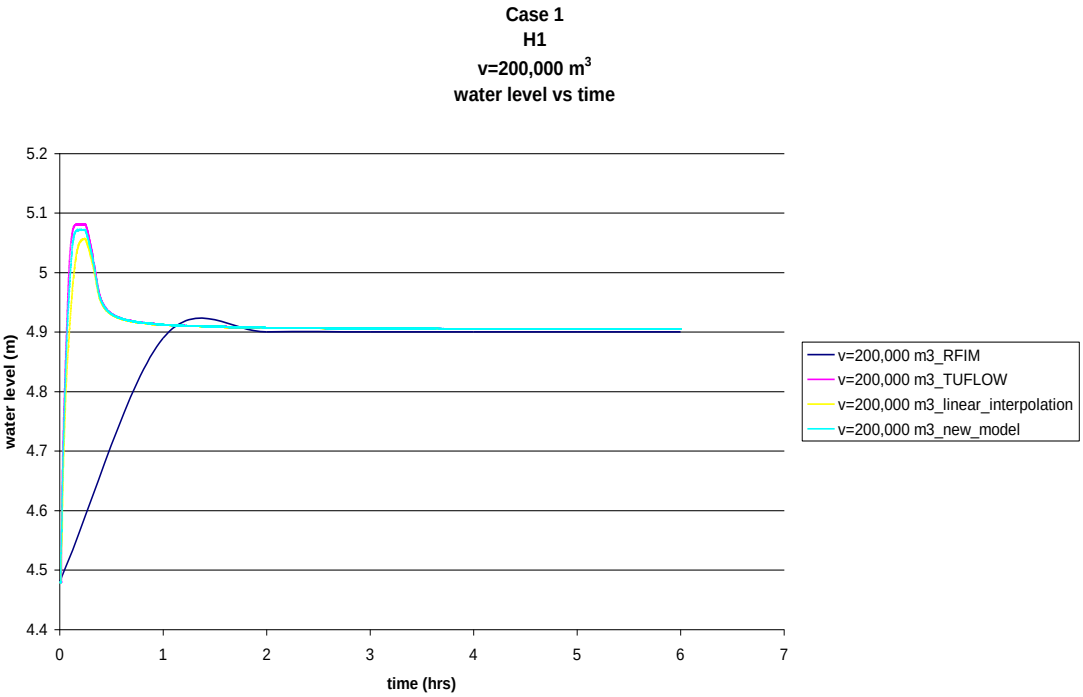

52b

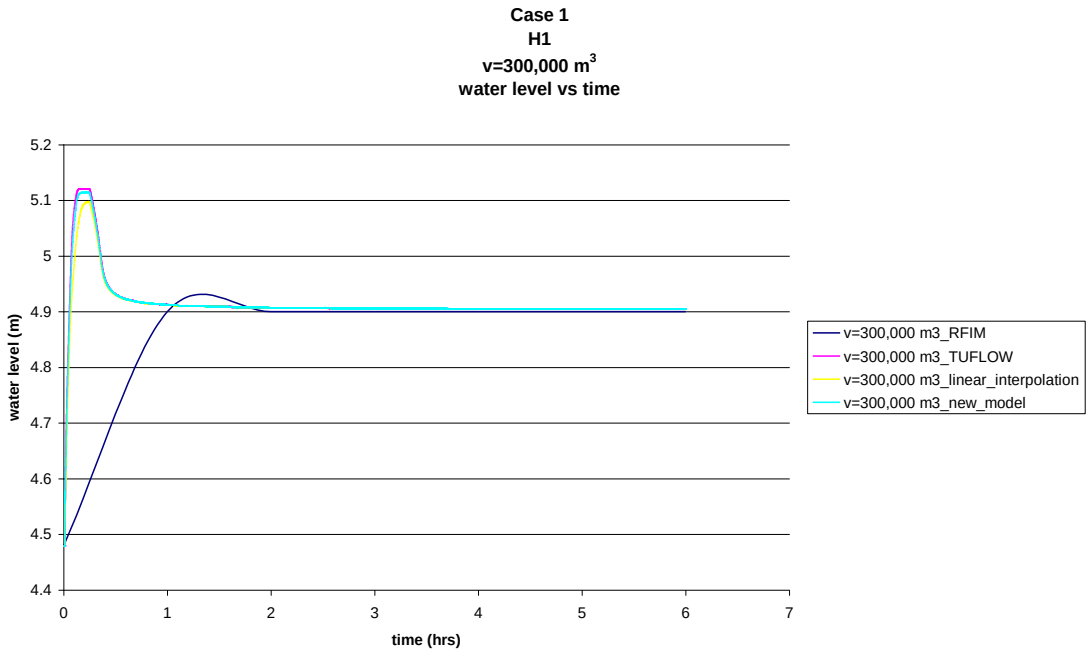

52c

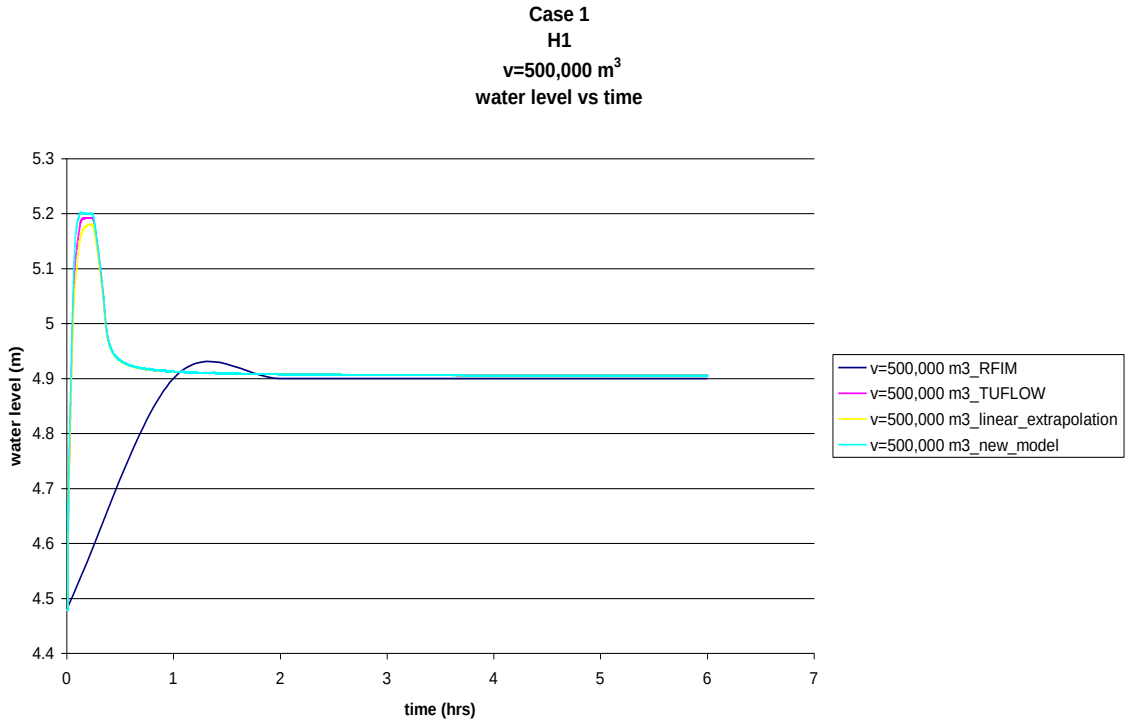

52d

Fig. 52 (a, b, c and d): water level predictions obtained from four different flood models

Another thing to notice is that TUFLOW, linear extrapolation and the new model display greater water level values than RFIM, and especially the new model predicts the largest one of all. The maximum RFIM predicted water level value is the same as predicted from all other models for their stable phase. The water level values of

TUFLOW, linear extrapolation and the new model at their stable phase is exactly the same and slightly greater than those predicted from RFIM.

It can be observed that Fig. 52b, c, d display the same characteristics of the same water level value and starting point as shown in Fig. 52a. Also, TUFLOW, linear interpolation/extrapolation and the new model display greater water level values than RFIM and especially at their stable phase the level values are slightly different if not exactly the same.

The water level values in Fig. 52b are slightly greater as it was expected since the volume to be investigated is greater.

TUFLOW displayed slightly greater values at the peak than the new model's results; however, this difference is negligible, thus, those predictions are very accurate.
The same two observations regarding the greater water level values due to greater volume and the slightly, but insignificant, greater predictions at the peak can also be seen in Fig. 52c.

The only difference between Fig. 52d and Fig. 52b, Fig. 52c is that in Fig. 52d the new model predicted slightly but insignificant greater values than TUFLOW; however, it can be said that those predictions are as accurate as TUFLOW.

- **H5**

The point H5 is shown in Fig. 51a (Chapter 3), is located at the east corner of the DTM. It has been selected because it is expected to flood not only because of the lack of barrier between the failure location and this particular cell, but also because of the slope of the DTM on the east direction (j axis).

It can be noticed that in Fig. 53 (Appendix B) TUFLOW, linear interpolation/extrapolation and the new model follow the expected pattern, meaning that the water level is stable for a short time period, then rises to its peak and then reduces until the point of its steady state. This is not the case for the RFIM which does not reach a peak point. It is noticeable that all models have the same starting point.

The water levels obtained from TUFLOW and the new model are greater than those from linear extrapolation and RFIM (Fig. 53a Appendix B); however, after a certain time RFIM predictions are larger than those predicted from simple linear extrapolation. Especially for the new model, although, its predicted values are greater than TUFLOW's, the difference between them is smaller than that between TUFLOW and linear extrapolation.

As the volume to be predicted increases (V=200,000 m^3, $Q_{max} = 13.88 m^3/s$) the difference between TUFLOW and the new model's predictions reduces (Fig. 53b, Appendix B). Once more, RFIM and linear interpolation predicted smaller values, most of the time, than the other two models.

As the volume to be predicted increases, the predicted water level values increase and the difference between TUFLOW and the new model reduces further (Fig. 53c, Appendix B), making the new model's results progressively move. It can also be noticed that although the difference between TUFLOW and linear interpolation reduced, it is still significant. RFIM retains a rising path.

Fig. 53d (Appendix B) demonstrates once more that the difference between the new model and TUFLOW is very small; however, for this particular case, TUFLOW displayed slightly greater values than the new model most of the time. Also, although, the difference between TUFLOW and linear extrapolation is small, the difference between TUFLOW and the new model is even smaller, thus, if there was a choice between the new model and linear extrapolation, the former would be chosen.

- **H15**

On the south-east corner of the DTM, the point H15 (Fig. 51a, Chapter 3) was selected because of the slope on the north-east direction of the DTM (i-j axes), since it is expected to flood.

It is noticeable in Fig. 54 (Appendix B) that RFIM predicted a smaller starting point value than the rest of the models.

In Fig. 54a (Appendix B) it is observed that RFIM's water levels are more accurate than those obtained from the new model and linear extrapolation, since there is a small

difference between it and TUFLOW. The horizontal shape of the TUFLOW curve implies that the cell was not flooded. As the new model and linear extrapolation are based on the extrapolation of results for V_{total}=100,000 m^3 ($Q_{max} = 6.94 m^3/s$) and V_{total}=400,000 m^3 ($Q_{max} = 27.77 m^3/s$), the shape of the curve follows the tidal nature of the inflow hydrographs.

Fig. 54b (Appendix B) shows that TUFLOW, linear interpolation and the new model follow the same pattern. The difference between TUFLOW and the new model is smaller than that between TUFLOW and linear interpolation, and also, although RFIM is close to TUFLOW predictions for certain time periods, it can be concluded that the new model predicted more accurate results than RFIM and linear interpolation.

The difference between TUFLOW and the new model's predictions reduces as the volume to be investigated increases (Fig. 54c, Appendix B), making the new model's results more and more accurate in relation to RFIM and linear interpolation.

Fig. 54d (Appendix B) shows, once more, that the new model displays very similar data as TUFLOW, although in this particular case the values are slightly greater. On the other hand, although the difference between TUFLOW and linear extrapolation is almost the same as the one between TUFLOW and the new model, the preference is towards the new model because its values are greater than TUFLOW's. RFIM shows lower values than the new model.

3.2 2nd CASE STUDY: Two walls at the crest of storage cells C, H and M:

- **H1**

Although the DTM in case study 2 is somewhat different than that in case study 1, the observations for point H1 (Fig. 51b, Chapter 3) are exactly the same as the ones made in Section 3.1 for H1. This happens because the conditions that hold for the particular flooded cell do not change, as H1 is located in the first cell to be flooded (defence failure location). In particular, if a wall is added at the crest of a cell or at the boundary between two cells, or the slope of the DTM changes slightly, this will not affect cell A.

So, as it can be observed in Fig. 55 (Appendix B), the predictions are exactly the same and follow the same pattern as the ones in Fig. 52 (Section 3.1), although it is a different DTM.

In particular all models display the same starting point and water level value (Fig. 55, Appendix B). TUFLOW, linear interpolation/extrapolation and the new model have very similar, if not exactly the same, predictions; however, RFIM always displays smaller values than the rest of the models. The same holds true, for all the remaining DTMs when referring to H1 (Fig. 58, 63, 67, 72, 76, 79, Appendix B).

- **H8**

Fig. 51b (Chapter 3) shows that point H8 is located at the centre of the cell which contains the gap between the two walls, thus, it is important to know the behaviour of the water as it transfers through it from one cell to the other.

Fig. 56 (Appendix B) displays the predictions of the water level for different volume magnitudes. The main observation in Fig. 56a (Appendix B) is that RFIM shows a greater time discontinuity in relation with the other predictions. Once again, the new model's predictions are very close to the ones obtained from TUFLOW. Also, the minimum predicted values come from the linear extrapolation.

The curves associated with each model follow the same pattern in Fig. 56b (Appendix B). TUFLOW displayed greater water level values than the other models; however, the difference between TUFLOW and the new model is insignificant.

The new model predicted the same water level values as TUFLOW most of the time (Fig. 56c, Appendix B). Also, RFIM predicted the same values as TUFLOW and the new model for the stable part of the curve.

The predicted values from linear extrapolation are very close to the ones obtained from TUFLOW (Fig. 56d, Appendix B); however, once again, the new model predicted closer, if not the same, values as TUFLOW, making them more accurate. RFIM predicted the same levels as TUFLOW and the new model at the constant phase of the curve.

- **H15**

Point H15 is located at the centre of the last cell of the DTM to be flooded (Fig. 51b, Chapter 3). It is examined in order to investigate the water behaviour after its transfer through the gap and its movement to that cell due to the slopes of the DTM.

Although, RFIM predicted smaller water level values than TUFLOW, it is deduced that for this particular investigation, they are more appropriate to be used than the two other predictions (Fig. 57a, Appendix B). The new model and linear extrapolation predicted greater values than TUFLOW, although that specific cell was not flooded at the particular volume of V_{total}=70,000 m^3 ($Q_{max} = 4.86 m^3/s$), due to the inclusion of linear extrapolation of V_{total}=100,000 m^3 ($Q_{max} = 6.94 m^3/s$) and V_{total}=400,000 m^3 ($Q_{max} = 27.77 m^3/s$).

The predicted water level values from TUFLOW, the new model and linear interpolation follow the same pattern (Fig. 57b, Appendix B). RFIM does not reach any particular peak point, but continues to rise throughout the run time. TUFLOW displayed greater values than the rest of the models; however, the difference between TUFLOW predictions and the new model's is smaller than that between TUFLOW and linear interpolation.

The same conclusions can be drawn for Fig. 57c (Appendix B), albeit the differences between the models are smaller.

The new model predicted larger values than the rest of the models (Fig. 57d, Appendix B). The difference between TUFLOW's predictions and the new model's is almost the same as the difference between TUFLOW and linear extrapolation; however, the new model is preferred because it is more accurate. RFIM does not reach a particular peak point but continues to rise throughout the run time.

3.3 3rd CASE STUDY: Two walls at the boundaries of the storage cells B, G and L:

- **H1**

For the particular point H1 (Fig. 51c, Chapter 3), as mentioned in Section 3.2, the same observations can be made as in Section 3.1. Therefore, Fig. 58 (Appendix B) is analysed in a similar manner.

- **H7**

The point examined here H7 (Fig. 51c, Chapter 3) is located at the centre of the flooded cell which contains the gap between the two walls at its boundary with its neighbouring cell. It is important to examine the behaviour of the water before it is transferred through the gap to the remaining cells.

The starting point of the water level is the same for all predicted curves for all 4 cases in Fig. 59 (Appendix B). It is observed that for all 4 cases the new model predicted greater values than the remaining models. In particular, in relation to TUFLOW, the new model predicted the same values for the majority of the run time, making it more appropriate to be used. As the volume to be investigated increases, the water level values increase as expected.

- **H8**

Point H8 (Fig. 51c, Chapter 3) was selected in order to examine the water behaviour after it passes through the gap between the two walls.

It is observed in Fig. 60a (Appendix B) that TUFLOW, the new model and linear extrapolation follow the same pattern, although TUFLOW displays a greater time discontinuity. Most of the time the predicted values from the new model are exactly the same as the ones obtained from TUFLOW. Another important thing to note is that RFIM, for this particular inflow volume predicted that H8 does not flood, as the water follows the lowest link and travels to the south instead of passing through the gap and flooding it.

For the examination of a greater volume (i.e. V=200,000 m^3) the new model predicted almost the same values as TUFLOW (Fig. 60b, Appendix B). On the other hand, linear interpolation predicted smaller values than the remaining models. RFIM shows a greater time discontinuity. Also, after a certain time it predicts the same values as TUFLOW and the new model.

Fig. 60c (Appendix B) shows TUFLOW and the new model to have predicted only slightly different water level values. The linear interpolation predictions are close to the ones predicted from TUFLOW. RFIM predicted the exact same values as TUFLOW and the new model, once half the run time has elapsed.

The new model predicted very similar values, most of the time, as TUFLOW; however, its predicted peak point is slightly greater (Fig. 60d, Appendix B). The predicted values from linear extrapolation are very close to the ones obtained from TUFLOW. RFIM displays the same values as TUFLOW and the new model after half of the total run time has passed.

- **H12**

Point 12 is located in the storage cell which contains one of the walls at its boundary with its easterly neighbouring cell (Fig. 51c, Chapter 3). Thus, it is necessary to examine the water behaviour as it reaches a barrier.

It is observed that both the new model and linear extrapolation have a small time discontinuity in relation to the other models (Fig. 61a, Appendix B). TUFLOW, linear extrapolation and the new model follow the same pattern, although the new model predicted greater values than the others. On the other hand, RFIM does not follow a tidal pattern as expected.

In Fig. 61b (Appendix B) all flood models display the same pattern and especially for TUFLOW and RFIM, they predicted the exact same water level values after a certain point. For this particular case, RFIM predictions are more accurate than the new model's and linear interpolation's, since they are closer to TUFLOW predictions.

A similar observation as presented in Fig. 61b is shown in Fig 61c (Appendix B); however, the water level values were greater as expected and also the difference between TUFLOW and linear interpolation, and also the difference between TUFLOW and the new model is smaller. Once again, for this particular case RFIM predictions are closer to TUFLOW results, thus, they are more appropriate to be used.

Finally, in Fig. 61d (Appendix B) the main observation is that the new model predicted very similar results to TUFLOW's. Although RFIM after a certain time predicts the same values as TUFLOW, the new model's predictions (although they are greater than TUFLOW's) are more reliable, since they are more consistent throughout the run.

- **H15**

Fig. 51c (Chapter 3), presents the last point to be flooded (i.e. H15). The slope of the terrain is the contributing issue for the flooding of the cell.

TUFLOW and RFIM predicted that for a small amount of flood water (i.e. V_{total}=70,000 m^3 ($Q_{max} = 4.86 m^3/s$)) the cell that contains point H15 does not flood (Fig. 62a, Appendix B). However, both linear extrapolation and the new model predicted that it floods, because these models are based on the linear extrapolation of V_{total}=100,000 m^3 ($Q_{max} = 6.94 m^3/s$) and V_{total}=400,000 m^3 ($Q_{max} = 27.77 m^3/s$).

For Fig. 62b (Appendix B) the new model predicted resembling water levels as TUFLOW. The water levels predicted from TUFLOW are greater than the ones obtained from the other models. Linear interpolation predicted smaller values than the other models. The highest point that RFIM reaches is the same as the peak point of TUFLOW.

Similar to Fig. 62b (Appendix B), the observations are the same in Fig. 62c (Appendix B). However, the highest water level value for RFIM is greater than the peak value of TUFLOW. Also, the predicted water levels are greater as expected.

Once more, the results shown in Fig. 62d (Appendix B) are corresponding to the ones in Fig. 62b, c (Appendix B), although the new model predicted greater values than the other models and also the difference between TUFLOW and the new model, and between TUFLOW and linear extrapolation is smaller.

The new model's results are more appropriate to be used as they are closer to the ones obtained from TUFLOW.

3.4 4th CASE STUDY: Two walls at the boundaries of storage cells B, G and L, decreasing the slopes on both directions i and j:

- **H1**

For the particular point H1 (Fig. 51c, Chapter 3), as mentioned in Section 3.2, the same observations can be made as in Section 3.1. Therefore, Fig. 63 (Appendix B) is analysed in a similar manner.

- **H6**

Point H6 is located at the cell immediately next to the cell where the defence failure occurs (Fig. 51c, Chapter 3).

For all inflow volume scenarios in Fig. 64 (Appendix B), it is observed that linear interpolation/extrapolation predicted the exact same results as the new model. This maybe attributed to the fact that the slope was steeper than in other case studies (i.e. i=0.001, j=0.001). Also, TUFLOW always predicts greater values than the rest of the models (i.e. RFIM, linear interpolation/extrapolation and the new model).

One important thing to note is that in the case of linear extrapolation (i.e. Fig. 64a, d, Appendix B) the difference between TUFLOW and the new model is smaller in comparison to the cases of linear interpolation (i.e. Fig. 64b, c, Appendix B).

In most cases RFIM predicted smaller values than the remaining flood models.

For this particular case, both the new model and linear interpolation/extrapolation can be used for water level predictions.

- **H7**

For all cases in Fig. 65 (Appendix B) linear interpolation/extrapolation predicted identical water level values as the new model. This maybe attributed to the fact that the slope was steeper than in other case studies (i.e. i=0.001, j=0.001).These values and RFIM's were always smaller than those obtained from TUFLOW; however, the difference between TUFLOW and the new model is reducing further as the inflow volume increases.

In Fig. 65a, b, c (Appendix B), RFIM follows an increasing path without reaching a peak point; however, in Fig. 65d (Appendix B) it follows a tidal shape.

Both the new model and linear interpolation/extrapolation are appropriate to be used for water level prediction.

- **H12**

Once again, the new model's predictions were identical to linear interpolation/extrapolation for all cases investigated in Fig. 66 (Appendix B). This maybe attributed to the fact that the slope was steeper than in other case studies (i.e. i=0.001, j=0.001). TUFLOW predicted greater water level values than the other models (Fig. 66b, c, d, Appendix B); however, for a small inflow volume of V_{total}=70,000 m^3 TUFLOW predicted that the cell does not flood (Fig. 66a, Appendix B).

The difference between TUFLOW and the new model reduces as the inflow volume to be examined increases (Fig. 66 b, c, d, Appendix B).

RFIM does not reach a peak point for inflow volumes of V_{total}=70,000 m^3 ($Q_{max} = 4.86 m^3/s$) and V_{total}=200,000 m^3 ($Q_{max} = 13.88 m^3/s$) (Fig. 66a, b, Appendix B). However, for V_{total}=300,000 m^3 ($Q_{max} = 20.83 m^3/s$) and V_{total}=500,000 m^3 ($Q_{max} = 34.72 m^3/s$) it follows a tidal shape (Fig. 66c, d, Appendix B).

3.5 5th CASE STUDY: Two walls at the boundaries of the storage cells B, G and L, reducing the slopes on both directions i and j:

- **H1**

For the particular point H1 (Fig. 51c, Chapter 3), as mentioned in Section 3.2, the same observations can be made as in Section 3.1. Therefore, Fig. 67 (Appendix B) is analysed in a similar manner.

- **H2**

The cell that contains point H2 is the easterly neighbour of the cell where the defence failure occurs (Fig. 51c, Chapter 3).

TUFLOW, linear interpolation/extrapolation and the new model have similar tidal shape in all case studies (Fig. 68, Appendix B). This is also the case for RFIM but only for cases shown in Fig. 68c, d (Appendix B). In Fig. 68a, b (Appendix B) RFIM does not reach a peak point but follows an increasing path.

As the inflow volume increases, the difference between TUFLOW and the new model reduces, making the new model more appropriate to be used for water level prediction purposes.

Linear interpolation/extrapolation always displays smaller values than the other flood models.

- **H6**

The examination of point H6 which is located at the centre of the southern neighbour of the defence failure location (Fig. 51c, Chapter 3) displays the same results and thus, follows the same analysis as point H2 as expected (Fig. 68, 69, Appendix B). This expectation is based on the fact that the DTM was equally inclined (i=0.001, j=0.001), so, the water should spread in the same way in both easterly and northerly direction.

- **H7**

TUFLOW and RFIM predicted that the cell that contains point H7 does not flood for this particular inflow volume (Fig. 70a, Appendix B). However, both the new model and linear extrapolation predicted water levels that follow a tidal pattern. This occurs because these two models are based on the linear extrapolation of V_{total}=100,000 m^3 ($Q_{max} = 6.94 m^3/s$) and V_{total}=400,000 m^3 ($Q_{max} = 27.77 m^3/s$) for which volume the cell floods.

For the remaining case scenarios (i.e. Fig. 70b, c, and d, Appendix B) TUFLOW, linear interpolation/extrapolation and the new model have similar tidal shapes. This is also the case for RFIM for an inflow volume of V_{total}=500,000 m^3 ($Q_{max} = 34.72 m^3/s$) (Fig. 70d, Appendix B). However, for V_{total}=200,000 m^3 ($Q_{max} = 13.88 m^3/s$) and V_{total}=300,000 m^3 ($Q_{max} = 20.83 m^3/s$), RFIM's water level values increase throughout the run time.

For most cases, the new model's predictions are close to the ones obtained from TUFLOW, thus, they are more accurate than the other predictions obtained from the remaining models.

- **H11**

Point H11 is analysed in a similar manner as Fig. 70 (Appendix B), as the graphical representation of the results is almost identical (Fig. 70, 71, Appendix B). The difference between the two Figures is that the water level values are greater in Fig. 71 (Appendix B).

3.6 6th CASE STUDY: Two walls at the boundaries of storage cells B, G and L, decreasing the elevation of the area between the walls by 0.5 m:

- **H1**

For the particular point H1 (Fig. 51c, Chapter 3), as mentioned in Section 3.2, the same observations can be made as in Section 3.1. Therefore, Fig. 72 (Appendix B) is analysed in a similar manner.

- **H7**

In all inflow volume cases, all models predicted water level values that follow the expected tidal pattern (Fig. 73, Appendix B).

The new model predicted very similar, if not exactly the same, water level values for all case scenarios as TUFLOW, making it more appropriate to be used for water level predictions.

For all cases, after a certain run time has elapsed, all flood models display the same water level value.

- **H8**

It can be observed in Fig. 74 (Appendix B) that all flood models have a similar tidal shape, and that linear interpolation/extrapolation predicted the smallest values of all models.

The water level values obtained from the new model are similar, close to the beginning of the run, to the ones obtained from TUFLOW, and after a certain time they are the same. Similarly for RFIM after a certain time period the results are identical to those from TUFLOW, although at earlier times they are much smaller.

- **H15**

Fig. 75a (Appendix B) presents a flat line for the prediction of TUFLOW and RFIM denoting that the cell does not flood. However, the remaining two flood models predicted that this particular cell floods, with water levels following a tidal shape.

For Fig. 75b, c (Appendix B) TUFLOW predicted greater values than the rest of the models for most of the time; however, for Fig. 75d (Appendix B) the new model predicted greater values than the others.

The difference between TUFLOW and the new model reduces as the volume to be examined increases, making them more and more accurate. In the same way, the difference between TUFLOW and linear interpolation/extrapolation decreases as the volume to be predicted rises.

In cases shown in Fig. 75b, c, d (Appendix B), RFIM does not present a clear tidal shape.

3.7 7th CASE STUDY: Two walls at the boundaries of storage cells B, G and L, reducing the elevation of the area between the walls by 0.5 m and reducing the area between the wall from 100m to 2m:

- **H1**

For the particular point H1 (Fig. 51c, Chapter 3), as mentioned in Section 3.2, the same observations can be made as in Section 3.1. Therefore, Fig. 76 (Appendix B) is analysed in a similar manner.

- **H2**

In all cases presented in Fig. 77 (Appendix B) TUFLOW, linear interpolation/extrapolation and the new model displayed similar predictions. On the other hand, RFIM predicted smaller values than the rest of the models.

As the inundation volume to be investigated increases, the difference between TUFLOW and the new model's predictions reduces, as well as the difference between TUFLOW and linear interpolation/extrapolation.

- **H7**

The results displayed in Fig. 78 (Appendix B) present a great similarity with the results in Fig. 77 (Appendix B), therefore the observations made through their analysis is the same. This can be attributed to the fact that the water travels from the cell where point H2 is located to the cell which contains point H7. The smaller gap between the walls at the boundary of the cell containing point H7 implies that the water transferring to this cell will not move through the gap to flood other cells. Therefore, both points (i.e. H2 and H7) will behave similarly.

3.8 8th CASE STUDY: Four walls at the boundaries of some storage cells:

- **H1**

For the particular point H1 (Fig. 51d, Chapter 3), as mentioned in Section 3.2, the same observations can be made as in Section 3.1. Therefore, Fig. 79 (Appendix B) is analysed in a similar manner.

- **H7**

All models predicted, in all cases, a similar tidal shape (Fig. 80, Appendix B).

The difference between TUFLOW and the new model is small and reduces as the inflow volume to be examined increases. In the same way, the difference between TUFLOW and linear interpolation/extrapolation decreases as the volume to be investigated increases. However, the new model's predictions are always closer to TUFLOW's than those obtained from linear interpolation/extrapolation and RFIM, making them more accurate to be used for water level prediction.

- **H8**

For V_{total}=70,000 m^3 ($Q_{max} = 4.86 m^3/s$) (Fig. 81a, Appendix B) both TUFLOW and RFIM predicted that the cell which contains point H8 does not flood, meaning that the water does not travel through the gap to that cell. On the other hand, both the new model and linear extrapolation displayed a flooded cell.

Fig. 81b, c and d (Appendix B) display similar tidal shape for the predictions of all models. In particular, for TUFLOW and the new model their predictions are becoming more and more similar as the inflow volume to be examined increases. This is also the

case for the difference between TUFLOW and linear interpolation/extrapolation which reduces as the volume to be investigated increases.

RFIM after a certain time predicted the exact same water level values as TUFLOW.
For this particular case, the new model is more accurate, thus, more appropriate to be used in water level prediction than the rest of the flood models.

- **H9**

On a similar basis to Fig. 81, Fig. 82 (Appendix B) presents the results from the analysis from point H9. The main difference is the smaller water level values, whereas the shapes and behaviour of the models are the same as described for the investigation of point H8. The greater water level values of H8 may be attributed to the fact that the cell was the first to be flooded as the water passes through the gap.

- **H12**

Fig. 83 (Appendix B) shows that all models predicted similar tidal shape. In all cases linear interpolation/extrapolation predicted the smallest values of all models. The new model displayed very similar water level values as TUFLOW which become alike, if not the same, as the volume to be predicted increases. RFIM predicted the exact same values as TUFLOW after a certain time step.

CHAPTER 4 – DISCUSSION

❖ RFIM and TUFLOW comparison observations:

In Chapter 2, a series of DTMs were examined for both RFIM and TUFLOW, in order to investigate the water behaviour. These DTMs included impermeable barriers, and/or variation in the terrain slope, and/or alteration of the size of the gap between two barriers. Flood volumes used (as mentioned in Chapter 2) varied from V_{total}=70,000 m^3 to V_{total}=400,000 m^3.

Comparisons between RFIM and TUFLOW simulations were satisfactory for a number of the cases considered here; the exception being where inertia has a significant influence on flood propagation. The general finding is that the RFIM is fit for purpose, particularly, for low inflow volume values. In these scenarios RFIM predictions are similar to the ones obtained from TUFLOW. Therefore, the short computation time of RFIM establishes it as fit for purpose in these low inflow volume scenarios. On the other hand, for higher inflow volume values TUFLOW predicts additional flooded cells with significant amount of water. As a result, the necessity arises for TUFLOW to be used in these scenarios. Some issues for each case study are given below.

➢ *1st Case study: Introduction of flat areas around the lowest link*:

The flood extent changes as the water increases from V_{total}=70,000 m^3 to V_{total}=100,000 m^3 for both models, as expected. More flooded cells are predicted for both models; however, the flood extent (and flooding order) remain the same for both models as the water volume increases to V_{total}=200,000 m^3, V_{total}=300,000 m^3 and V_{total}=400,000 m^3, this implies that those cells have reached their maximum flood volume capacity. In particular, for both models, the flood volume contained within the first 4 flooded cells (i.e. storage cells A-D) remains the same although the inflow volume increases. Also, the predicted water levels for those cells are the same for both models and remain the same despite the increase in the inflow volume. The predicted flood extent from both models is completely different in all case scenarios. This is a result of the effect of inertia which is not captured by RFIM.

For the cases V_{total}=100,000 m^3 to V_{total}=400,000 m^3 both models have predicted the same flooded cells which contain the maximum amount of flood water (i.e. storage cells E, J and O). This suggests that the slope of the terrain has an important effect on the

flood extent, a combination with the fact that no impermeable barriers are introduces in the DTM.

The smallest percentage of flood volume difference is +0.1% (for all cases) and it is displayed at storage cell A (where the defence failure occurs); however, the maximum difference occurs at storage cell E for cases V_{total}=200,000 m^3, V_{total}=300,000 m^3 and V_{total}=400,000 m^3. For the former, the effects of inertia are not very noteworthy, since, in that the defence failure occurs, whereas, for the latter, the effects of the momentum are significant.

For V_{total}=70,000 m^3, where the % of flood volume difference is very small, both models could be used for inundation prediction purposes. For all other volume scenarios, where the % of flood volume difference is great and the flood extent difference is more obvious, TUFLOW is more appropriate to be used, since the effects of inertia are more significant.

- ***2nd Case Study: Introduction of flat areas around the lowest link and two walls at the crest of the Storage cells C, H & M:***

The flood extent changes for RFIM as the water increases from V_{total}=70,000 m^3 to V_{total}=200,000 m^3, as one would expect, but then is the same until V_{total}=400,000 m^3, where the predicted flooded cells reached their maximum capacity of flood volume. On the other hand, TUFLOW predicted different flood extents as the water increases from V_{total}=70,000 m^3 to V_{total}=300,000 m^3 and then remains the same for V_{total}=400,000 m^3. In general, however, in all inflow volume scenarios, TUFLOW displays a greater number of flooded cells than RFIM.

For both models the flood volume contained in the storage cells A, B, C and H remains the same, although the inflow volume increases from V_{total}=70,000 m^3 to V_{total}=400,000 m^3, due to the location of the walls. Also, as the inflow volume increases from V_{total}=200,000 m^3 to V_{total}=400,000 m^3 the volume contained in storage cells E, J and O increases by approximately 30,000 m^3 for each cell, for both models, since all other flooded cells have reached their maximum flood volume capacity, any increase of the Vtotal will be contained with those last cells to be flooded. Also, for TUFLOW the volume increases by 4,000 m^3 for storage cells F, G, M and N from V_{total}=200,000 m^3 to

V_{total}=300,000 $m^3$and from V_{total}=300,000 m^3 to V_{total}=400,000 m^3. The location of the walls displays a great role in this.

From V_{total}=100,000 m^3 to V_{total}=400,000 m^3 both models have predicted the same flooded cells which contain the maximum amount of flood water (i.e. storage cells E, J and O).

The smallest percentage of flood volume difference is +0.1% (for all cases) and it is displayed at the storage cell A (where the defence failure occurs), as explained in 1st case study. However, the maximum difference occurs at storage cell I for V_{total}=70,000 m^3, at storage cell O for V_{total}=100,000 m^3 and storage cell E for V_{total}=200,000 m^3, V_{total}=300,000 $m^3$and V_{total}=400,000 m^3, which are the last cells to flood in each of the corresponding volumes. The locations of the barriers, as well as the slope of the terrain, display a great role in this.

For the inflow volume of V_{total}=70,000 m^3, both flood models are appropriate to be used for flood inundation prediction purposes. However, for all the remaining of the inflow volume scenarios, TUFLOW is more applicable, since the additional cells contain a significant amount of flood volume, which cannot be ignored.

- ***3rd Case Study:* Introduction of flat areas around the lowest link and two walls at the boundaries of the Storage cells B, G &L:**

The flood extent changes as the inflow volume increases. For RFIM this is the case for V_{total}=70,000 m^3 until V_{total}=200,000 m^3. From there until V_{total}=400,000 m^3 the flood extent is the same. On the other hand, for TUFLOW the flood extent is changing from V_{total}=70,000 m^3 until V_{total}=200,000 m^3. From there until V_{total}=300,000 m^3 the flood extent is the same. However, from V_{total}=300,000 m^3 to V_{total}=400,000 m^3 the flood extent changes. In general, as the V_{total} increases, the number of flooded cells rises. Once the previous flooded cells have reached their maximum flood volume capacity, the remaining flood volume is transferred to cells that have not flooded yet. This process continues until the entire amount of flood volume is spread.

For V_{total}=200,000 m^3, V_{total}=300,000 m^3 and V_{total}=400,000 m^3 both flood models predicted that the maximum amount of flood volume was contained in storage cell O

(the last cell to flood). Both the location of the barrier and the slope of the terrain have a role to play in this.

The smallest percentage of flood volume difference is +0.1% for all scenarios and it is located at the storage cell A (where the defence failure occurs), as analysed in 1st case study. However, the maximum difference occurs at storage cell I for V_{total}=100,000 m^3 and it is +96.8%. The maximum difference for V_{total}=70,000 m^3 occurs at storage cell L and it is -92.5%, for V_{total}=200,000 m^3 the maximum difference occurs at storage cell E and it is 48.6%, for V_{total}=300,000 m^3 it occurs at storage cell E and it is -12.5%, and for V_{total}=400,000 m^3 it occurs at storage cell E and it is -14.2%. The simplified representation of the hydraulic processes of the RFIM (Krupka, M. (2008), in combination with both the location of the barriers with the slope of the terrain lead to differences of the predicted flood extent, and so, flood volume difference in the corresponding flooded cells.

The predicted final water levels from both flood models for the corresponding flooded cells, for all inflow volume scenarios, were very similar, with TUFLOW displaying slightly greater values than RFIM.

Generally, for this particular case study and the majority of the inflow volume scenarios (apart from V_{total}=70,000 m^3), TUFLOW is more suitable to be used for flood inundation prediction purposes, since the dynamic effects of inertia are significant.

- ***4th Case Study:* Introduction of flat areas around the lowest link and two walls at the boundaries of the Storage cells B, G & L, decreasing the slopes on both directions I and j:**

For RFIM, the flood extent remains the same for V_{total}=70,000 m^3 and V_{total}=100,000 m^3. From V_{total}=200,000 m^3 to V_{total}=400,000 m^3 the number of flooded cells increases gradually. For TUFLOW, the flood extent changes in all inflow volume scenarios. The number of flooded cells increases gradually, as the total volume to be spread increases. In all case studies the flood extent displayed by both models is very similar, due to the same slopes on both i and j directions; however, TUFLOW displayed additional flooded cells than RFIM for most of the flood volume scenarios.

For all inflow volume scenarios and for both models, storage cells A, B and F contain the same flood volume, implying that they have reached their maximum flood volume capacity from the first case of V_{total}=70,000 m^3. Especially, for RFIM and for V_{total}=300,000 m^3 and V_{total}=400,000 m^3 it could be concluded that the majority of the predicted cells contain the same volume (apart from storage cells N and O), meaning that they reached their maximum capacity of flood water. Another important point to notice is that from V_{total}=100,000 m^3 to V_{total}=400,000 m^3 for both models storage cell L contains the maximum amount of flood volume, implying that for this particular scenario the walls (and not the slope of the DTM), play the major role in terms of the water spreading.

The smallest percentage of flood volume difference is for all inflow volume scenarios +2.3% and it is located at the cell where the failure occurs, as explained in 1st case. However, the maximum difference occurs at storage cell L for V_{total}=100,000 m^3 and it is -42.6%. For V_{total}=70,000 m^3 and V_{total}=200,000 m^3 the maximum percentage of the difference is 10.0% and it is located at the storage cell F for both cases. For V_{total}=300,000 m^3 the maximum percentage is -41.3% and for V_{total}=400,000 m^3 it is -33.0%. From these it could be concluded that there is a large fluctuation of the maximum percentage of the flood volume difference as the inflow volume increases. The slope of the terrain plays a great role in the determination of the flood extent, and in extension, the flood volume contained in the corresponding flooded cells.

For V_{total}=70,000 m^3, V_{total}=200,000 m^3 and V_{total}=300,000 m^3, both flood models can be used to predict the flood extent; however, for V_{total}=100,000 m^3 and V_{total}=400,000 m^3, TUFLOW is more suitable for the inundation extent prediction. One additional flooded cell was predicted from TUFLOW than RFIM (in both scenarios), which contains a significant amount of water that cannot be ignored. Therefore, it is considered necessary to use the more accurate flood model (i.e. TUFLOW) to capture the effect of these additional flooded cells in the flooding. The appearance of these additional cells is due to the flat slopes of the terrain, which only allow for the water spreading in extent when specific volume values are reached (i.e. V_{total}=100,000 m^3 and V_{total}=400,000 m^3). This could be a topic for further investigation.

- ***5th Case Study:* Introduction of flat areas around the lowest link and two walls at the boundaries of the Storage cells B, G & L, reducing the slopes on both directions i and j:**

For RFIM the flood extent remains the same for V_{total}=70,000 m^3 and V_{total}=100,000 m^3 and for V_{total}=200,000 m^3 and V_{total}=300,000 m^3. For V_{total}=400,000 m^3 only one more cell was predicted (6 flooded cells). For TUFLOW the same flood extent is obtained for V_{total}=70,000 m^3 and V_{total}=100,000 m^3. From V_{total}=200,000 m^3 to V_{total}=400,000 m^3 the number of the predicted flooded cells increases gradually. For V_{total}=70,000 m^3, V_{total}=100,000 m^3 and V_{total}=200,000 m^3 both models predicted the exact same flood extent. For V_{total}=300,000 m^3 and V_{total}=400,000 m^3, TUFLOW always predicted one additional flooded cell than RFIM.

In all cases of inflow volume for RFIM, storage cells B and F, G and K had the same or very similar flood volume values, due to the flat terrain. Storage cell A contained the same volume in all case studies, as explained in 1st case study. Storage cells B and F contained the same volume from V_{total}=200,000 m^3 to V_{total}=400,000 m^3, meaning that they reached their maximum flood volume capacity. On the other hand, for TUFLOW for V_{total}=300,000 m^3 and V_{total}=400,000 m^3 the flood volume values for storage cells A and B, and F and G were very similar, due to the flat slopes of the terrain.

Both flood models predicted that at V_{total}=400,000 m^3**,** storage cell L contained the maximum flood volume, implying that for this particular scenario the walls, rather than the slope of the terrain, played the major role in terms of the water spreading.

The smallest percentage of the flood volume difference was +2.0% which was located at the cell B, which is the on the easterly direction of the defence failure location, and the maximum percentage was -54.3% for V_{total}=200,000 m^3. For V_{total}=70,000 m^3 the maximum percentage was -36.6%, for V_{total}=100,000 m^3 it was -13.1%, for V_{total}=300,000 m^3 it was -51.2% and for V_{total}=400,000 m^3 it was -17.1%. It is important to mention that for V_{total}=70,000 m^3 the minimum percentage was +2.5% and was located at the cell where the failure occurs. The slope of the terrain is responsible for the flood extent, mostly contained within the cells westerly of the barriers, in extension; it affects the predicted flood volume enclosed in the corresponding flooded cells.

For inflow volumes from V_{total}=70,000 m^3 to V_{total}=200,000 m^3, both models predicted the exact same flood extent; however, for larger inflow volumes (i.e. V_{total}=300,000 m^3 to V_{total}=400,000 m^3) the effects of inertia become more significant, thus, TUFLOW is more appropriate to be used.

- ***6th Case Study:* Introduction of flat areas around the lowest link and two walls at the boundaries of the Storage cells B, G & L, decreasing the elevation of the area between the walls by 0.5m:**

For RFIM, the number of flooded cells increased gradually from V_{total}=70,000 m^3 to V_{total}=200,000 m^3. From there the flood extent was the same until V_{total}=400,000 m^3, implying that the predicted flooded cells reached their maximum flood volume capacity. On the other hand, for TUFLOW the number of flooded cells increased gradually from V_{total}=70,000 m^3until V_{total}=300,000 m^3. From there the flood extent was the same until V_{total}=400,000 m^3. The flood extent obtained by both flood models is very similar, following a similar flow path. However, in all inflow volume scenarios, TUFLOW displays a greater number of flooded cells than RFIM, due to the simplified representation of the hydraulic processes of RFIM (Krupka, M. (2008)).

For all inflow volume scenarios, for RFIM, storage cells A, B, G and H contained the same flood volume, meaning that they reached their maximum capacity of flood volume from the first inflow volume scenario. Storage cells A and B contain the same amount of flood water from V_{total}=70,000 $m^3$to V_{total}=400,000 m^3 for TUFLOW, meaning that they reached their maximum flood volume capacity from the first inflow volume scenario. Both models predicted from V_{total}=200,000 m^3 until V_{total}=400,000 m^3 that cells E, J and O, which are located on the easterly direction of the DTM, contained higher flood volumes. The steep slopes of the terrain imply that these last cells to be flooded will attract more water. Especially for cell O, which is the last cell to be flooded, it contained the maximum flood volume.

The smallest percentage of the flood volume difference for the corresponding flooded cells was +0.1% (at the cell where the failure occurs) for all inflow volume scenarios, as analysed in 1st case study. The maximum percentage of the difference was -57.9% for V_{total}=70,000 m^3 and was located at cell I. For the remaining inflow volume scenarios the maximum difference was +22.1% for V_{total}=100,000 m^3at cell J, -34.7% for V_{total}=200,000 m^3 at cell E, -28.0% for V_{total}=300,000 m^3at cell E and -24.5% for

V_{total}=400,000 m^3 at cell E, which are the last cells to flood. This implies that the slope of the terrain plays a great role in this.

For the same flooded cells, for both models, there appears to be similar final water levels. TUFLOW displayed slightly greater values than RFIM.

For an inflow volume of V_{total}=70,000 m^3 and from V_{total}=200,000 m^3 to V_{total}=400,000 m^3 TUFLOW can be utilised in terms of flood inundation extent, since it predicted more flooded cells (containing a significant amount of flood volume) than RFIM. However, this was not the case for V_{total}=100,000 m^3, in which case, both models could be used to predict the flood extent.

- ***7th Case Study:* Introduction of flat areas around the lowest link and two walls at the boundaries of the Storage cells B, G & L, reducing the elevation of the area between the walls by 0.5m and reducing the area between the walls from 100m to 2m:**

For RFIM the number of flooded cells increases gradually from V_{total}=70,000 m^3 to V_{total}=200,000 m^3. From V_{total}=200,000 m^3 to V_{total}=400,000 m^3 the flood extent is the same, following the same flow path. On the other hand, for TUFLOW the flood extent is identical for all inflow volume scenarios. The predicted flood extents from the two models display different flood extent for all inflow volume scenarios. RFIM predicted that the water travels through the gap and floods the cells on the easterly direction of the walls. So, it could be concluded that for this particular case, the decrease of the elevation of the area close to the gap assisted, so, most of the flood volume be spread to the cells on the easterly direction of the walls, since RFIM is based on the lowest link. On the other hand, TUFLOW which does not have such a limitation predicted flooded cells only on the westerly direction of the walls. So, the small gap between the walls prevented the flood volume be spread to the easterly direction of the walls, thus, most of the flood volume was stored in the cell on the south (i.e. storage cell L).

For RFIM predictions, storage cells A, B, G and H contained the same amount of flood volume in all inflow volume scenarios, implying that they reached their maximum flood volume capacity from the first inflow volume scenario (i.e. from V_{total}=70,000 m^3). This is also the case for cell I for the scenarios from V_{total}=100,000 m^3 to V_{total}=400,000 m^3. Cells E, J and O had each an almost constant increase of approximately 30,000 m^3 from V_{total}=100,000 m^3 to V_{total}=400,000 m^3, implying that the increase of 100,000 m^3 from

one inflow scenario to the next was split almost equally between those cells. For TUFLOW, only the cell where the failure occurs (i.e. storage cell A) contained the same amount of flood volume. The remaining of the predicted cells had a gradual increase. Especially cells B, G and L, which contain a wall on their boundary, each had a constant increase of approximately 30,000 m^3, for each of the scenarios from V_{total}=100,000 m^3 to V_{total}=400,000 m^3.

The smallest percentage of flood volume difference was +0.1% in all inflow volume scenarios and it was located at the cell where the failure occurs (i.e. storage cell A). The maximum percentage of the flood volume difference is +709.5% for V_{total}=400,000 m^3 and occurred at cell G. The other maximum percentages for the remaining of the scenarios where predicted at cell G and were +25.2% for V_{total}=70,000 m^3, +76.8% for V_{total}=100,000 m^3, +292.6% for V_{total}=200,000 m^3 and +501.5% for V_{total}=300,000 m^3. The smaller size of the gap between the two barriers does permit TUFLOW flood cells beyond it. Thus, this difference increases as the V_{total} rises.

For the corresponding flooded cells the final water levels were very similar. TUFLOW displayed greater values than RFIM.

Although, RFIM predicted more cells (in all flood volume scenarios) than TUFLOW, and one would expect this to be the most appropriate flood model for inundation extent prediction, this is not the case, since in real life situations some effects of inertia would exist.

- ***8th Case Study: Introduction of flat areas around the lowest link and four walls at the boundaries of some Storage:***

For RFIM the flood extent remains the same for V_{total}=70,000 m^3 and V_{total}=100,000 m^3, and then increases gradually for the remaining V_{total}. On the other hand, for TUFLOW the inundation extent is the same for V_{total}=70,000 m^3 and V_{total}=100,000 m^3, from there it increases as the V_{total} rises gradually. For V_{total}=70,000 m^3 and V_{total}=100,000 m^3 the predicted flood extent obtained by both models is very similar; however, TUFLOW displayed one additional flooded cell compared to RFIM. Although, the total number of flooded cells is the same for both models when the total volume is V_{total}=200,000 m^3 these cells are not the same in terms of location. For a V_{total}=300,000 m^3 and V_{total}=400,000 m^3 the inundation is very similar for both models; however, once again,

TUFLOW displayed 2 additional flooded cells than RFIM. In general, it could be concluded in both models follows the same path.

For all inflow volume scenarios storage cells A, B, G, and L for RFIM contained the same flood volume, meaning that those cells have reached their maximum flood volume capacity from the first inflow volume scenario (i.e. from V_{total}=70,000 m^3). This is also the case for cells H, I and L for V_{total}=200,000 m^3 until V_{total}=400,000 m^3. For TUFLOW for all inflow volume scenarios storage cells A, B, G and L contain the same amount of flood water, implying that they have reached their maximum flood volume capacity from the first inflow volume scenario (i.e. from V_{total}=70,000 m^3). This is also the case for V_{total}=200,000 m^3 until V_{total}=400,000 m^3 for storage cells H, I and M. The remaining of the predicted cells increase their flood volume as the V_{total} rises. One important observation to be made is that storage cells E, J and O contain high flood volume values, due to the interaction of the location of the gap between the walls and the slopes of the terrain In particular, storage cell O for V_{total}=400,000 m^3 contains the maximum flood volume of all cells.

The smallest percentage of flood volume difference is +0.1% for all inflow volume scenarios and it is located at the cell where the failure occurs (i.e. storage cell A), as explained in 1st case study. The maximum percentage of flood volume difference is -54.4% for V_{total}=70,000 m^3 and it is located at cell M. The maximum percentage of the other scenarios is -14.6% at cell M for V_{total}=100,000 m^3, +19.2% for V_{total}=200,000 m^3 at cell J, -18.4% at cell E for V_{total}=300,000 $m^3$and -13.0% for V_{total}=400,000 m^3at cell E. The location of the barriers has an important effect on the flood extent.

For the corresponding flooded cells the predicted final water levels are very similar for both models, although TUFLOW displayed slightly greater values than RFIM.

Both flood models can be used to predict the flood extent in all inflow volume scenarios, since the dynamic effects of the flood wave propagation are insignificant.

GENERAL OBSERVATIONS:

In general, RFIM predicts results comparable to those obtained from TUFLOW in most of the cases and inflow volume scenarios. Their differences are attributed to the effects of inertia captured by the momentum equation, included only in TUFLOW.

Consequently, in terms of accuracy TUFLOW is the most appropriate flood inundation model to be used; however, the small computation time of RFIM makes it as applicable as TUFLOW, in the prediction of flood parameters, particularly, when small inflow volumes are investigated.

The inflow volume values were restricted from V_{total}=70,000 m^3 to V_{total}=400,000 m^3 as representative values of a typical tidal or storm surge event. Higher values were avoided in order to prevent potential failures of the impermeable barriers in the DTMs. Such failures were not addressed in this thesis; however, they could be topics for further research.

An important observation is that the % of flood volume difference between the two models in the flooded cell where the failure occurs (i.e. storage cell A) has the same value of +0.1% for most of the case studies and inflow volume scenarios as analysed in 1st case study.

For this piece of work, it can be observed that the differences in the predicted results from both the RFIM and TUFLOW are considered to be the effect of the simplified representation of the hydraulic processes of the RFIM as mentioned in Krupka, M. (2008).

The DTMs developed were considered to be the most effective in capturing the majority of flood event scenarios. However, other forms of the DTMs could be used, such as a network of inverted pyramids with circular plan (Liu, Y. et al 2010) instead of a rectangular plan. Also, the size or the location of the impermeable barriers could change. Finally, the defence failure could be placed at a different location. The predictions of the flood parameters are not expected to display great differences with the ones obtained in this thesis, if these changes are made.

The RFIM was applied only to a number of artificial DTMs; however, it can also be applied to real topographies as Krupka, M. (2008) and Alevyzaki, S. (2007) did at Greenwich and Thamesmead Embayments (both sites are densely populated and could be subject to severe consequences on the occasion of flood events).

❖ **New Rapid Flood Modelling technique:**

The combination of accuracy and small computation time would be ideal for a flood inundation model. This was the reason for the development of a new RFIM. The main results obtained from the analysis of the new RFIM are mentioned below:

- In all case studies for most of points investigated the RFIM predictions are smaller than those obtained from TUFLOW, linear interpolation/extrapolation and the new model. As expected, the results obtained from linear interpolation/extrapolation and the new RFIM are very similar to those obtained from TUFLOW in most of the points examined, since, those model techniques are closely linked. On the other hand, RFIM water level predictions are disimilar to those obtained from the rest of the models, may be due to the simplified representation of the hydraulic processes as mentioned in Krupka, M. (2008).
- For all case scenarios point H1 does not display a large time discontinuity as it occurs for all other points. It seems that the water level rises as soon as the defence failure occurs. In all case studies, for all models point H1 follows the same typical tidal pattern, with its values rising as the V_{total} investigated increases. This implies that storage cell A, which is the first cell to flood (since it contains the defence failure), is not affected by the location of the impermeable barriers in neighbouring cells. Thus, changes in the DTMs' layout would not affect the general water level predictions at H1.
- Especially, for point H1 all TUFLOW data, meaning TUFLOW, linear interpolation/extrapolation and the new model are very similar to each other. In particular, the new model's results are the same as TUFLOW's, making them as accurate as TUFLOW's. As mentioned before, this may be attributed to its location at the storage cell (i.e. A), where the defence failure occurs.
- In case study 4, for all points examined (i.e. H1, H6, H7, H12) and for all inflow volume scenarios, the new model predicted the exact same water level values as linear interpolation/extrapolation. This is a result of the flat slope of the terrain (i.e. i = 0.001, j = 0.001); however, this is not the case for case study 5 where the terrain is almost completely horizontal.
- In general, for most of the cases investigated the new model displayed similar water level values as TUFLOW and the difference between these values reduces as the inflow volume to be investigated increased. Therefore, for large inflow volume scenarios, the new RFIM serves its purpose giving as accurate as TUFLOW results.

However, this is not the case for low inflow volume values, (e.g. V_{total}=70,000 m^3) where the new RFIM predicted dissimilar water level values to TUFLOW, due to the extrapolation of V_{total}=100,000 m^3 and V_{total}=400,000 m^3. In particular, for some points (e.g. H15) that are not predicted as flooded from TUFLOW, appear flooded in both the new RFIM and linear interpolation/extrapolation, since the flood volume value is the effect of extrapolation. So further investigation is recommended for future work.

CHAPTER 5– CONCLUSIONS

❖ RFIM and TUFLOW comparison observations:

This thesis investigated the comparison of the predicted flood parameters in different scenarios, between the RFIM and TUFLOW, in order to examine in which case RFIM predicts as accurate results as TUFLOW. Therefore the main conclusions of this piece of research are:

- The gradient of the terrain has an important effect on the flood extent. For topographies that have steep slopes (i.e. i = 0.0002 and j = 0.002) the number of flooded cells rises as the inflow volume increases (i.e. from V_{total}=70,000 m^3 to V_{total}=400,000 m^3), as expected. This is the case for both the RFIM and TUFLOW. On the other hand, for DTMs with flat slopes (i.e. i = 0.001, j = 0.001 and i = 0.0002, j = 0.0002) the number of flooded cells starts to increase, only when inflow volume values become large (e.g. V_{total}=300,000 m^3) for both flood models.
- Similar to the inundation extent, the contained flood volume in each flooded cell (apart from the failure location cell) increases as the V_{total} rises, depending both on the slopes of the terrain and the location of the barriers.
- Another important observation regarding the effect of the inclination is the small percentage of the flood volume difference between the two flood models on the failure location cell, for most of the case studies and for all inflow volume scenarios. Both flood models predicted almost identical food volume values on the failure location, since, for the first cell to flood, the effects of inertia are insignificant.
- For the same inflow volume and different slopes on the i (i = 0.0002) and j (j = 0.002) axes the predicted flood extent for both the RFIM and TUFLOW is relatively the same. The flooding order is different apart from the cell that the failure occurs and its neighbour cell.
- For the same slope on the i (i=0.0002) and j (j=0.0002) axes and different volumes the flood extent and the flooding order are exactly the same for RFIM and TUFLOW for most of the volume scenarios tested. This is a result of the flat terrain.
- The water level for all cases of investigation was very close for both models. However TUFLOW displays a greater value of flood depth.
- One of the most important differences between the RFIM and TUFLOW is the run time. TUFLOW (it takes almost 1 hour to run) requires more run time in order to predict the inundation extent, the flooding order, the flood depths and all the other flood parameters than RFIM (it only needs 10-15 minutes to run both routines).

- Another important difference between the two models is that the RFIM displays a greater value of flood volume for the corresponding flooded cells with TUFLOW for most of the cases, due to the prediction of smaller flood extent than TUFLOW.
- In general, for this piece of work it can be concluded that the differences of the results between the two models can be attributed to the fact that TUFLOW contains the momentum equation which allows it to simulate the effect of inertia. However, RFIM does not capture this. Therefore, in some cases, the effects of the momentum are more important and although RFIM is faster, TUFLOW would be preferred as it captures this effect.

❖ **New Rapid Flood Modelling technique:**

The limitations of the RFIM in comparison to TUFLOW led to the development of a more accurate Rapid Flood Model (i.e. new RFIM). Comparisons between TUFLOW simulations and the new Rapid Flood modelling technique show some potential in predicting water level and timing of inundation. For most of the inflow volume cases investigated the new model displayed similar water level values as TUFLOW and the difference between these values reduced as the inflow volume to be investigated increased. However, the comparisons, in terms of water level prediction, deteriorated at the extremities of the flood extent, because of the fact that in some cases the flood volume is obtained through extrapolation as mentioned in Chapter 4. For large inflow volume scenarios the new RFIM combines both the accuracy of TUFLOW and small computation time, so, it is appropriate to be used. For low inflow volume scenarios TUFLOW is more applicable to be used. In general, it can be concluded that the new Rapid Flood Model fulfilled the aim of this thesis, namely, achieving a short run time similar to RFIM, and producing as accurate results as TUFLOW. Further detailed analysis is necessary to finally determine the potential of this method.

FUTURE WORK:

Future analysis could include the examination of higher inflow volume scenarios in order to investigate the behaviour of the water when a failure (overtopping or breaching) of impermeable barriers occur (as briefly mentioned in Chapter 2). The new RFIM can be extended to examine other flood parameters such as water depth and flow velocity. Finally, it could be applied to real topographies in order to be examined under real life conditions.

REFERENCES

1. **Alevyzaki, S.,** (2007), ***Investigation of the Flooding at a Coastal Site, using a Flood Inundation Model,*** MSc Thesis – Department of Civil Engineering, University of Glasgow
2. **Baldassarre, G., Castellarin, A., Montanari, A., Brath, A.,** (2009), ***Probability weighted hazard maps for comparing different flood risk management strategies: a case study,*** Natural Hazards. doi: 10.1007/s11069-009-9355-6
3. **Baldassarre, G., Schumman, G., Bates, P., Freer, J., Beven, K.,** (2010), ***Flood-plain mapping: a critical discussion of deterministic and probabilistic approaches,*** Hydrological Sciences Journal, 55:3, 364-376
4. **Balica, S.F., Wright, N.G., Van der Meulen, F.,** (2012), ***A flood vulnerability index for coastal cities and its use in assessing climate change impacts,*** Natural Hazards, DOI: 10.1007/s11069-012-0234-1
5. **Balica, S.F., Popescu, I., Beevers, L., Wright, N.G.,** (2013), ***Parametric and physically based modelling techniques for flood risk and vulnerability assessment: a comparison,*** Environmental Modelling and Software, volume 41, March 2013, pp. 84-92
6. **Ballinger, J., Jackson, B., Pechlivanidis, I., Reis, W.,** (2011), ***Potential flooding and inundation on the Hutt River,*** New Zealand Climate Change Research Institute Victoria University of Wellington
7. **Bamford, T., Balmforth, D., Digman, C., Waller, S., Hunter, N.,** (2008), ***Modelling Flood Risk Assessment, an Evaluation of Different Methods,*** WaPUG Autumn Conf. 2008
8. **Bates, P.D., De Roo, A.P.J.,** (2000), ***A simple raster – based model for floodplain inundation,*** Journal of Hydrology, 236, pp. 54-77
9. **Bates, P.D., Dawson, R.J., Hall, J.W., Horitt, M.S., Nicholls, R.J.,Wicks, J.,Hassan, M.A.A.M.,** (2005), ***Simplified two-dimensional numerical modelling of coastal flooding and example applications,*** Coastal Engineering 52 (2005), pp 793,810
10. **Beevers, L., Douven, W., Lazuardi, H., Verheij, H.,** (2012), ***Cumulative impacts of road developments in floodplains,*** Transportation Research Part D: Transport and Environment, volume 17, issue 5, July 2012, pp. 398-404
11. **Beven, K.J., Freer, J.,** (2001), ***Equifinality, data assimilation, and uncertainty estimation in mechanistic modelling of complex environmental systems,*** Journal of Hydrology. 249, 11-29

12. **Bradbrook, K.,** (2006), ***A multiscale two – dimensional dynamic model,*** Water and Environment Journal 20, pp 79-86
13. **Burns, T.,** (2009), ***Applied statistics and strength of Materials,*** 2nd Edition, eISBN 9781467285339
14. **Deb, K.** (2001), ***Genetic Algorithms for Optimization,*** Department of Mechanical Engineering, Indian Institute of Technology Kanpur
15. **Deb, K.,** (2004), ***Genetic Algorithms for optimisation,*** In D. Kundu and A. Basu (eds.), Statistical Computing: Existing Methods and Recent Developments, New Delhi, India: Narosa Publishing House, pages 85-123
16. **DEFRA,** (2006), ***Engineering Guide to Emergency Panning for UK Reservoirs,*** Appendix A: Emergency Planning Generally, Draft Guide: Volume 1
17. **DHI Water and Environment,** (2001), ***MIKE 3, Estuarine and Coastal Hydraulics and Oceanography***
18. **East London SFRA,** Embayment Risk Assessments, Appendix G
19. **Environment Agency,** (2005), ***The Mersey Estuary Catchment Flood Management Plan,*** Scoping Report-November 2005
20. **Environment Agency,** (2009), ***Desktop review of 2D hydraulic modelling packages,*** Science report – SC080035/SR (EXCERPT)
21. **Fleming, G.,** (2002), ***Learning to live with rivers – the ICE's report to government,*** Proceedings of ICE, Civil Engineering 150, May 2002, pp 15-21, Paper 12774
22. **Gouldby, B., Sayers, P.B., Mulet-Marti, J., Hassan, M.A.A.M and Benwell, D.,** (2008), ***A methodology for regional-scale flood risk assessment,*** Proceedings of the Institution of Civil Engineers, Water Management 161, issue WM3, pp. 169-182 (June 2008)
23. **Hall, J.W., Meadowcroft, I.C., Sayers, P.B. and Bramley M.E.,** (2003), ***Integrated Flood Risk Management in England and Wales,*** Natural Hazards Rev., Volume 4, Issue 3, pp. 126-135 (August 2003)
24. **Hall, J.W.,** (2003), ***Handling uncertainty in the hydroinformatic process,*** IWA Publishing 2003, Journal of Hydroinflormatics 05.4, 2003
25. **Hall, J.W., Solomatine, D.,** (2008), ***A framework for uncertainty analysis in flood risk management decisions,*** International Journal of River Basin Management 6 (2),85-98

26. **Hartanto, I.M., Beevers, L., Popescu, I., Wright, N.W.,** (2011), ***Application of a coastal modelling code in fluvial environments,*** Environmental Modelling and Software, 26 (12), 1685-1695
27. **Horritt, M.S. and Bates, P.D.,** (2001), ***Predicting floodplain inundation: raster – based modelling versus the finite – element approach,*** Hydrol. Process. 15, pp 825-842
28. **Horritt, M.S., Pender, G.,** (2008), ***Research Outcomes in the Application of 2D Flood Inundation Models for Flood Risk Management,*** FRMRC WP5.3 University and Industry partners
29. **Huang, S., Vorogushyn, S., Lindenschmidt, K.E.,** (2007), ***Quasi 2D hydrodynamic modelling of the flooded hinterland due to dyke breaching on the Elbe River,*** Advance in Geosciences, 11, pp. 21-29
30. **Hunter, N.M., Bates, P.D., Neelz, S., Pender, G., Villanueva, I., Wright, N.G., Liang, D., Falconer, R.A., Lin., B., Waller, S., Crossley, A.J. and Mason, D.C.,** (2008), ***Benchmarking 2D hydraulic models for urban flooding,*** Proceedings of the ICE –Water Management, 161, (1), pp13-30, ISSN, University of Reading
31. **Jonkman, S.N., Vrijling, J.K.,** (2008), ***Loss of life due to floods,*** Journal of Flood Risk Management 1, 43-56
32. **Kennedy, M.C., O' Hagan, A.,** (2000), ***Predicting the Output from a Complex Computer Code when Fast Approximations are Available,*** Biometrica, 87(1), pp1-13
33. **Krupka, M., Wallis, S.G., Pender, G. and Neelz, S.,** (2007a), ***Some Practical Aspects of Flood Inundation Modelling,*** Publs. Inst. Geophys. Pol. Aca. SC., E-7 (401), 2007
34. **Krupka, M., Pender, G., Wallis, S.G., Sayers, P.B. and Mulet-Marti J.,** (2007b), ***A Rapid Flood Inundation Model,*** Proc. 32nd IAHR Congress, Venice 1-6 July, paper SS05-04-O
35. **Krupka, M.,** (2008), ***A Rapid Inundation Flood Cell Model for Flood Risk Analysis,*** PhD Thesis – School of the Built Environment, Heriot-Watt University
36. **Leandro, J.,** (2008), ***A Dynamic – Objective- Function algorithm to calibrate a 1D/1D coupled hydraulic model versus a 1D/2D model,*** 11th International Conference on Urban Drainage, Edinburgh, Scotland, UK
37. **Lhome, J., Sayers, P., Gouldby, B., Samuels, P., Wills, M., Mulet-Marti and J.,** (2008), ***Recent development and application of a rapid flood spreading method,*** HR Wallingford, Howbery Park, Wallingford, Oxfordshire

38. **Li, B., Phillips, M., Fleming, C.A.,** (2006), ***Application of 3D hydrodynamic model to flood risk assessment,*** Proceedings of the Institution of Civil Engineers, Water Management 159, Issue WMI, pp. 63-75
39. **Liang, Q.,** (2010), ***A new adaptive grid based shallow flow model for flood simulation,*** IAHR 2010 European Congress, Edinburgh, UK
40. **Lin, B., Wicks, J.M., Falconer, R.A. and Adams, K.,** (2006), ***Integrating 1D and 2D hydrodynamic models for flood simulation,*** Proceedings of he Institution of Civil Engineers, Water Management 159, Issue WMI, pp 19-25
41. **Liu, Y.** (2008), ***A comprehensive survey of flood inundation models,*** School of the Built Environment, Herriot-Watt University, Edinburgh
42. **Liu, Y, Pender, G.**(2010), ***A new Rapid flood model,*** 1st IAAR European Congress, Edinburgh, UK
43. **McCall, J.,** (2005), ***Genetic algorithms for modelling and optimisation,*** Journal of Computational and Applied Mathematics 184, pages 205-222
44. **Mitchell, M.,** (1996), ***An Introduction to Genetic Algorithms,*** Cambridge, MA: MIT Press, ISBN 9780585030944
45. **Motte, A.,** (1846), ***Andrew Motte's English translation: Newton Isaac (1846), Newton's Principia: the mathematical principles of natural philosophy,*** New York: Daniel Adee, p. 72
46. **Neelz,. S., Pender, G., Villanueva, I., Wilson, M., Wright, N.G., Bates, P., Mason, D. and Whitlow, C.,** (2006), ***Using remotely sensed data to support flood modelling,*** Proceedings of the Institution of Civil Engineers, Water Management 159, issue WMI, pp 35-43
47. **Neelz, S., Hall, J. and Pender, G.,** (2007a), ***Improving the performance of fast flood inundation models by incorporating results from very high resolution simulations,*** Proc. Second IMA International Conference on Flood Risk Assessment
48. **Neelz, S. and Pender, G.,** (2007b), ***Parameterisation of square-grid hydrodynamic models of inundation in the urban area,*** Proceedings of the CONGRESS – INTERNATIONAL ASSOCIATION FOR HYDRODYNAMIC RESEARCH, CONF 32, VOL. 1, pp 41
49. **Neelz, S. and Pender, G.,** (2008), ***Grid resolution dependency in inundation modelling: a case study,*** in Allsop, W., Samuels, P., Harrop, J., Huntington, S., eds, Flood Risk Management Research and Practice, CRS Press, Chapter 13

50. **Neelz, S., Pender, G.,** (2009), ***Desktop review of 2D hydraulic modelling packages,*** Science Report SC080035, Joint DEFRA / Environment Agency Flood and Coastal Erosion Risk Management R & D Programme
51. **Oakley, J.E., O' Hagan, A.,** (2004), ***Probabilistic sensitivity analysis of complex models: a Bayesian approach,*** J. R. Statist. Soc. B(2004) 66, Part 3, pp. 751-769
52. **Ole, M., Sutat, W., Chusit, A., Surajate, BA., Slobodan, D.,** (2004), ***Potential and limitations of 1D modelling of urban flooding,*** Journal of Hydrology, volume 299, issues 3-4, pages 284-299, Urban Hydrology
53. **Pappenberger, F., Beven, K.,** (2006), ***Ignorance is Bliss: or 7 Reasons not to use Uncertainty Analysis,*** Water Resources Research, 42, W05302, DOI: 10.1029/2005WR004820
54. **Pender, G. and Neelz, S.,** (2007), ***Use of computer models of flood inundation to facilitate communication in flood risk management,*** ELSEVIER, Environmental Hazards 7 (2007), p. 106-114
55. **Pender, G. and Neelz, S.,** (2008), ***Developments in Floodplain Inundation Modelling,*** Inst. Geophys. Pol. Acad. Sc., E-10 (406)
56. **Pender, G. and Neelz, S.,** (2008), ***Hydrodynamic floodplain modelling in the urban area using remotely sensed digital elevation models,*** School of the Built Environment, Herriot-Watt University, Edinburgh
57. **Pender, G.,** (2011), ***A New Flood Inundation Modelling,*** FRMRC, Flood Mapping Workshop, 15th June 2011, Herriot Watt University, Edinburgh, UK
58. **Pender, G.,** (2011), ***Introduction to Inundation Modelling,*** FRMRC, Flood Mapping Workshop, 15th June 2011, Herriot Watt University, Edinburgh, UK
59. **Pender, G., and Liu, Y.,** (2012), ***Rapid Flood Inundation Modelling: Meta-Modelling of 2D Hydrodynamic Model Using Artificial Intelligence Techniques-Support Vector Regression, Modified Linear Interpolation and Cellular Automata,*** FRMRC Research Report WP1.3
60. **Penning-Rowsell, E., Werrity, A.,** (2008), ***FLOOD ERA Report for England and Scotland: Schematisation, evaluation and context conditions of structural and non structural measures for flood risk reduction,*** CRUE Research Report No 1-1
61. **Plate, E.J.,** (2002), ***Flood risk and flood management,*** Journal of Hydrology 267 (2002) 2-11
62. **Reeder, T. and Tarrant, O., Environment Agency,** (2007), ***Issues in Risk Science Future Flood: Risk Management in London and along the Tidal Thames,*** Benfield UCL Hazard Research Centre

63. **Robinson, P., Wicks, J., Pati, S., Niforatos, C.,** (2012), ***Saving money in Flood Risk Mapping – more bang for your buck,*** AWRA 2012 Spring Specialty Conference, New Orleans, Louisiana
64. **Sayers, P.B., Hall, J.W and Meadowcroft, I.C.,** (2002), ***Towards risk-based flood hazard management in the UK,*** Proceedings of ICE, Civil Engineering 150, May 2002, p. 36-42, paper 12803
65. **Smemoe, C.M., Nelson, E.J., Zundel, A.K., Miller, A.W.,** (2007), ***Demonstrating Floodplain Uncertainty Using Flood Probability Maps,*** JAWRA Journal of the American Water Resources Association, volume 43, issue 2, pp 359-371
66. **Syme, W.J.,** (2001), ***TUFLOW – Two & one – dimensional Unsteady FLOW software for Rivers, Estuaries and Coastal Waters,*** IEAust 2D Seminar, Sydney, Feb. 2001
67. **Syme, W.J., Pinnell, M.G., Wicks, J.M.,** (2004), ***Modelling Flood Inundation of Urban Areas in the UK Using 2D / 1D Hydraulic Models,*** The Institution of Engineers, Australia, 8th National Conference on Hydraulics in Water Engineering, ANA Hotel Gold Coast, Australia 13-16 July 2004
68. **Syme, B.,** (2006), ***2D or not 2D? –An Australian perspective,*** DEFRA 2006
69. **Syme, B.,** (2011), ***Pros and Cons of 1D and 2D Modelling,*** FMA Conference, San Diego, USA, Sep. 2011
70. **Tarrant, O., HR Wallingford, Environmental Agency,** (2006), ***Thames Estuary 2100, Rapid flood spreading methodology (RFSM),*** Final Report, Technical Note DT4, December 2006
71. **TUFLOW User Manual, GIS Based 2D/1D Hydrodynamic Modelling,** June 2006
72. **Tunstall, S.M., Johnson, C.L. and Penning –Rowsell, E.C.,** (2004), ***Flood Hazard Management in England and Wales: From Land Drainage to Flood Risk Management,*** Proceedings of World Congress on Natural Disaster Mitigation, 19-21 February 2004
73. **Van Vuren,** (2005), ***Stochastic Modelling of River Morphodynamic,*** PhD Thesis, Delft University of Technology, IOS Press, Amsterdam, Netherlands, ISBN: 90-407-2605-1
74. **Vapnik, V.K.,** (1999), ***An overview of Statistical Learning Theory,*** IEEE Transactions on Neural Networks, vol. 10, No. 5
75. **Wang, Z.B., Bruinsma, R.,** (1997), ***A Detailed 2D-Hydrodynamic Model for the Nieuwe Merwede,*** Prepard for: Rijkswaterstaat RIZA, delft hydraulics

76. **Wang, T., Yang, Z., Khangaonkar, T.,** (2010), ***Development of a Hydrodynamic and Transport model of Bellingham Bay in Support of Nearshore Habitat Restoration,*** Prepared for the U.S. Department of Energy under Contract DE-AC05-76RL01830
77. **Warmink, J., Janssen, J., Booij, M., Krol. M.,** (2010), ***Identification and classification of uncertainties in the application of environmental models,*** Environmental Modelling and Software. 25. 12: 1518-1527
78. **Weiyan, T.,** (1992), ***Shallow Water Hydrodynamics,*** Elsevier Oceanography Series, 55
79. **Whitley, D.,** (1994), ***A genetic algorithm tutorial,*** Statistics and Computing 4, (2): 65-85, doi: 10.1007/BF00175354
80. **Wicks, J., Syme, J., Hasaan, M.A.A.M., Lin, B., Tarrant, O.,** (2004), ***2D modelling of floodplains – is it worth the effort?,*** Proceedings of the River and Coastal Flooding Conference, Defra, UK, 1-10
81. **Willems, P., Vaes, G., Popa, D., Timbe, L., Berlamont, J.,** (2002), ***Quasi 2D river flood modelling,*** River Flow 2002, volume 2, 1253-1259, ISBN: 90 5809 509 6
82. **WUP-FIN,** (2003), ***Introduction to Modelling,*** Introductory training course, 2-4 November 2003, Can Tho

WEBPAGES

I. **PAGASA**, (2009), www.pagasa.dost.gov.ph/genmet/floods/cause_types.html
II. www.old.ima.org.uk/Conferences/Flood%20Risk%202007/contents_page.htm
III. www.TUFLOW.com
IV. http://evidence.environment-agency.gov.uk/FCERM/en/FluvialDesignGuide
V. www.eia.fi/wup-fin/training/material/presentations/EIA-overview.pdf
VI. www.earthzine.org/2011/03/21/is-flood-risk-management-identical-to-flood-disaster-management/
VII. www.nesdb.go.th/Portals/0/news/nesdbnews/flood
VIII. www.technion.ac.il/~dalyot/docs/Intro-DTM.pdf
IX. www.tuflow.com/Presentations.aspx
X. www.floods.org.au
XI. **Association of British Insurers (ABI)**, (2013). https://www.abi.org.uk/News/News-releases/2010/11/massive-rise-britains-flood-damage-bill-highlights-the-need-for-more-help-for-flood-vulnerable-communities-says-the-abi.aspx accessed 16th August 2013

XII. UK Parliament, (2013). Current parliamentary material available on flooding, http://www.parliament.uk/topics/Flooding.htm accessed 16th August 2013

XIII. www.sciencedirect.com